COMPARE UAV LASER AND IMAGE DATA FOR FLOOD MODELLING

KATEBE SAKALA
JUNE, 2020

SUPERVISORS:
dr.ir., S.J., Oude Elberink
dr., C .M., Gevaert

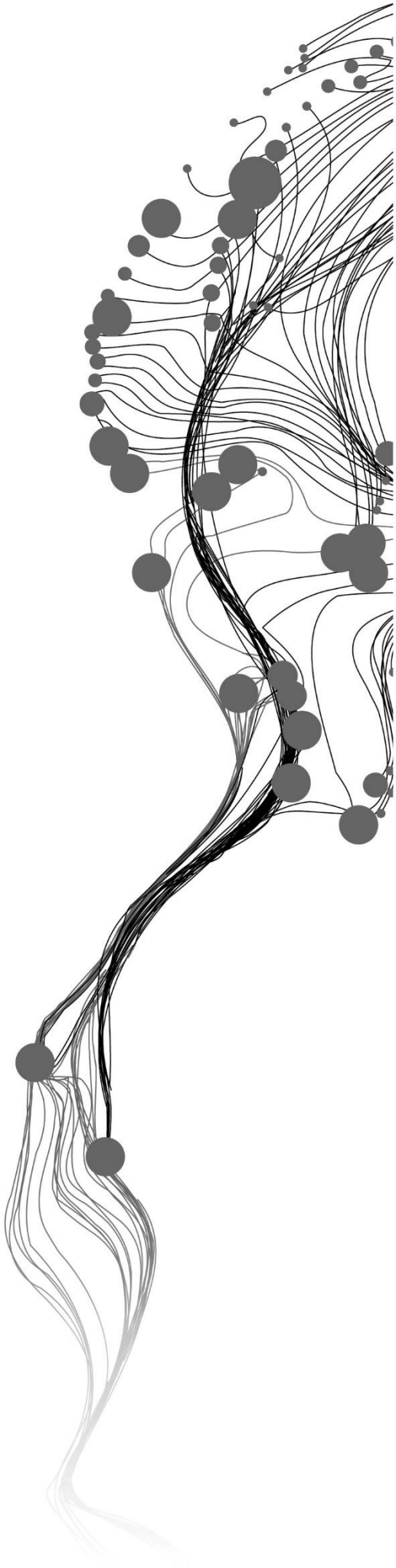

COMPARE UAV LASER AND IMAGE DATA FOR FLOOD MODELLING

KATEBE SAKALA
ENSCHEDE, THE NETHERLANDS, JUNE, 2020

Thesis submitted to the Faculty of Geo-Information Science and Earth Observation of the University of Twente in partial fulfilment of the requirements for the degree of Master of Science in Geo-information Science and Earth Observation.
Specialization: Geoinformatics

SUPERVISORS:
dr.ir., S.J., Oude Elberink
dr., C.M., Gevaert

THESIS ASSESSMENT BOARD:
Prof.dr.ir., M.G., Vosselman (Chair)
dr., R.C., Lindenbergh (External Examiner, TU Delft, Dept of Geoscience & Remote Sensing)

ABSTRACT

Floods are a significant challenge that can cause considerable damage and impede development. There is a need to capture data that can help control, manage, and mitigate this disaster. The emergence of UAVs has made the capture of this data more accessible, and at very high resolution. UAVs mounted with a camera or laser system can be an excellent choice for this. But looking at the cost of these systems, which data can be used for flood modeling in the Msimbazi river basin, located in the city of Dar es Salaam in Tanzania, which is prone to flooding. Hence the purpose of this study was to analyze and compare the quality of DTMs generated using UAV laser and UAV image data to demonstrate the application in flood modeling.

Therefore to produce DTMs suitable for flood modeling, filtering of the point clouds into ground and non-ground is very important. So for this purpose, the PTIN algorithm, as implemented in Lasground, was used in this study. Six parameters that are crucial in the tuning of this algorithm are step, spike, bulge, standard deviation, offset, and sub. These parameters were tuned in both the LiDAR and DIM data and accuracy assessment done on both the point clouds and DTMs. Furthermore, an investigation was done to ascertain how tuning these parameters affect flood modeling in terms of extent, velocity, water surface elevation, and depth. The findings from the comparison of the LiDAR and DIM DTMs and point clouds indicate that as the parameters are being tuned, this heavily influences what gets added to the produced surface. This filtering consequently affects flooding. HEC-RAS modeling software was used for flood modeling.

The analysis also showed that different landcover influence parameter settings when filtering. Also, the study showed that as the resolution of DTM reduces, flood extent increases because the DTM is more simplified at coarser resolutions, hence things like ramps, riverbanks, embankments may be removed. It was found that different parameter settings either increase or decrease the flooding effect. The analysis also showed that parameters that had the most significant influence when tuning the LiDAR data were bulge, step, and spike. And for DIM, the settings with the most significant impact were step, bulge, and offset.

From the findings, it was observed that both LiDAR and DIM could be used for flood modeling. The only considerations should be landcover and terrain characteristics in the study area. Also, it is essential to know the limitations of both datasets, questions, like where does LiDAR work best and where does DIM work best should be answered. The most important thing is the removal of macro objects such as buildings, vegetation, bridges, and the preservation of ramps, riverbanks, embankments, dividers, etc., especially when the DTM is for flood modeling.

Keywords: Ground filtering, DTM, accuracy assessment, LiDAR, DIM, Flood modeling

ACKNOWLEDGEMENTS

First and foremost, I would like to thank the Lord God Almighty for giving me the grace to continue with my studies. I give Him all the glory for this.

I would like to thank my supervisors, dr.ir. Sander Oude Elberink and dr. Caroline .M. Gevaert for their support, encouragement, and push. It has been worthwhile, and their input has been invaluable, and made this journey worth taking, made me grow in the whole process. I also want to thank my mentor drs. Wan Bakx, thank you for your guidance when I needed it most.

I would also want to thank my employer Zesco Ltd for allowing me to pursue my dream of studying at one of the best institutions in the world.

My gratitude goes to OKP for offering me the scholarship that has enabled me to undertake my master's program.

I would like to thank my friends and colleagues at ITC, SADC family, Forward in Faith church family, you made the journey worthwhile and enjoyable. Thank you, Wisdom, Mulimba, Mulala, Viollа, Jeff, Dickson, to mention but a few, you were excellent support. God bless you.

Last but not least, my special thanks goes to my lovely wife Kaluba, for always encouraging, praying for me, being a pillar for my children in my absence. Thank you to Fanny, Matamando, Takondwa, and Madalitso for your patience. I love you, and may God richly bless you.

TABLE OF CONTENTS

LIST OF FIGURES

LIST OF TABLES

1. INTRODUCTION

1.1. Background

Unmanned Aerial Vehicle (UAV) platforms are an essential alternative and solution for examining and researching our environment and are a capable source of laser and imaging data for many applications (Nex & Remondino, 2014). UAV platforms are used for many applications such as forestry, natural disaster monitoring, precision agriculture, topographic mapping, volumetric calculations, building, and road engineering (Izumida et al., 2017). Further, UAVs are considered viable and less costly compared to conventional manned aerial vehicles because they require less time for data acquisition, especially if the area is not too big (Martínez-Carricondo et al., 2018). Technological advances on the weight of sensors have made it feasible for the UAV platform to be mounted with different sensors, such as camera and light detection and ranging (LiDAR) (Zeybek & Şanlıoğlu, 2019).

LiDAR uses an actively emitted laser beam as its base for measuring the physical characteristics of objects and can provide data on the vertical structure of objects above the ground through scanning with a pulse (Begashaw, 2018). LiDAR is the most popular method of generating Digital Terrain Models (DTM) by filtering ground points from the entire point cloud. While photogrammetry needs image matching to generate a point cloud for filtering purposes, LiDAR obtains point cloud directly without additional processing (Rizaldy, 2018).

UAV Photogrammetry is an up-to-date, mobile, simple, and cost-effective remote sensing area mapping technology that uses a digital camera mounted on a small, low-cost UAV system. High image quality is a massive influence on the effectiveness and quality of mapping products, such as DTMs and Orthophotos. The accuracy of these products depends heavily on camera resolution, flight height, and accuracy of Ground Control Points (GCPs) (Berteška & Ruzgienė, 2013). UAV photogrammetry is also very useful for obtaining an image-based dense point cloud. Therefore it is possible to say that UAV photogrammetry is another data source for point cloud in place of LiDAR (Polat & Uysal, 2018). Berteška & Ruzgienė (2013) were able to show that UAV data is suitable for the creation of 3D models and meets the requirements for large-scale topography and GIS needs. Further, they showed that the evaluation of DTM, generated from UAV images, is necessary if the final mapping product is to be accurate.

A DTM is a digital depiction of the earth's surface without objects on it like vegetation, buildings, street furniture, etc. (Briese, 2010). The bare earth is a boundary between ground and objects attached to the ground; thus, DTM contains elevation information of solid ground without anything on it. Some applications that use a DTM are flood management, infrastructure and engineering planning, and environmental protection (Rizaldy, 2018). LiDAR point clouds are usually the preferred choice for DTM extraction; This is because they give first, intermediate and last pulse data, which is necessary for the classification of the ground and non-ground points (Yilmaz & Gungor, 2018). However,3D elevation models can likewise be obtained from UAV photogrammetry within a reasonable period, and good accurate DTMs can be produced from this same technology.

Polat & Uysal (2018) studied the precision of Digital Surface Models (DSMs) and DTMs, which were generated from 4 different LiDAR data and UAV Photogrammetry. The quality metrics they used for this comparison were correlation coefficient and Root Mean Square Error (RMSE). Their main goal was to

exemplify that the image-based dense point cloud was as accurate as the LiDAR point cloud. Their study showed that for a relatively small area, UAV photogrammetry could generate digital elevation models as precise as LiDAR-derived. Harwin & Lucieer (2012) also supported this by showing the viability of Multi-view stereo (MVS) and proving that UAV image data can be used for fine-scale landform change monitoring, focused on coastal erosion monitoring, which requires sub-decimetre dense and accurate 3D point clouds.

Similarly, Javernick et al.(2014) were able to show that structure from motion(SfM) applied in a dataset of UAV images can deliver high-quality terrain datasets competitive with those obtained by LiDAR, and suitable for studying how rivers or coastal areas are affected by flooding. Further, Yilmaz & Gungor (2018), in their study, showed that the use of UAV image-based point clouds enables the generation of accurate DTMs and may be an alternative for LiDAR technology. The research, therefore, will evaluate which dataset is ideal for flood modeling between UAV laser and UAV image data.

The Msimbazi river valley found in the city of Dar es Salaam in Tanzania. People settling in the flood-prone area, deforestation, and soil erosion have contributed to the basin failing to keep water naturally. Substantial and prolonged rainfall characterized by recurrent and severe flooding has been a big challenge that is faced here (Fintling, 2006). Hence flood plain mapping using drones is helping to bring up mitigation measures, which can bring down the risks associated with flooding by helping to create detailed terrain models. The data from this region is what the researcher used to conduct the research (WorldBank, 2019).

It is foreseen that the research will result in better knowledge regarding DTMs for flood modeling in the Msimbazi river valley basin, and it would also show which method performs better in the study area's terrain between UAV LiDAR and UAV photogrammetry. The players who would benefit from this data are the government, private sector, and development partners. Accurate monitoring and mapping of the DTM and flood extent are critical to assess flooding risk, develop wide-ranging relief efforts immediately after flooding, and provide damage estimates in both spatial and temporal dimensions (Hashemi-Beni et al., 2018). Therefore, the results of this research will contribute to the scientific literature on flood modeling on the use of UAV laser and UAV image data.

1.2. Research problem

From both UAV image and laser data, high-density point clouds and DTMs are derived. The accuracy of the point cloud will influence the quality of the DTM product, and so there is a need to investigate how accurate this point cloud data is. Several studies have focused on the accuracy of DTM derived in forest areas and mine areas (Begashaw, 2018; Obeng-manu, 2019) and some specifically on Digital Elevation Model (DEM) from UAV photogrammetry compared to SAR images for flood water level monitoring (Mantong, 2018). Others focused on Lightweight UAV data derived digital elevation models and orthoimage for environmental applications, focusing on data accuracy evaluation, the capacity for river flood risk modeling, predicting the effects of sea-level rise to flooding and erosion risk (Coveney & Fotheringham, 2011). Some studies like Yang & Chen (2015) integrated UAV laser, and image data since the reasons for integration are prompted by the significant deviations from direct geo-referencing of laser with image data. This co-registration method registers mini-UAV image data and LiDAR data successfully with an error of less than one pixel.

Therefore, it is necessary to study the accuracy of the DTMs derived from LiDAR or digital image matching (DIM) to find out whether they can be used for flood modeling in the study area. Thus it is vital

to determine if UAV LiDAR or UAV DIM data can be used independently for flood modeling in the Msimbazi river basin.

1.3. Research objectives

The main research objective is to analyze and compare the quality of DTMs generated using UAV laser and UAV image data to demonstrate application possibilities for flood modeling. This objective will be achieved through the following sub-objectives:

1.3.1. Sub-objectives

1. To focus on the optimization of filtering LiDAR and DIM DTMs for flood modeling by conducting a parameter sensitivity analysis using the TIN algorithm.
   a. What are the crucial parameters that affect the final LiDAR and DIM DTM products?
2. To determine how data processing methods affect the final LiDAR/DIM DTM product
   a. How do the produced DTMs differ from each other?
   b. Can the produced DTMs be used for flood modeling in the Msimbazi river valley basin?
3. To compare the influence of different DTMs for flood models produced from the parameters with the biggest influence.
   a. How do the different DTMs compare to each other in terms of flood depth, extent, and velocity?
   b. What is the effect of optimizing all relevant parameters on the output DTMs for flood modeling?
   c. Which parameters do have the most impact when analyzing DTM produced for flood modeling?
   d. What effects does filtering DTMs of different resolutions have on flood extent?

1.4. The innovation of the study

The research aims at combining parameter optimization of DTM filtering and flood modeling. The novelty will be to investigate how different parameter combinations influence the flooding extent, velocity, and depth. This would indicate how the filtering has either preserved objects like riverbanks, ramps, curbs, or removed macro objects like bridges, vegetation, and buildings.

1.5. Structure of Thesis

The research thesis is composed of five chapters. Chapter 1 is an introduction that looks at problem statement, research gap, objectives, and research questions. Chapter 2 is literature review; this chapter presents related works in line with the thesis. Chapter 3 is the Methodology it describes the methods used to achieve the sub-objectives. Chapter 4 is results and discussion; this presents the evaluation and discussion of the results. Chapter 5 is the conclusions and recommendations; this gives a conclusion based on the findings drawn from answering the research questions, and finally, recommendations are proposed.

2. LITERATURE REVIEW

2.1. UAV Photogrammetry

Photogrammetry is a system that is centered on the processing of images for the production of DTMs, DSMs, orthoimages, 2D and 3D reconstruction, etc. (Remondino et al., 2012).UAV Photogrammetry can generate very high-resolution datasets, which make it possible to generate 3D models (Micheletti et al., 2015). An example of image acquisition is shown in figure 1.

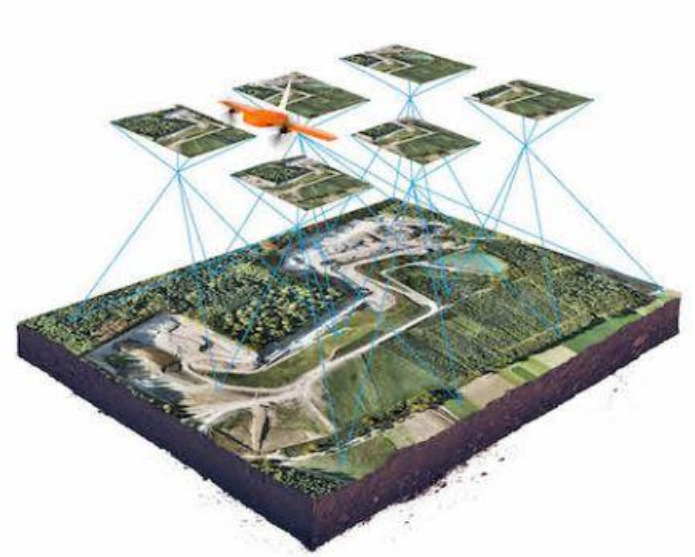

Figure 1: Example of UAV Photogrammetry data acquisition
(source: www.wingtra.com)

Among many other applications of UAV photogrammetric system, one of the essential ones is the capture of high-resolution images. Multi-view stereopsis (MVS) and SfM methods can be used to produce a dense 3D point cloud from UAV image data acquired through UAV photogrammetry (Harwin & Lucieer, 2012). DIM or SfM is a process that tries to match common features between images which are then used to establish both interior and exterior orientation parameters, after which a dense point cloud is extracted (Micheletti et al., 2015; Höhle & Potuckova, 2011;Polat & Uysal, 2017).
From their study Uysal, Toprak, and Polat (2015) were able to show that UAV photogrammetric data can be as accurate as RTK GPS data and can be used to generate DTMs using photogrammetric techniques. (Shahbazi et al., 2015) also reiterated this by stating that the generation of DTMs,3D point cloud, photo mosaic, and DSM are produced through the application of photogrammetric processes.

2.2. UAV LiDAR system

LiDAR is an optical remote sensing technique within which scattered light properties are measured to work out the variety and alternative information of an object (Guo et al., 2010). LiDAR data may be used to generate comprehensive high-resolution DTMs by using suitable interpolation techniques (Chu et al., 2014). Airborne LiDAR has many applications, some of which are DTM extraction, generation of 3D

building models, road extraction, forest parameter estimation, etc. (Hui et al., 2019). How data is captured using UAV LiDAR is shown in figure 2.

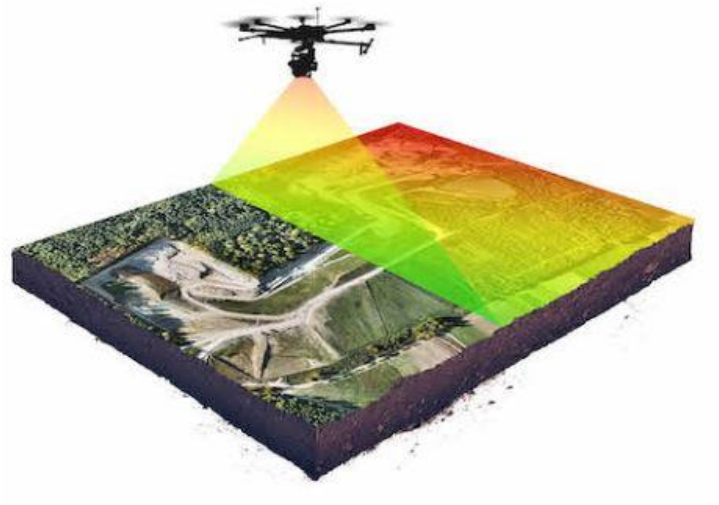

Figure 2: Example of UAV LiDAR data acquisition (source: www.wingtra.com)

LiDAR is one of the faster techniques for acquiring 3D laser data. Airborne laser systems use a laser beam emitted to record 3D information about a phenomenon through which the laser pulse bounces off. This can be done from helicopters, fixed-wing aircraft, or since recently UAVs (Siwiec, 2019). Axelsson (2000) further stated that the 3D point clouds acquired from the laser scanning system are capable of giving more than one unique z-value, which makes it possible to have different height attributes. Polat & Uysal (2017), in their study, emphasized that LiDAR has become a powerful means of collecting 3D information because it can do this efficiently, accurately, and on time. This is also highlighted by (Höhle & Potuckova, 2011).

The major difference between Photogrammetry and Airborne Laser Scanning (ALS) data is that with ALS measurements, it is almost difficult to make out what something is without the use of additional optical sensors. In contrast, photogrammetry, you can easily interpret what something is because of its advantage of color (RGB) imaging. One other significant difference is the ability of LiDAR systems to penetrate through vegetation canopies and hence provide ground points even in forested areas. On the other hand, DIM systems can only offer elevation data top of the canopy, as they are not able to provide ground information in thick, dense vegetation. So, the two point clouds would be very different from the two systems around vegetated areas.
Generally, LiDAR point clouds are considered more accurate than the DIM point clouds due to the latter containing several outliers below the terrain level (Zeybek & Şanlıoğlu, 2019). Therefore, the processing of the two point clouds would be different to consider the outliers (low points). In terms of point density and size, the DIM point cloud is denser and thereby larger than the LiDAR (Salach & Bakuła, 2018). However, both the DIM data and LiDAR data must go through the process of filtering before the process of DTM generation.

2.3. Filtering of point clouds

Filtering is the removal of all non-terrain objects to come up with a bare earth. The ground filtering is an essential step in the separation of points which are part of the ground surface and those which are not (Polat & Uysal, 2015;Zeybek & Şanlıoğlu, 2019; Moudrý et al., 2020; Liu, 2008). Separating ground and

non-ground points can be a very demanding task, especially in areas where there is a lot of variability in terrain. Therefore the accuracy of the DTM is dependent on the removal of non-ground points (Polat & Uysal, 2015).

Filtering results also depend upon the filtering algorithm used. The differences in the filtering processes can be checked through qualitative and quantitative methods. Qualitative methods include cross-sections profiles, Hillshaded DTMs, while quantitative methods include correlation coefficient, DEM of difference, RMSE, cloud to cloud compare among others (Anders et al., 2019;Sithole & Vosselman, 2004; Polat & Uysal, 2015).

Different filtering algorithms may produce different DTMs because they have different strengths and weaknesses, this is due to the parameter settings they use to fit different field data (Polat & Uysal, 2015;Nie et al., 2017; Zeybek & Şanlıoğlu, 2019). Zeybek & Şanlıoğlu (2019) further stated that some algorithms require some tuning of parameters, thereby giving the user power to influence the outcome of the filtering results. In their work of comparing different filters, Sithole & Vosselman (2004) show that the best filter algorithms and the optimal parameters are influenced by the landscape being investigated. Cățeanu & Arcadie (2017) in their work state that parameter optimization starts from default values, and then either these values are increased or decreased for each parameter value until the optimal one is arrived at (one that yields the lowest RMSE).

The algorithm for classifying ground and non-ground can be put in four different categories according to (Sithole & Vosselman, 2004): slope based, surface-based, clustering/segmentation, and block minimum algorithms. The most used algorithms are the surface-based because they use more context compared with other algorithms in the filtering process. Surface-based filtering algorithms can further be categorized into three: morphological-based filters, iterative-interpolation-based filters, and progressive-densification-based filters (Nie et al., 2017). Progressive TIN(PTIN) is a commonly used algorithm for filtering airborne LiDAR data (Nie et al., 2017;Polat & Uysal, 2015).

However, PTIN has weaknesses in that in steep terrain areas, it finds it difficult to find all possible ground points, and it tends to misclassify lower objects as ground points (Nie et al., 2017). Moudrý et al. (2020) show that though PTIN removes some ground points, misses some steep slopes, and did not perform well where there is dense vegetation, it was able to conserve the topography well. They further identified three conditions that may cause the filtering algorithms to fail in classifying ground and non-ground, namely: (i) sharp ridge/steep slope (ii) very dense vegetation (iii) vegetation on the slope or in ditches. On the other hand (Sithole & Vosselman, 2004) identified two more, namely outliers in the data and objects that are attached to the terrain.

Moudrý et al. (2020) state that to achieve optimal filtering performance, the choice of algorithm and tuning of parameter settings should be directed by the prevalent landscape in the study area. This process, according to them, is applied in Lastools, which allows users to select a set of parameters for a particular landscape in the study area. Lastools are developed for the processing of LiDAR data, and the Lasground tool is for the classification of ground and non-ground points. This tool uses an improved version of the TIN algorithm developed by Axelsson (Zeybek & Şanlıoğlu, 2019). In their study, Cățeanu & Arcadie (2017) show that Lasground performed better as compared to the other eight filters in mountainous terrain, steep slopes, and forestry vegetation. Zhang et al.(2018) in their study concluded that standard LiDAR filters like Lasground could be used to filter DIM point clouds preceding DTM generation. They further argued that the filtering results could be improved if a ranking filter is used before applying the ground filtering algorithm.

A description of how PTIN algorithm works is described by (Nie et al., 2017; Silva et al., 2018;Polat & Uysal, 2015), and it works by improving on the TIN algorithm developed by (Axelsson, 2000) by adding a step to enhance the densification using an algorithm similar to the Douglas-Peuker algorithm which builds an improved TIN to ensure that no ground points are under the improved TIN. And secondly, the

iterative judgment criteria is changed in that only a point with minimum distance to the corresponding TIN surface is selected as the ground point. Figure 3 depicts how the PTIN works:

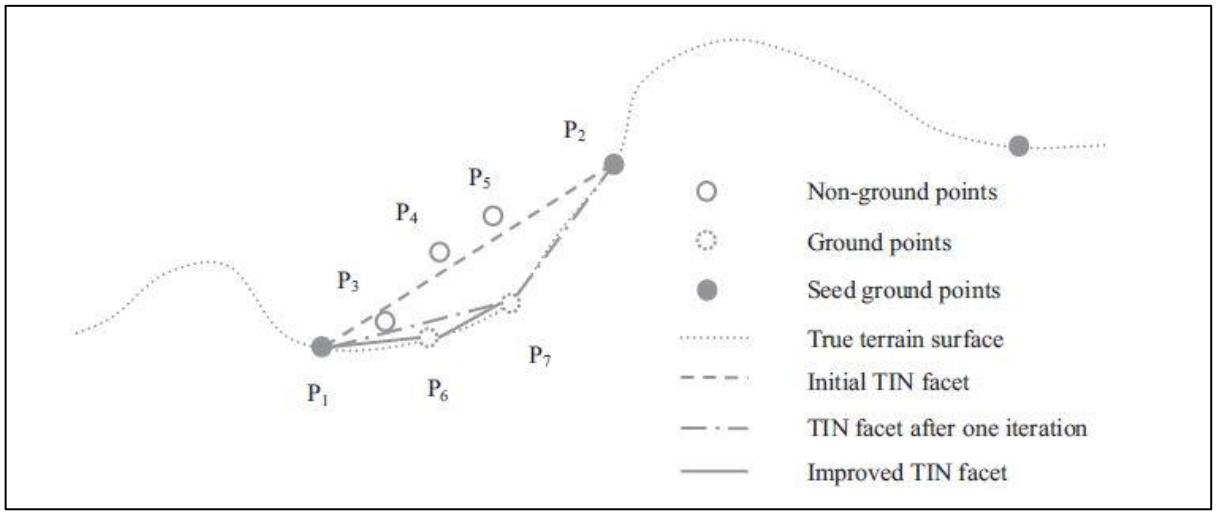

Figure 3: How PTIN works. Source: (Nie et al.,2017)

2.4. DTM accuracy

Jakovljevic et al.(2019) in their study listed four elements that affect the accuracy of a DTM, namely: (i) Point cloud accuracy and point density, (ii) efficiency of ground filtering algorithm, (iii) the interpolation method used and the, (iv) DTM resolution.

2.4.1. Quantitative assessment

The accuracy of LiDAR and DIM point clouds are assessed by using two methods: DEM of Difference (DoD) and cloud-to-cloud (C2C). DoD is the most used method of point cloud comparison, it works on a pixel-by-pixel difference, thereby highlighting vertical uncertainties and change detection (Jakovljevic et al., 2019; Salach & Bakuła, 2018;Leitão et al., 2016). The Root Mean Square Error (RMSE) and Mean Average Error (MAE) of the elevations were calculated in the LiDAR and UAV point clouds compared to the reference. MAE is a metric used to identify the overall bias in the data, thereby showing underestimation and overestimation in the elevations per land use/land cover (Jakovljevic et al., 2019; Salach & Bakuła, 2018; Ismail et al., 2015).

Polat and Uysal (2018) in their study used correlation coefficient to compare the similarities between LiDAR and DIM surfaces to illustrate that the DIM point cloud is as accurate as the LiDAR one(Cao et al., 2019;Peterson et al., 2019). Further, Pa'suya et al.(2019) also used linear correlation when analyzing differences between SRTM and GDEM surfaces against mean sea level reference surfaces.

The spatial variability of point cloud accuracy is assessed in CloudCompare using the C2C tool, which computes the cloud to cloud differences. Consequently, the mean absolute distance (MAD) and standard deviation (SD) were calculated based on the absolute distance between the two point clouds (Jakovljevic et al., 2019).

2.4.2. Qualitative assessment

Visual methods provide the first assessment of DTMs and require a higher level of adaptation to specific problems; Hillshaded DTMs are one such example (Podobnikar, 2009). Hillshaded DTMs aid in analyzing terrain as it shows the simplicity and complexity of the terrain, it also shows a realistic view on the depth in the DTM (Wilson & Gallant, 2000;Zhang et al., 2018). This visual inspection can help to ensure that things like riverbanks and ramps are not filtered out if the resultant DTM is meant for flood modeling. Therefore, shaded relief can be used to assess the quality of DTMs qualitatively, as shown by (Leitão et al., 2016;Cao et al., 2019).

Terrain profiles are also an effective way of visually assessing DTM quality, and these visualizations reflect the methods used, leading up to DTM production (Podobnikar, 2009). Jakovljevic et al. (2019) similarly used cross-sections in various land use/land cover to assess the accuracy of the DTMs. Equally, Salach & Bakuła (2018) also showed in their work that the cross-section method is a valuable assessment of filtering results and DTM accuracy. Finally, Peterson et al. (2019) further proved that a profile could be used to compare two surfaces by using the extracted centreline of a road.

2.5. Flood Modelling

Urban flooding is an inescapable scenario for many cities around the world, and the challenges which are caused by this can vary from minor ones to major ones that cause massive inundation (Mark et al., 2004). The authors went on to further state that urban drainage modeling is a good case study in developing countries, because of the extent and frequency of the flooding in their cities as flood data is available. Hence it is essential to model these floods to analyze and understand the existing conditions so that mitigation measures can be implemented.

Urban flood modeling has several input parameters, and one crucial one is a DTM because it affects the flow direction, flow velocity, flood extent, and flood depth (Abdullah et al., 2009;Jakovljevic et al., 2019; Muller, 2015). Anders et al. (2019) further state that the choice of filtering technique for hydrological modeling is vital if the correct modeling outputs are to be achieved. The characteristics of DTMs for urban flood application is that objects like bridges, buildings, vegetation, flyovers, and light rail train line should be removed, while ramps, curbs, and dividers should be preserved (Abdullah et al., 2009; Leitão & Sousa, 2018;Meesuk et al., 2015). Mark et al. (2004) also state that the characteristics of data in a flood-prone area, such as the base and curb level of the road, the general topography of each catchment, and the height data of low and high points, should be correctly obtained.

Abdullah et al. (2009) used MIKEFLOOD software to do the flood simulation to analyze the outcome of the filtering process (produced DTM). 2D flood models were created for each of the filters and analyzed. The authors argued that Urban flood application is dependent on how the DTM surface closely represents the real surface.

Abdullah et al. (2009) also did an evaluation and comparison of 8 different filtering algorithms to ascertain which one produces a DTM that is suitable for urban flood applications. The DTMs were analyzed in terms of flood depth and flood extent compared to reference flood depth and flood extent data. Figure 4 shows the results of their work depicting DTMs from 5 filters (1) Elevation threshold Elevation Window (ETEW), (2) Morph2D, (3) Poly two surface (4) Slope and (5) Adaptive TIN.

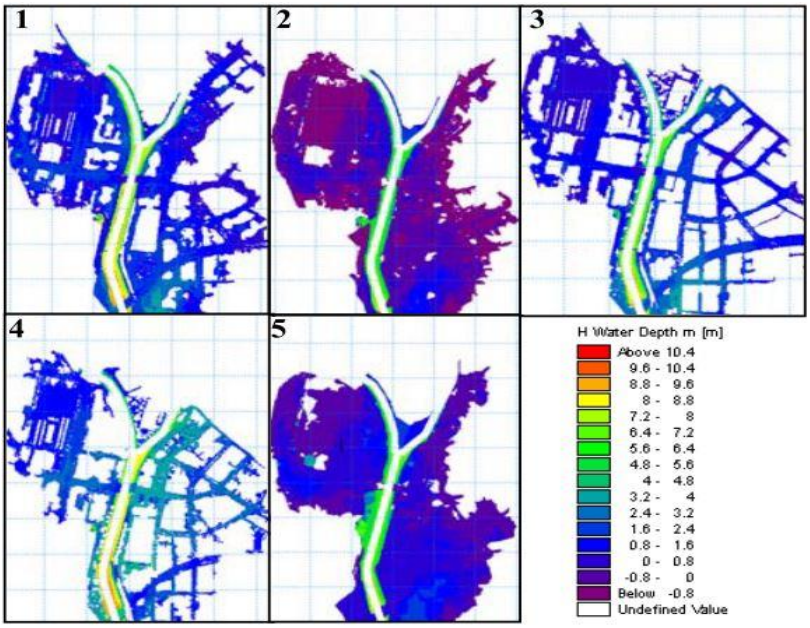

Figure 4: Urban Flood model Simulation from 5 filters
Source: Abdullah et al., 2009

Abdullah et al. (2009) conclude that the adaptive TIN flood simulation in terms of flood depth and extent gave results that were close to the reference data. This is because of its ability to remove macro objects, and its resultant DTM is closer to the surface of the study area. Similarly, in their work Abdullah et al.(2012) showed that the performance of the ATIN filter for creating a suitable hydrological DTM was second overall only to their developed modified progressive morphological filter. Anders et al. (2019) went on to show that the TIN densification algorithm is suitable for producing a bare-earth DTM.

In their study, Jakovljevic et al. (2019) showed that though LiDAR data is a recommended source of hydrological data, an alternative is a DIM data that can perform well in many land cover classes, and it's also cost-effective. These findings are in agreement with (Escobar Villanueva et al., 2019). This was also reiterated by (Leitão et al., 2016), who added that image classification could be the basis for urban drainage modeling. Langhammer et al.(2018) went on further to show how different DTMs can depict different flood extents and flood depth in each scenario. They further proved that DTMs from DIM could be used to model floods, as did (Meesuk et al., 2015).

There are several flood modeling applications, as highlighted in Table 1 below. In this study, HEC-RAS was used; it is a software that can perform one and two-dimensional hydraulic calculations for both natural and man-made networks (Ben Khalfallah & Saidi, 2018). A number of studies have been conducted by using this model since its development, some of which are those highlighted in Table 1. One of the main inputs in HEC-RAS is a DTM, which is essential for the development of a hydraulic model; others are geometric data and map layers. Geometric data in HEC-RAS includes things like river cross-section data, 2D flow area, boundary conditions, breaklines, structures, etc. (Brunner, 2016). Boundary conditions are conditions that are linked to the 2D flow area, and they permit the program to

perform computations among them are flow hydrograph, stage hydrograph, normal depth, rating curve, and precipitation.

Table 1: Flood Modelling applications

Application	Applied by
SOBEK	(Tamiru & Rientjes, 2001)
MIKEFLOOD	(Meesuk, 2017) (Abdullah et al., 2009) (Abdullah et al., 2012)
LISFLOOD	(Anuar bin Md, 2018)
HEC-RAS	(Anuar bin Md, 2018) (Alho et al., 2009) (Nandurkar et al., 2017) (Alaghmand et al., 2014) (Ben Khalfallah & Saidi, 2018)
PCRaster	(Muller, 2015)
OPENLISEM	(Pratomo, 2015) (Bout & Jetten, 2018) (Habonimana, 2016)

The main features of HEC-RAS are modeling 1-D steady flow, 1 and 2-D unsteady flow calculations, sand deposit transport, and water quality modeling (Brunner, 2016). Examples of expected output from HEC-RAS in terms of flood depth, velocity, water surface elevation, and flood extent are shown the figures 5-8 below.

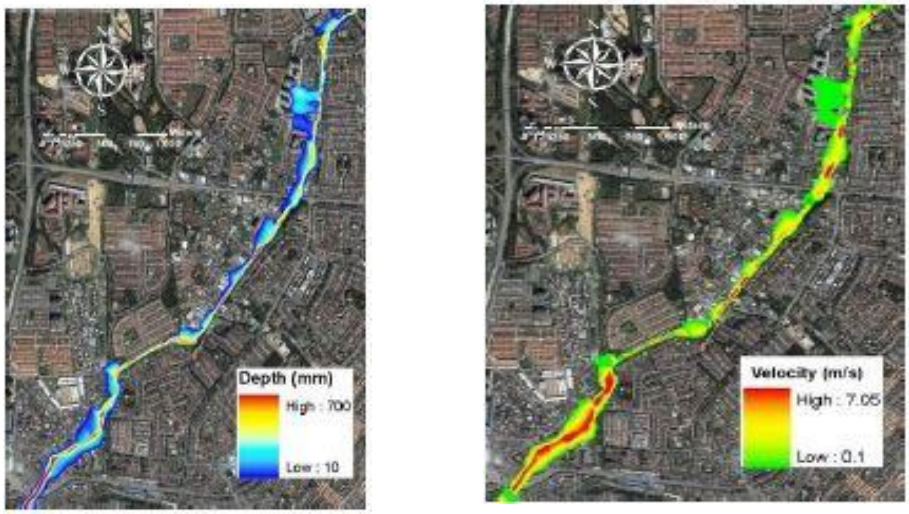

(a) (b)

Figure 5:(a)water depth map and (b) water velocity map

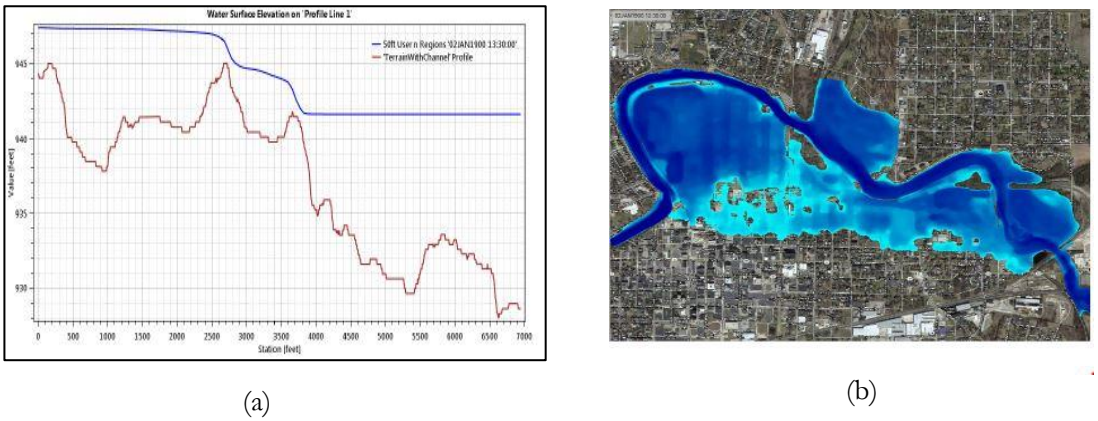

(a) (b)

Figure 6: (a) Water surface elevation and (b) flood extent map

From the literature review, it can be noted that different DTMs can be generated based on different parameter settings in the filtering algorithm. It can also be concluded that the PTIN algorithm is a considerably good filter that can be used to filter point clouds, specifically for flood scenario generated DTMs. Further, it is essential to conduct both qualitative and quantitative assessment of the DTMs produced.

This research aims at using the PTIN algorithm in LAStools to carry out the parameter optimization and investigate using the flood modeling software HEC-RAS the effects of the different parameters on flooding in the study area.

3. METHODOLOGY

3.1. Study Area

The case study area is the Msimbazi river valley basin in Dar es Salaam, Tanzania. The Msimbazi watercourse flows across Dar es Salaam town from the upper regions of Kisarawe within the coastal zone and discharges its waters in the Indian ocean(de Risi et al., 2013). This area is susceptible to flooding, and hence, there is a need to model the flooding in this area so that some mitigation measures can be put in place to help the people who live along the river, figure 7 shows the study area.

Data sources

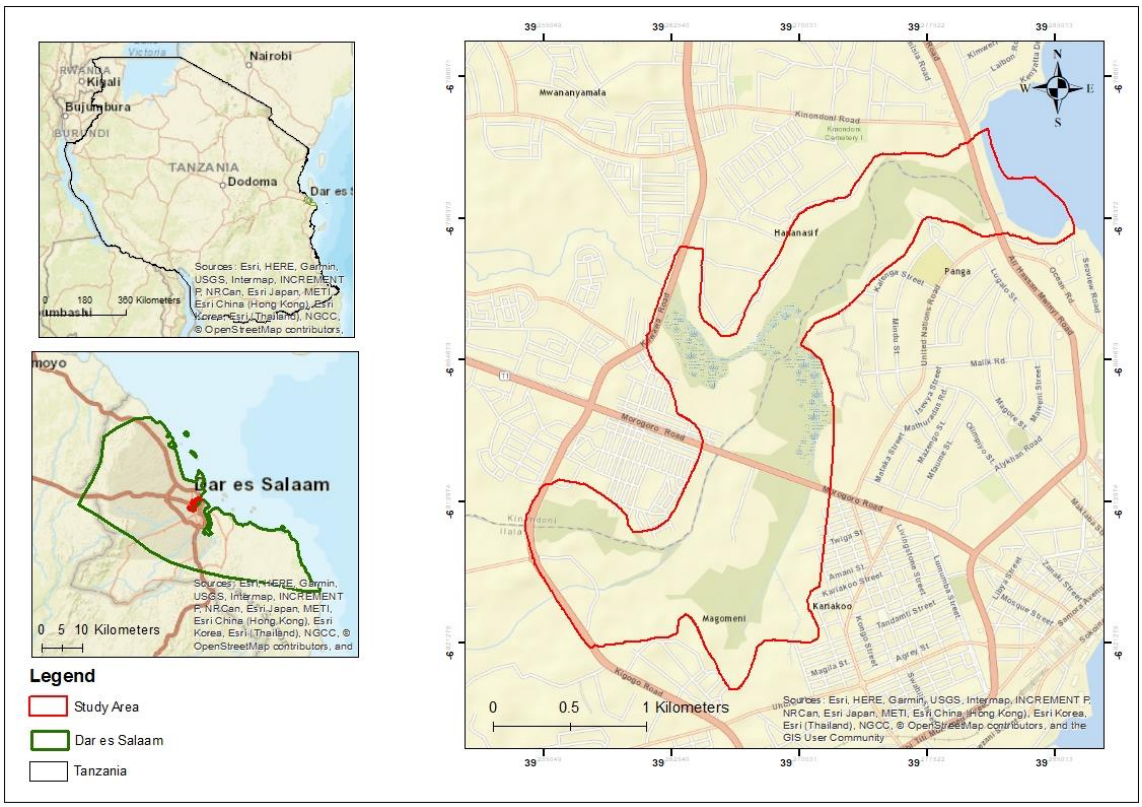

Figure 7: Study Area (Msimbazi river basin)

The source of the Photogrammetric and LiDAR data was CDR international (2019). The LIDAR data was obtained in March 2019, while the Photogrammetric data was obtained in September 2019. These datasets were made available as point clouds in Laz format for use in this research. Also, a total of 8 control points were marked around the study area, and these are shown in Table 2. The coordinate system used was WGS84 UTM 37S. figures 8 and 9 show the LiDAR and DIM raw point clouds.

Table 2: Ground control points in WGS84 UTM 37S

Point ID	Easting(m)	Northing(m)	Z(m)
GCP-01	531075.061	9248766.414	-22.901
GCP-02	530353.151	9248436.971	-15.157
GCP-03	528969.653	9248158.025	-19.218
GCP-04	529402.167	9247131.435	-21.621
GCP-05	529380.292	9246798.731	-21.800
GCP-06	528103.916	9246751.987	-16.458
GCP-07	528995.062	9246548.000	-19.485
GCP-08	529861.105	9247022.124	-20.736

Figure 8: Subset of LiDAR point cloud

Figure 9: Subset of DIM point cloud

3.2. Methodology workflow

The research questions were addressed by applying three methods in the research: filtering, accuracy assessment, and flood simulation of the dense 3D point clouds and DTMs from the two datasets. Figure 10 shows the flowchart of the methodology.

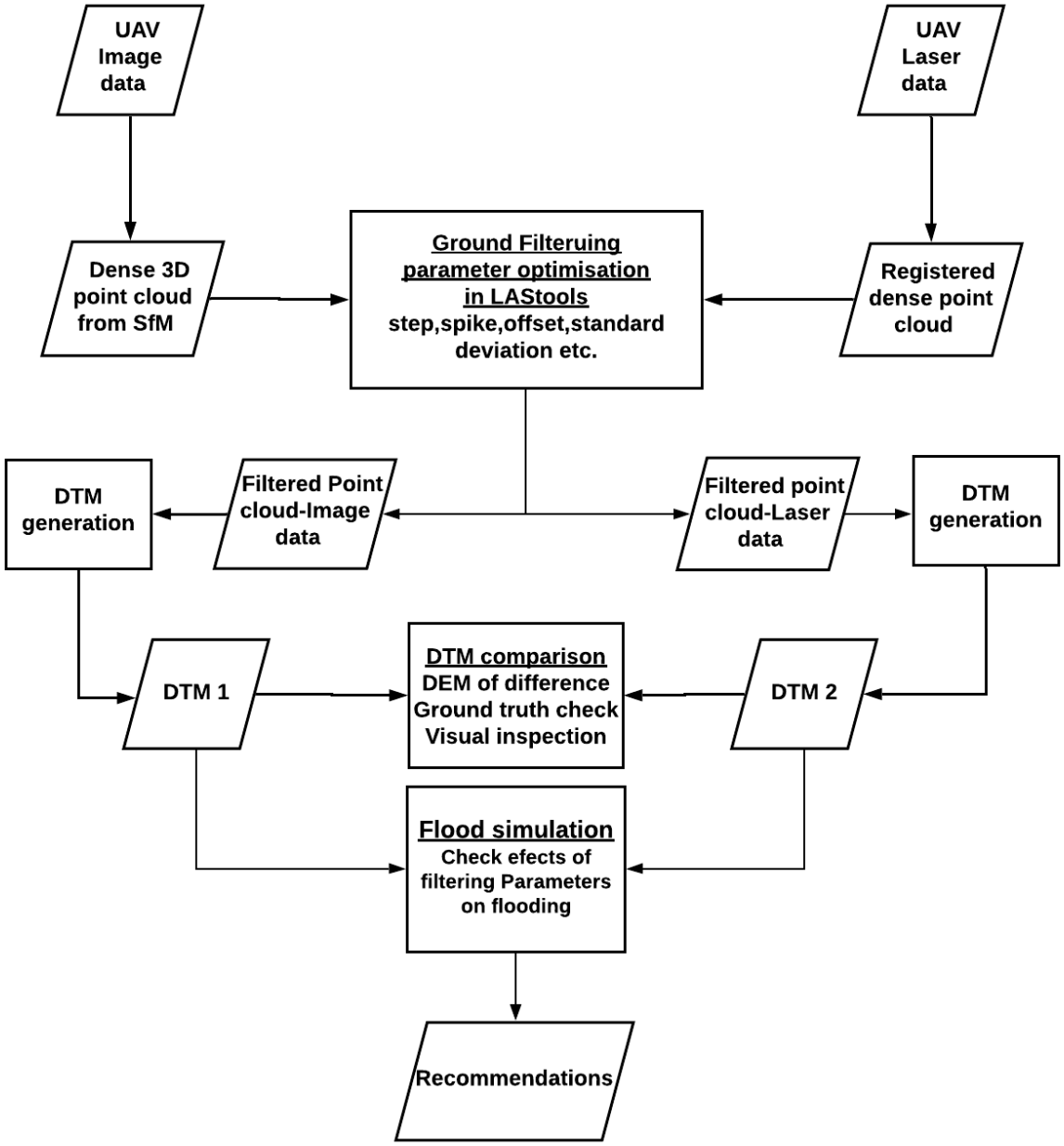

Figure 10: Workflow of the Methodology

3.3. Filtering parameter optimization

The filtering method adopted in this research is the TIN algorithm, as implemented in LAStools. The way this algorithm works is by; first, initial parameters are calculated using the data; secondly, seed points are chosen; thirdly, iterative densification of the TIN is done by calculating parameters for each iteration from any point included in the TIN. If a point meets the threshold, it is added. Fourthly, this process continues until all pints are classified as ground or non-ground. According to Mantong (2018), the TIN algorithm is used for flood modeling because it gives an accurate portrayal of the geometry of channels, riverbanks, dikes, etc., and it's able to model elevation changes and breaks in gradient.

Several parameters, such as step, spike, and offset, will be optimized to investigate which ones have more influence on the DTMs for flood modeling. The meaning of these terms is as follows; Step is the measure

of setting the resolution of the grid. Spike sets the threshold of spikes that can be removed (up-spike and down-spike), and offset sets the margin within which points above the specified ground can be included. This algorithm was chosen because it can handle complex scenes, lower-resolution data, and its ability to handle type I (rejection of ground points) and type II (acceptance of non-ground points) errors. Since this algorithm can process 3D point clouds from both UAV laser data and UAV images, it would make it easier to compare which dataset produces a suitable DTM for Flood Modelling in the study area. This is essential because the DTMs will have been produced using the same methods.

Cățeanu and Arcadie (2017) analyzed nine LiDAR filtering algorithms, and from their findings, the adaptive TIN algorithm provided better results than the others. Other studies which have used the adaptive TIN algorithm to filter point clouds from either Image or laser data are (Anders et al., 2016; Axelsson, 2000; Anders et al., 2019;Wallace et al., 2016).

Also, to produce a DTM, all non-ground points are removed or filtered. Rapidlasso (2019) published several articles on their website, highlighting how the adaptive TIN algorithm in Lasground can be applied in the processing of both UAV image and LiDAR data. They showed how photogrammetric produced 3D point clouds could be processed, from denoising, filtering, and consequently, up to the production of DTM.

In this research, the optimization of these parameters to remove the non-ground points was investigated to produce DTMs that can be used for flood modeling from the UAV image and laser data. The relevant investigated parameters are optimized to produce DTMs that can be useful for flood simulation in the study area. To come up with the parameters that would influence the accurate processing of point clouds, parameter combinations for the different LAStools algorithms were set to default values. Then their behavior is monitored when increased or decreased until they reach a point where they cannot be optimized any further (Cățeanu & Arcadie, 2017).

3.3.1. LiDAR point cloud processing steps in LAStools

To carry out the analysis, a subset of the point cloud was used for the processing and subsequent parameter tuning. A batch script from LAStools (Rapidlasso, n.d.-b) was modified to be used for the data preparation and derivative production (Appendix B). The following steps were used to execute the work;

Step 1: create a buffered tiling of 200m x 200m and buffer of 30m, from the original LiDAR point cloud using lastile

Step 2: Lasground was used to classify ground and non-ground points

Step 3: lasheight was used to remove low and high points

Step 4: lasclassify was used to classify buildings and trees from the cleaned tiles

Step 5: lastile was used to remove the buffers from the classified tiles

Step 6: las2dem was used to create raster DTM from the ground points

Step 7: blast2dem was used to generate hillshade DTMs and actual elevation DTMs in tiff format

3.3.2. Preliminary steps for DIM point cloud

Since the DIM point clouds covered a bigger area than the LiDAR data, it was necessary to create a boundary around the LiDAR points, which would then be used to clip the DIM points cloud.

Step 1: Lasboundary was used to generate a shapefile of the LiDAR point cloud.

Step 2: Using lasclip the boundary from LiDAR was used to clip the photogrammetric point cloud and merged

Step 3: Lasduplicate was used to remove duplicate points that were similar in terms of X, Y, and Z. The purpose of the above steps was to ensure that the two point clouds covered the same study area.

3.3.3. DIM point cloud processing steps in LAStools

To carry out the analysis, a subset of the point cloud was used for the processing and subsequent parameter tuning. Similarly, for the DIM point cloud a photogrammetric batch script from LAStools (Rapidlasso, n.d.-b) was modified to be used for the data preparation and derivative production (Appendix B). The following steps were used to execute the work;
Step 1: create a buffered tiling of 200m x 200m and buffer of 30m from the original photogrammetric point cloud lastile
Step 2: lasthin was used mark points whose z coordinate corresponds to certain percentile
Step 3: lasnoise was used to remove isolated low points from marked points of step 2
Step 4: lasground was used to classify ground and non-ground using remaining points from step 3
Step 5: lasheight was used to classify points above and below the ground
Step 6: lasthin was used to classify the lowest points that was not noise
Step 7: lasground was used to classify code 8 points into ground and non-ground
Step 8: las2dem was used to create a DTM from the ground points
Step 9: blast2dem was used to create a seamless DTM and hillshade DTM

3.4. DTM generation

Among the common DTMs used to represent the existing terrain, the most common ones are the regular, the triangular irregular network (TIN), and the contour line model (Ramirez, 2006). Based on the parameter optimization, several DTMs were generated for analysis from both the UAV image and laser data. This was done in LAStools.

3.5. DTM comparison

To access the DTMs of the two datasets, a comparison had to be made in selected landcover of the study area to ascertain how the different DTMs performed in these regions. To do this, a combination of methods were conducted:

3.5.1. Point cloud noise analysis in CloudCompare

A comparison was made to check and compare how noisy the filtered point clouds from both the LiDAR and DIM are compared to each other in different Landcover scenarios. Before the filtered point clouds could be analyzed, lassplit was used to split the final classified point cloud into its classified point clouds. The output required for this case is the ground filtered points only because the analysis was to check how noisy these ground filtered point clouds are.

Noise analysis of the filtered point clouds was carried out on a car park area using CloudCompare software. The area of interest was the same for all the surfaces analyzed, and to find out how noisy a point cloud is, a flat surface is preferred. This procedure involves fitting a plane through the point cloud and calculating the RMSE between the plane and the points in the selected point cloud. The RMSE is a measure of how noisy the point cloud, the lower it is, the less noisy the point cloud

3.5.2. Cloud to cloud accuracy assessment in CloudCompare

For the accuracy assessment in CloudCompare, first, the classified LiDAR and DIM point clouds are split into ground and non-ground for easy analysis using lassplit. The ground filtered point clouds were

compared to each other to check how the DIM point cloud differs from the LiDAR. The comparison was based on only the ground points since they are the ones used to produce the DTMs for LiDAR and DIM. For this assessment the LiDAR point cloud was taken as a reference.

3.5.3. Cross-section accuracy assessment

One way of making a comparison between two surfaces is to compare their corresponding cross-sections/profiles. Profile lines are a qualitative measure for comparison of surfaces. Profile lines at different filtering parameter settings were compared, assuming the LiDAR as the reference in this case. In this study, four areas were examined, namely: built-up, vegetated, bare/open grassland, and man-made. Khalid et al. (2016), in their study, used profile sections to do a visual inspection of generated DTMs in comparing them to the reference.

3.5.4. DEM of difference

Difference models are a qualitative comparison of DTM surfaces. Podobnikar & Vrečko (2012) used the DEM of difference to assess the differences between DTMs produced from different filtering algorithms. In this study, the difference models were created using ArcGIS software. The LiDAR DTM was taken as the reference, so the Z value of the DIM DTM was subtracted from the LiDAR DTM pixel by pixel. This yielded a surface that shows the differences between the two, and this difference map displays the areas where the LiDAR and DIM data differ, and where there is little or no difference.

3.5.5. DTM comparison using correlation coefficient

For this study, the points for the calculation of the correlation coefficient were made in ArcGIS software using a subset from the study area. Random points were extracted on both the LiDAR and DIM surfaces. These points were then assigned Z values using the corresponding surfaces. Finally, by using RStudio, the correlation coefficient in different regions of the study area was calculated (Appendix C).

Two quantitative continuous variables can be investigated using a technique known as correlation, one common one is the Pearson's correlation which is a measure of how related the two variables are (Boslaugh, 2012). Khalid et al. (2016) used the correlation coefficient to evaluate and compare how the heights in open-source DEM and LiDAR compare to each other. Therefore, the correlation coefficient is an excellent way to evaluate the differences between the two DTMs.
For this study, the points for the calculation of the correlation coefficient were made in ArcGIS software. Random points were extracted on both the LiDAR and DIM surfaces. These points were then assigned Z values using the corresponding surfaces. Then using RStudio, the correlation coefficient in different regions of the study area was calculated.

3.6. Flood simulation in HEC-RAS 5.0.7

For the flood simulation, open-source software called HEC-RAS was used, is open-source modeling software that can perform one-dimensional steady flow, one and two-dimensional unsteady flow calculations and many more such as sediment transport/mobile bed computations, and water temperature/water quality modeling (Brunner, 2016; Alzahrani, 2017). HEC-RAS version 5.0.7, which was used in this research, allows 2D unsteady flow calculations. In this way, a river network and floodplain could be modeled through a 2D flow computational mesh (Alzahrani, 2017). This study focused on applying a 2D HEC-RAS model on the Msimbazi river basin.

According to, Abdullah et al.(2009), flood simulation uses as its input, the DTM for flood modeling. They also stated that the DTM could be analyzed by direct comparison of the flood depths and flood extent of the model in contrast to that at gauging stations. Hence flood simulation levels can indicate the accuracy of the DTM. Coveney and Roberts (2017) stated that DTM derived from several platforms could be used for flood modeling and consequently flood prediction, this is very important as it points out that the resolution and accuracy of the DTM directly affect the flood simulation.
This research involves three methods in HEC-RAS, namely (i) hydrological modeling, (ii) hydraulic modeling, and (iii) flood mapping. Figure 11 shows the workflow for the 2D flood simulation.

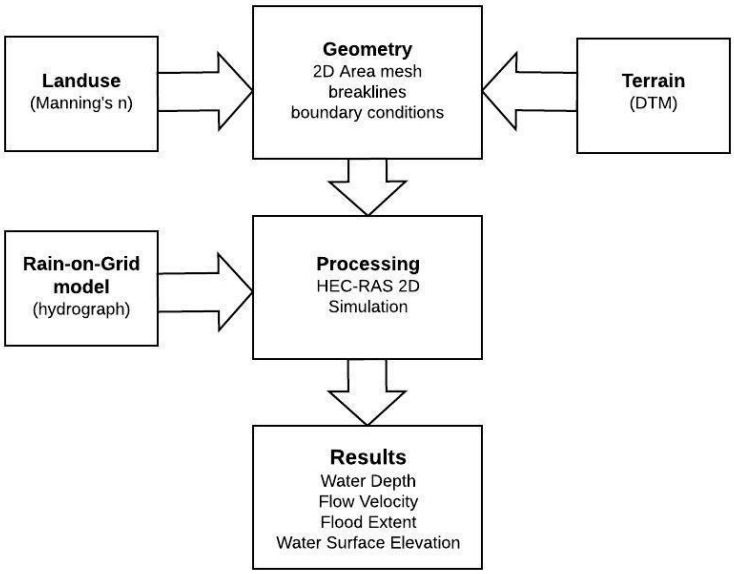

Figure 11: Workflow for the 2D flood simulation in HEC-RAS

3.6.1. Data preparation

3.6.1.1. Rainfall

The rainfall data needed as an input in the hydrological model was of a period at which the study area experienced flooding, in this case, the month of May 2019 (WorldBank, 2019). Rainfall data was downloaded from the NASA website as a text file; this was after selecting the area of interest and time step (temporal resolution of half-hourly). After that, using the script shown below. Wget software was used to download actual rainfall data from the NASA Giovanni internet protocol.

wget --http-user=kats2050 --http-password=methodGEO2020 --load-cookies .urs_cookies --save-cookies .urs_cookies --keep-session-cookies --auth-no-challenge -r --reject "index.html" -np -e robots=off --content-disposition -i Dar_UAV.txt*

This script is run through the command prompt. A total of 1440 images (NetCDF format) were obtained for May; this is the cumulative rainfall in mm/hr. Figure 12 is a sample of downloaded data from the website, which has a grid size of 11km. These images cover the whole world, and hence the area of interest had to be masked from it.

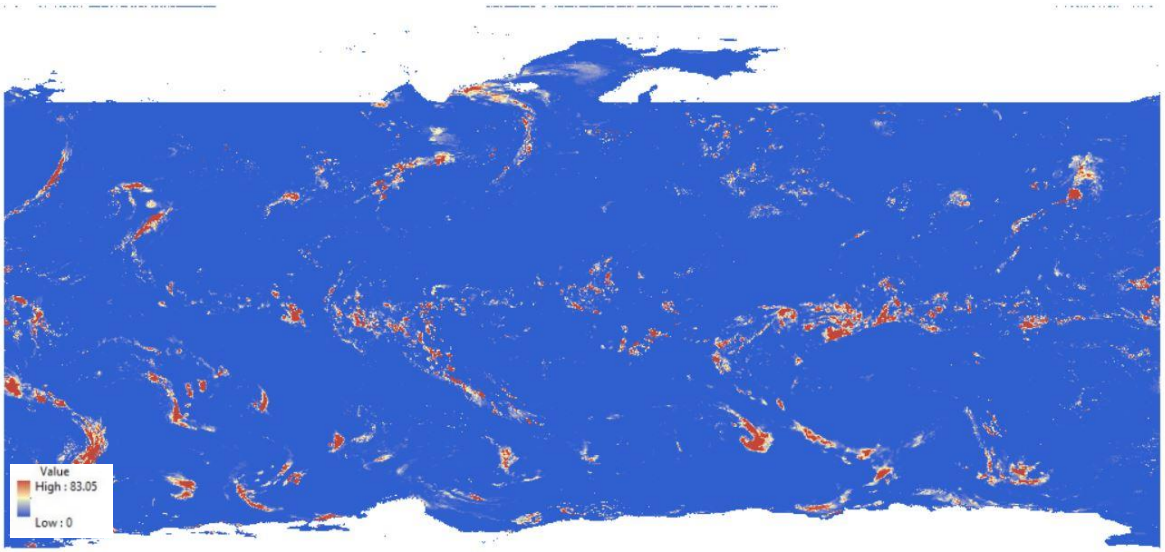

Figure 12:standard downloaded rainfall data from NASA

The next step was to convert the images from the netCDF format to Tiff. After that, using the ArcGIS model builder, a model was created which clips out the area of interest where the study area is located and uses the shapefile of the area of interest to mask the rainfall data. See Figure 13.

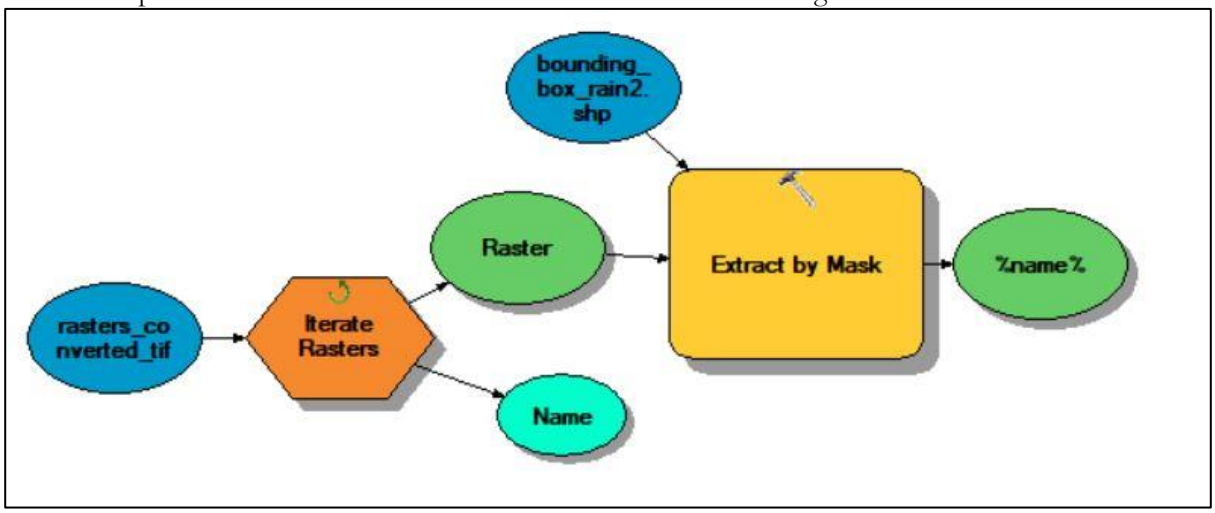

Figure 13: Model for clipping and masking rainfall data

Figure 14 shows the output of the masking operation, displaying the values for the two rainfall grid cells which cover the study area . The mask used was the study area polygon, the units are mm/hr for the rainfall, the same as the original netCDF files, but the format is now Tiff, and grid size maintained at 11km.

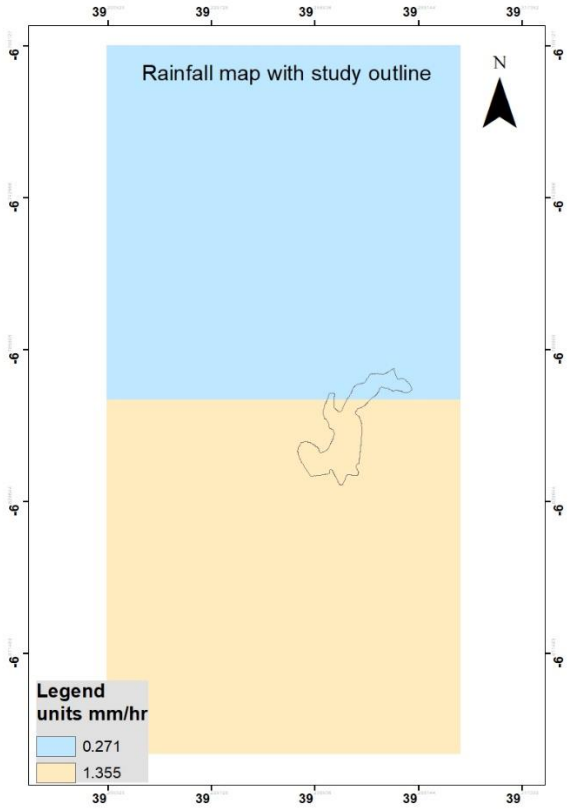

Figure 14:Sample Rainfall data on study area

3.6.1.2. Rainfall value extraction

Using the masked polygon, the rainfall values of the study area were extracted utilizing an R code (shown in Appendix A). The area of interest has longitude 39.2 and latitude -6.8, so cell values at this specific location were extracted; in total, 1440 masked images were obtained. Figure 15 shows the plot of the rainfall values obtained from the extraction.

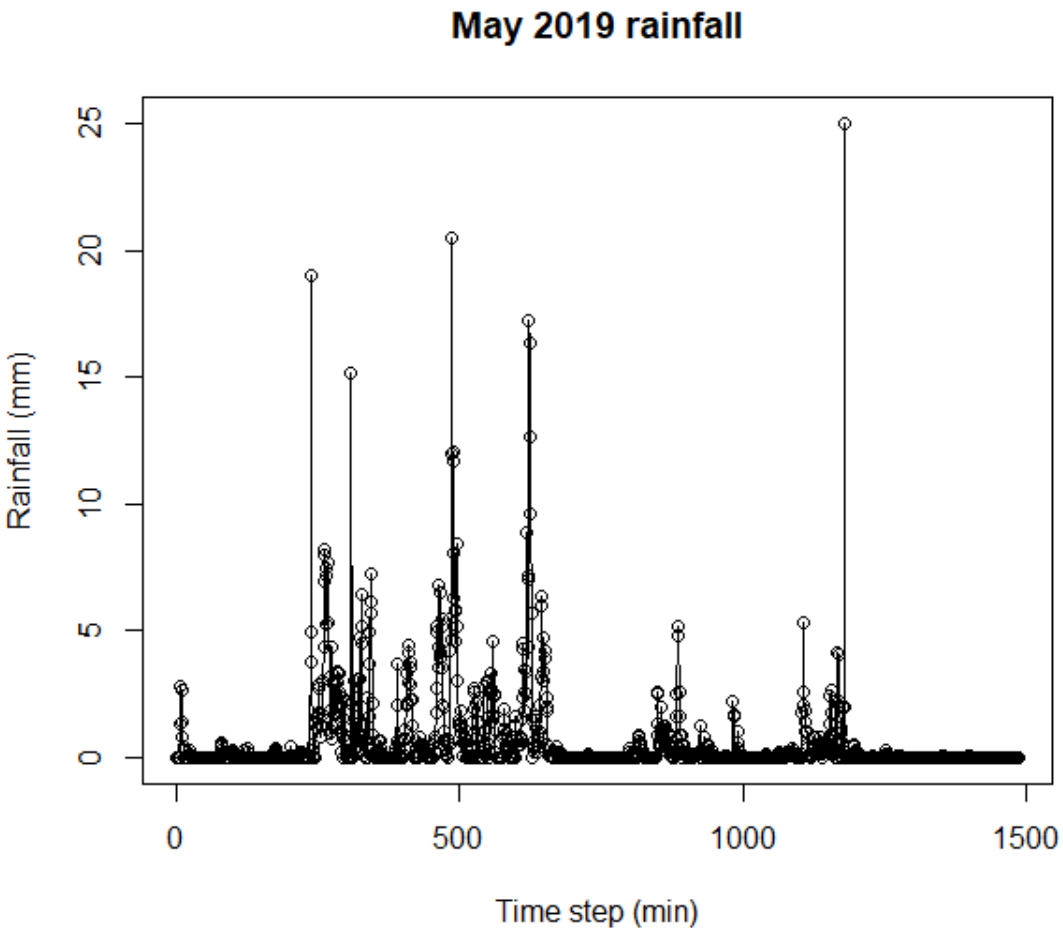

Figure 15:Plot of precipitation in May 2019

The processed direct precipitation was entered in the HEC-RAS hydrological model.

3.6.1.3. Landcover

The landcover map used for this study was downloaded from the RCMRD Geoportal site (http://geoportal.rcmrd.org/), which has open geospatial datasets and maps for Eastern and Southern Africa. The landcover map is of the year 2016, and this map was clipped using the 2D flow area shapefile, before being used in HEC-RAS, the map is shown in figure 16. The legend is the same as the one from the original classified dataset, and the classification codes with their corresponding Manning's number are shown in Table 3.

The manning's values for the study area are based on the tables by Chow (1959) and Syme (2008). The Manning's n values on the various landcover depict how the flow is affected, and these can give the simulation a more realistic depiction of how water flows (Dorn et al., 2014). Kalyanapu, Burian, & McPherson, (2009) state in their paper that the Manning's roughness coefficient is used to represent surface roughness in hydrological models, to show that runoff is connected to the Manning's value.

Further, they stated that when dealing with larger catchments, Landuse/Landcover is used to assign corresponding manning's values.
Therefore, Landuse is included in the hydraulic model to have specific Manning's number for the surface roughness because the flow, infiltration, etc. are affected by this. These values are obtained from standard tables with values corresponding to Landuse/Landcover.

Table 3: Manning's Roughness Coefficient for different Landuse (Chow,1959; Syme,2008)

Value	Landcover	Manning's n
1	Trees cover areas	0.16
2	Shrubs cover areas	0.1
3	Grassland	0.035
4	Cropland	0.035
5	Vegetation aquatic or regularly flooded	0.07
7	Bare areas	0.025
8	Built-up areas	0.15

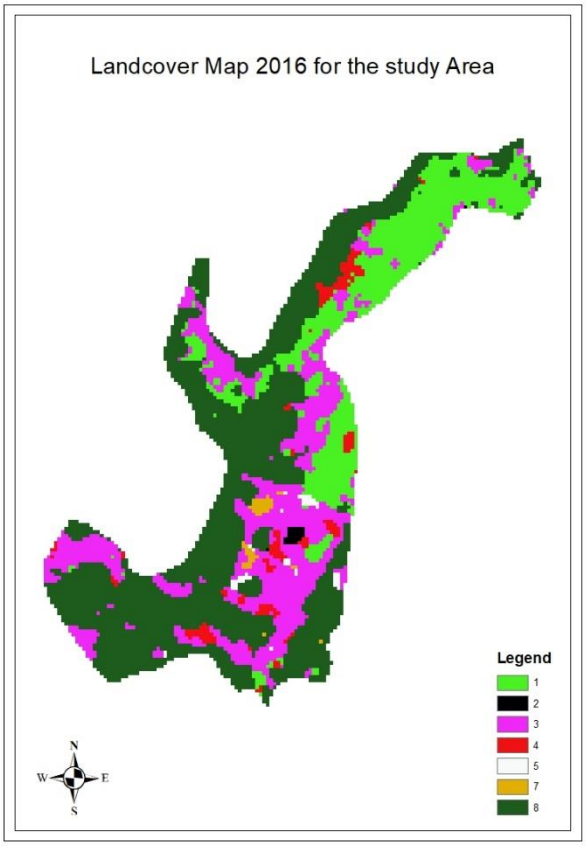

Figure 16:Landcover map 2016 clipped to 2D flow Area

3.6.1.4. DTM

The DTM as an input in both the hydrological and hydraulic models was generated in Lastools, from both LiDAR and DIM data. A total of 61 DTMs were used in the flood simulation, these covering the subsections, effect of optimized parameters, the effect of resolution on flooding, and the effects of different parameters on flooding.

3.6.2. 2D flow Simulation in HEC-RAS 5.0.7

3.6.2.1. Hydrological Modelling

Since the study area has no flow information, this had to be modeled from the precipitation. This involved modeling runoff hydrograph of the precipitation applied to the catchment. In the HEC-RAS manual, it is stated that the Precipitation boundary condition can be directly applied to the hydrological model to any 2D flow area (Brunner, 2016). In this study, the prepared rainfall data used to generate the flow hydrograph. The rain-on-grid model simulation time was for 16 hours, with the starting time 11:00 AM, 9th of June 2023. The hydrograph data was then used as input when conducting the hydraulic analysis.

The rain-on-grid model will have the same components as the ones described in the hydraulic model in the next section. The significant difference is in the placement of the boundary conditions, an internal boundary condition which acts as a breakline is the considerable difference; this is shown in figure 17. This is where the hydrographic data was extracted for the study area.

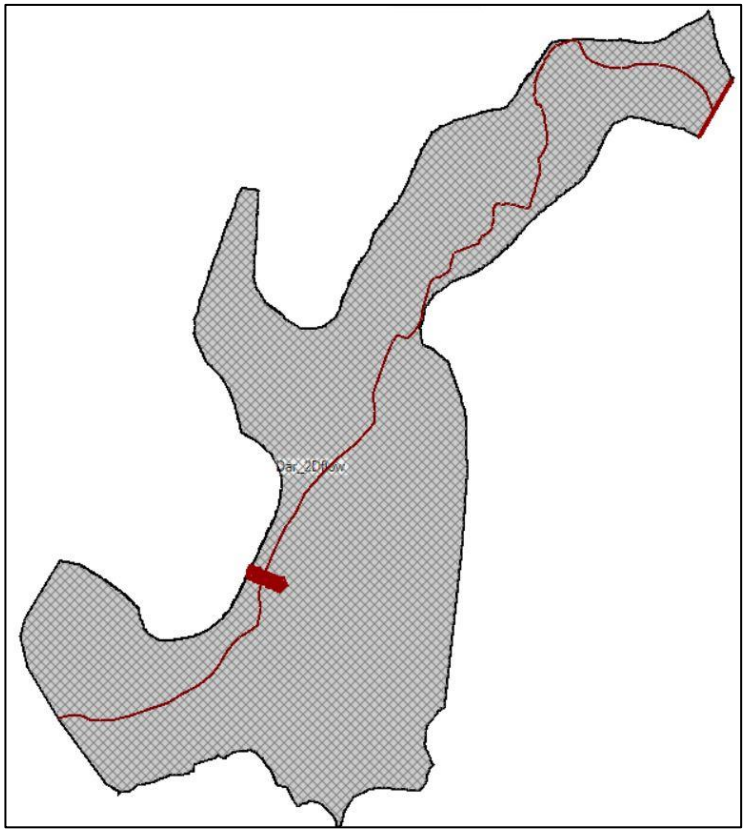

Figure 17: 2D flow mesh with internal and external boundary condition

3.6.2.2. 2D Hydraulic Modelling

For the HEC-RAS model used for the simulation, three input data sets used were DTM, Runoff hydrographs, and Landcover. There are several steps when implementing the 2D flow modeling, and these are highlighted below, and they can also be found in the HEC-RAS River Analysis system user manual (Brunner, 2016). Before creating the geometric data, the projection system for the project had to be set to WGS84 UTM zone 37S; this reference system for the HEC-RAS model was obtained from the spatial reference website (https://spatialreference.org/).

1. **Geometric data**

The geometric data component of HEC-RAS is where the 2D flow area, breaklines, boundary conditions were defined. A grid size of 10 was determined and a mesh computed, also the Msimbazi river centreline was added as a breakline and reinforced, this was used for all the models created. Two boundary conditions are defined in this case; both are external boundary conditions on the upstream and downstream. The near and far grid size for the breakline was put at 20 and 30, respectively. Figure 18 shows the created 2D mesh of the flood area with a breakline and boundary condition.

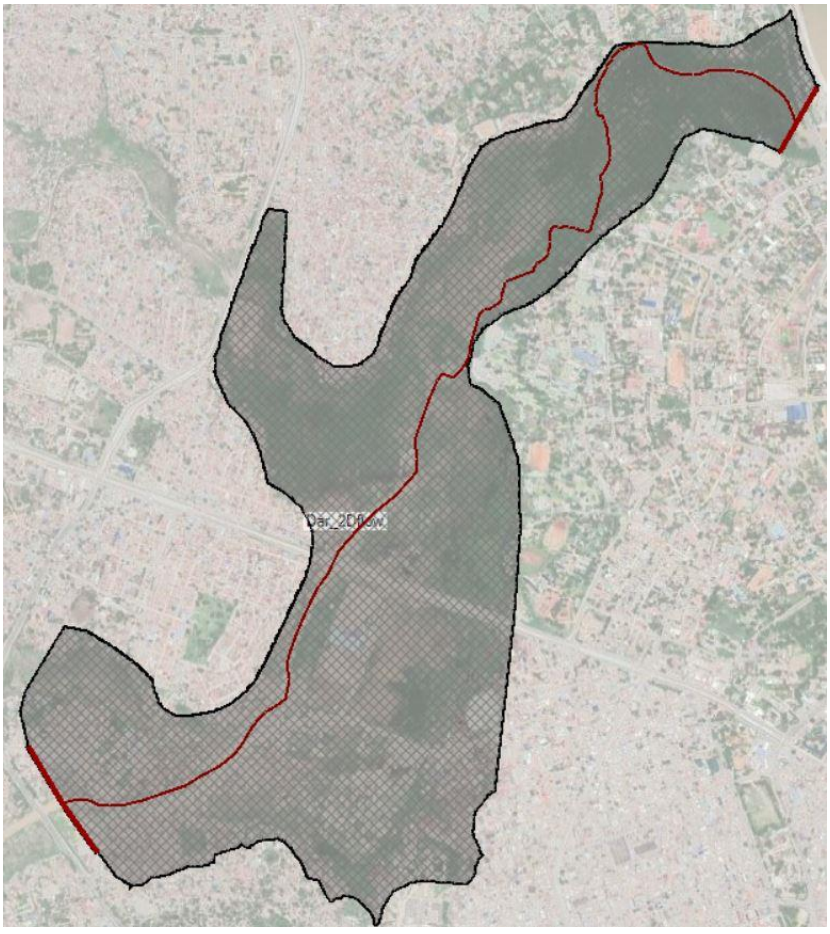

Figure 18:2D flow breakline and external boundary condition for hydraulic model

2. Breaklines

The Msimbazi river centreline was drawn and used as a breakline. As a general rule, any place which either hinders or controls flow should have a breakline added to it, and these breaklines can even be added after the mesh computation by simply enforcing it (Brunner, 2016).

3. Boundary conditions

The boundary condition used for the modeling is the flow hydrograph generated from the hydrological modeling. The flow hydrograph brings flow into the 2D flow area, and this was used at the upstream boundary, while for the downstream boundary condition, normal depth was used, which takes flow out of the 2D flow area (Brunner, 2016). For the unsteady flow hydrograph data, a multiplier of 10000 was used on flow to increase the amount of flooding in the study area. A time date interval of 30 minutes was used because the rainfall data used to generate the flow was of the same time step; this is shown in the figure 19.

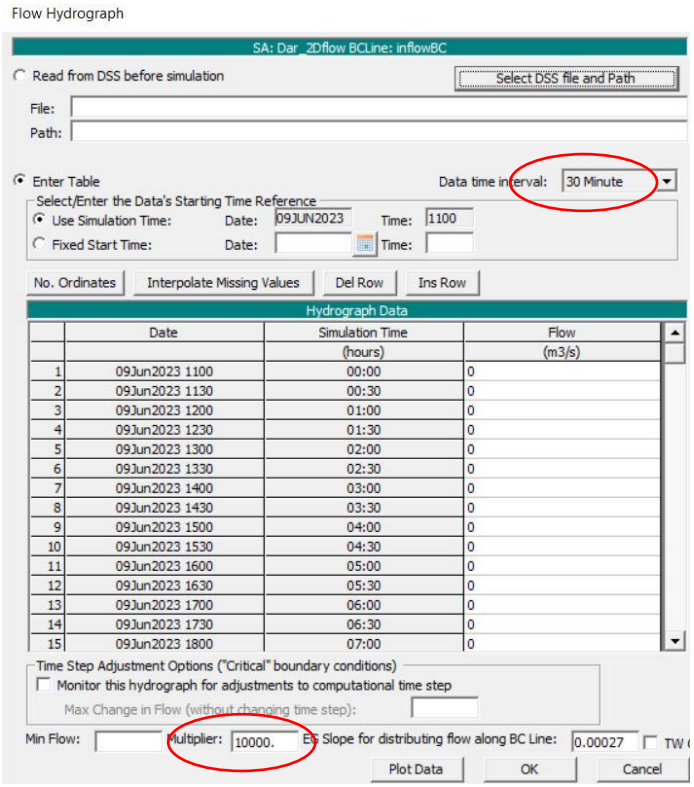

Figure 19: unsteady flow hydrograph

4. Manning's roughness coefficient

To have a spatially varying manning's roughness coefficient for the 2D flow area, a landcover map of 2016 was used for the study area. The landcover must be associated with the Geometry data before the Manning's values can be assigned for each landcover type. The values for the Manning's n were given with reference to the landcover; consequently, landcover was combined with the mesh in the 2D flow area for the computations (Dorn et al., 2014). If this were not done, a single value manning's n would have been assigned to the 2D flow area (Brunner, 2016). The Landuse for creating the varying manning's values is the same as shown in figure 16.

5. Running the Model

The model is run by creating a plan in the unsteady flow analysis. The start and end time of the simulation was entered; in this study, the model simulation time was from 9th June to 11th June 2023 for all the models created. This should correspond to the duration of the hydrograph information in the hydrograph boundary condition. Figure 20 shows the primary inputs of the unsteady flow analysis.

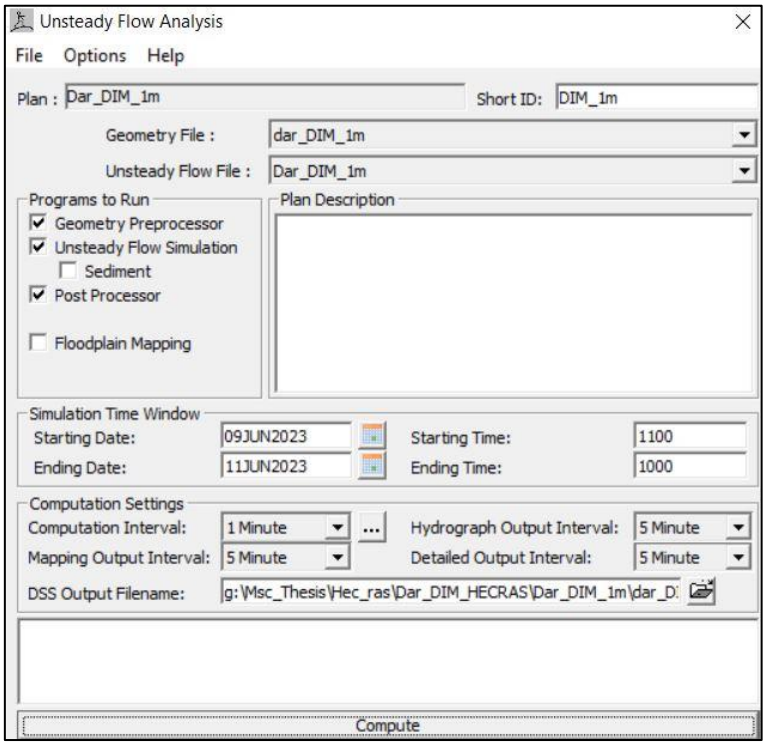

Figure 20:Unsteady flow analysis

3.6.2.3. Flood Mapping

After the unsteady flow computation is complete, RAS Mapper was opened to view the results. Four flood maps were generated, namely flood extent, floodwater depth, flow velocity, and water surface elevation. These maps were exported and further analyzed in ArcGIS so that information could be extracted. These outputs were generated from both LiDAR and DIM data for the various filtering parameter settings. And a comparison of the results was done to investigate the effect of optimized parameters, the effect of resolution on flooding, and the effects of different parameters on flooding. After that, a conclusion was made as to which data set is most appropriate for the Msimbazi river basin.

4. RESULTS AND DISCUSSION

4.1. Filtering parameter optimization LiDAR point cloud

Table 4: Default Parameters for 5 Lastools switches

	Step[m]	Sub	Spike[m]	Bulge[m]	Stddev[cm]	Offset[m]
Town	10	6	1	1	10	0.05
City	25	7	1	2.5	10	0.05
Wilderness	3	4	1	0.6	10	0.05
Metro	50	8	1	5	10	0.05
Nature	5	5	1	1	10	0.05

Note that the default for Lasground is nature

Using the ground points from the various switches as shown in Table 4, lascontrol was then used to check the quality of the TIN generated from the ground points as an indication of the quality of final DTM produced. The produced Hillshaded DTMs were visually inspected, and the results of the lascontrol indicated which switch's default parameters could be the starting point for the optimization. Table 5 shows the lascontrol results of the various switches.

Table 5: RMSE and Standard deviation of switches

Switch	RMSE (m)	Standard deviation (m)
City	0.339	0.313
Metro	0.346	0.323
Nature	0.224	0.195
Town	0.339	0.313
Wilderness	0.291	0.301

From the Table, nature gave a lower RMSE; hence these parameters can further be tuned to investigate how to obtain a DTM whose height is closer to the actual terrain elevation. These, in combination with the step size of 25m from city, is ideal for this study area because it can filter out the big warehouse buildings in the study area. Therefore, using the step of 25 and the other default parameters for nature, the optimization process was carried out, as explained in the next section.

4.1.1. Parameter Tuning LiDAR

To examine the influence of the six parameters in the Lasground algorithm, a visual hillshade view analysis was carried out on the generated surfaces per parameter. Table 6 shows the surfaces generated with their corresponding parameters, and the best representative surface as compared to the orthophoto of the area was chosen. The same area was processed 41 times using different parameter settings for step, spike, bulge, standard deviation, offset, and sub, each combination of these yielding a single surface per run. The effect of the different parameter combinations had to be checked on the DTM surfaces as a whole. The resultant surface is analyzed to check whether it's ideal for flood modeling or not by looking at how the river banks, curbs, embankments, etc. are preserved and also whether non-ground objects like buildings, vegetation, and bridges are filtered.

Table 6: LiDAR Parameter tuning

Parameter	DTM_surface	STEP[m]	SPIKE[m]	BULGE[m]	STDDEV[cm]	OFFSET[m]	SUB
STEP	surface1	50	1	1	10	0.05	5
	surface2	25	1	1	10	0.05	5
	surface3	10	1	1	10	0.05	5
	surface4	5	1	1	10	0.05	5
SPIKE	surface5	25	2.5	1	10	0.05	5
	surface6	25	2	1	10	0.05	5
	surface7	25	1.5	1	10	0.05	5
	surface8	25	1	1	10	0.05	5
	surface9	25	0.5	1	10	0.05	5
	surface10	25	0.25	1	10	0.05	5
	surface11	25	0.1	1	10	0.05	5
	surface12	25	0.05	1	10	0.05	5
	surface13	25	0.01	1	10	0.05	5
BULGE	surface14	25	2	3	10	0.05	5
	surface15	25	2	2.5	10	0.05	5
	surface16	25	2	2	10	0.05	5
	surface17	25	2	1.5	10	0.05	5
	surface18	25	2	1	10	0.05	5
	surface19	25	2	0.5	10	0.05	5
	surface20	25	2	0.25	10	0.05	5
	surface21	25	2	0.1	10	0.05	5
STDDEV	surface22	25	2	1.5	10	0.05	5
	surface23	25	2	1.5	6	0.05	5
	surface24	25	2	1.5	3	0.05	5
	surface25	25	2	1.5	1	0.05	5
	surface26	25	2	1.5	0.5	0.05	5
	surface27	25	2	1.5	0.2	0.05	5
	surface28	25	2	1.5	no_stddev	0.05	5
OFFSET	surface29	25	2	1.5	1	0.01	5
	surface30	25	2	1.5	1	0.02	5
	surface31	25	2	1.5	1	0.05	5
	surface32	25	2	1.5	1	0.1	5
	surface33	25	2	1.5	1	0.2	5
	surface34	25	2	1.5	1	0.5	5
	surface35	25	2	1.5	1	1	5
SUB	surface36	25	2	1.5	1	0.1	3
	surface37	25	2	1.5	1	0.1	4
	surface38	25	2	1.5	1	0.1	5
	surface39	25	2	1.5	1	0.1	6
	surface40	25	2	1.5	1	0.1	7
	surface41	25	2	1.5	1	0.1	8

The Sub parameter comprises the switches extra coarse, coarse, fine, extra-fine, and ultrafine, and it is for the initial search for the ground. Figures 21 and 22 show some output from the step and standard deviation analysis.

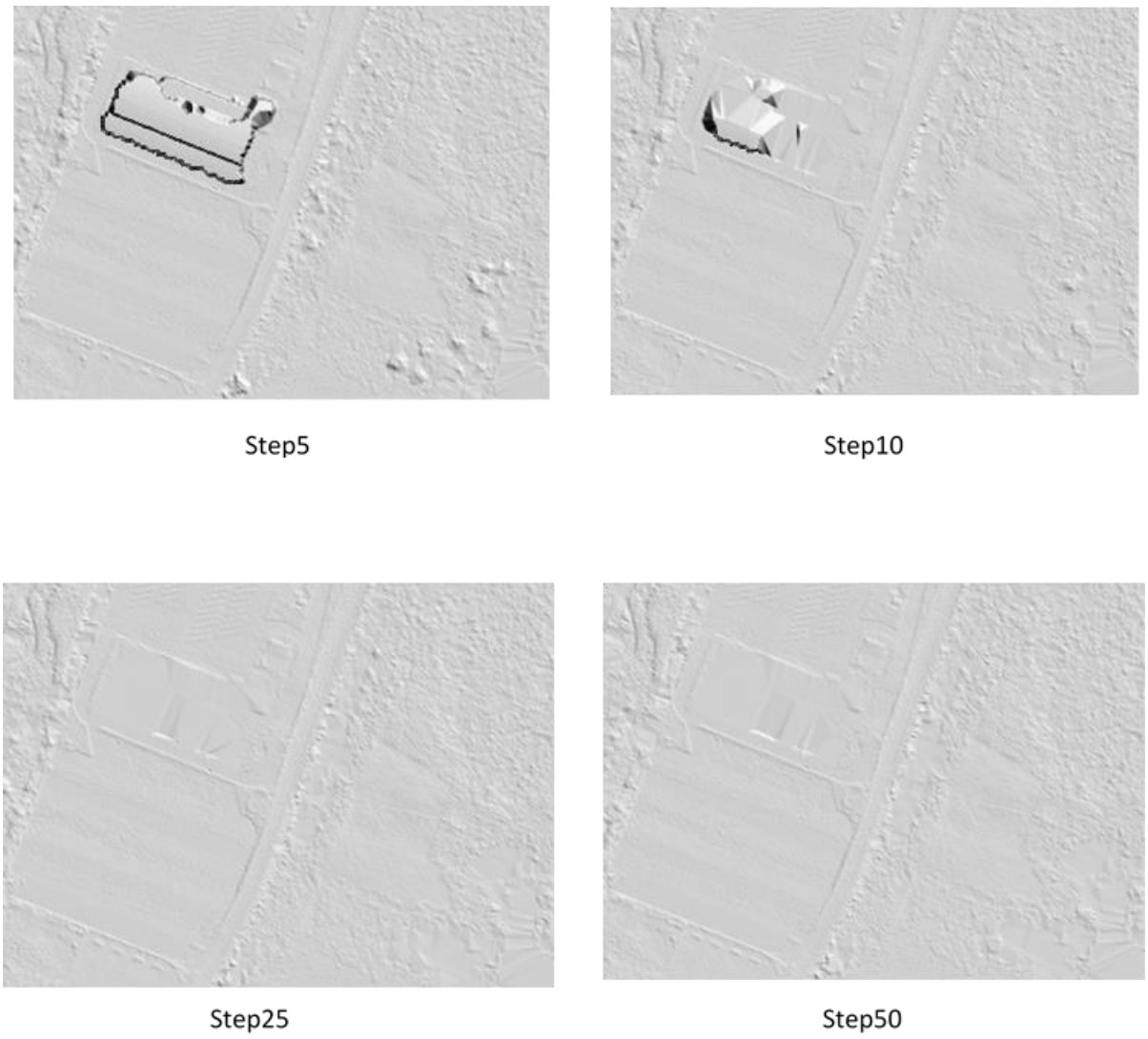

Figure 21:LiDAR Step parameter optimization

The step size of 25 was the one that gave a better outcome because it was able to filter out the big buildings in the study area. The step of 50 gave a distorted surface in some areas, so this was not chosen. As earlier indicated, the whole area must be looked at when investigating the effect of a parameter.

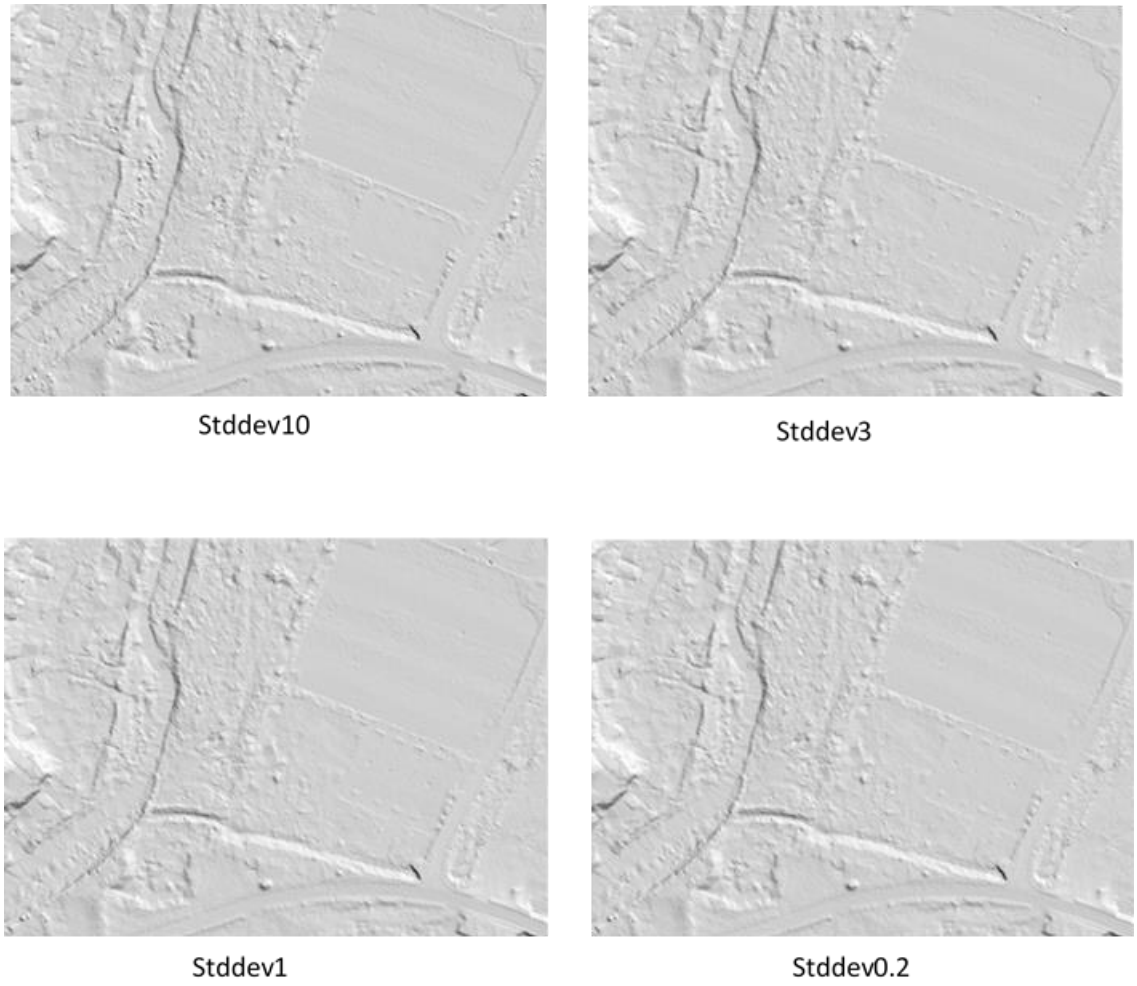

Figure 22: Standard deviation parameter optimization

The effect of the standard deviation is such that it removes objects that are close to the ground but are still not part of the ground. Hence, in this case, a smaller standard deviation gave a good result. The optimised parameters for the LiDAR data set were found to be: Step : 25, Spike: 2, Bulge: 1.5,Stddev: 1, Offset: 0.1, Sub: 5. The sub of 5 was chosen because the study area is a flood plain, so it is relatively flat.

4.1.2. Display of LiDAR ground classified point cloud in Fugroviewer

Figure 23 shows the classified ground points in purple and the non-ground in green of a river cross-section indicated by the grey line. The profile depicts the separation of ground and non-ground points.

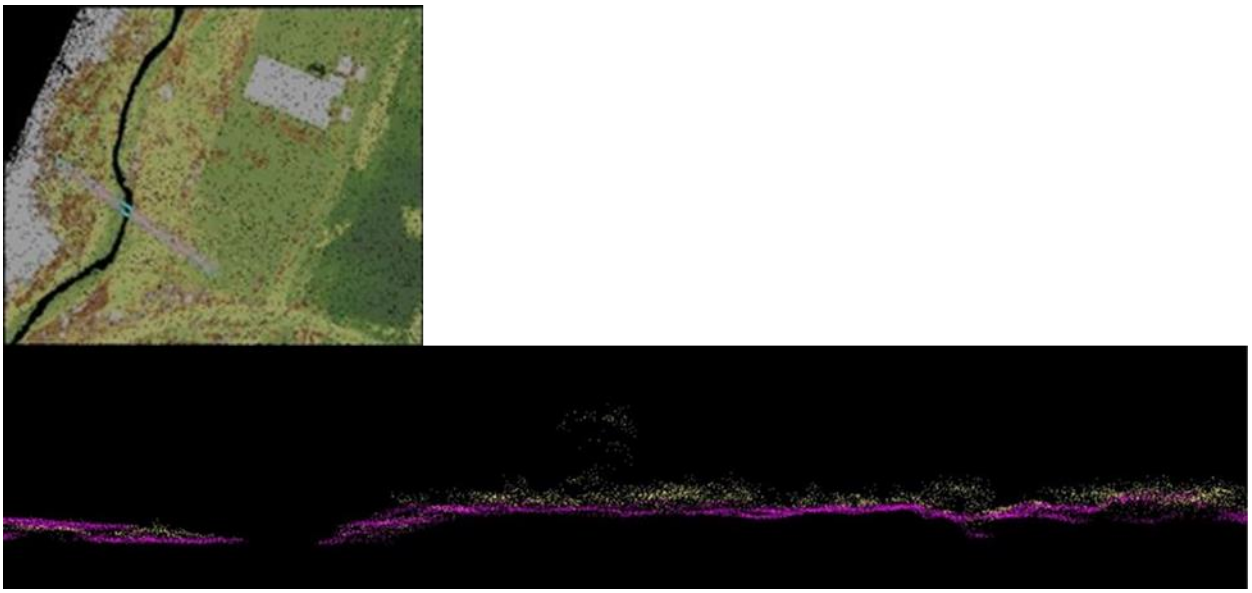

Figure 23: Cross-section profile ground and non-ground classified points

4.2. Filtering parameter optimization DIM point cloud

4.2.1. Parameter Tuning of DIM point cloud

The parameter tuning for the DIM point cloud was done the same way the LiDAR was, as described in section 4.1.1. also, in this case, a total of 41 surfaces corresponding to different parameter settings were generated. The modified batch script for the processing is found in appendix B. Table 7 shows the surfaces generated with their corresponding parameters. The optimised parameters for the DIM data set were found to be: Step: 25, Spike: 2.5, Bulge: 1.5, Stddev: 10, Offset: 0.1, Sub: 5.

The visual representation of the bulge and standard deviation parameter surfaces are shown in figures 24 and 25.

Table 7: DIM Parameter tuning

Parameter	DTM_surface	STEP[m]	SPIKE[m]	BULGE[m]	STDDEV[cm	OFFSET[m	SUB
STEP	surface1	50	1	1	10	0.05	5
	surface2	25	1	1	10	0.05	5
	surface3	10	1	1	10	0.05	5
	surface4	5	1	1	10	0.05	5
SPIKE	surface5	25	2.5	1	10	0.05	5
	surface6	25	2	1	10	0.05	5
	surface7	25	1.5	1	10	0.05	5
	surface8	25	1	1	10	0.05	5
	surface9	25	0.5	1	10	0.05	5
	surface10	25	0.25	1	10	0.05	5
	surface11	25	0.1	1	10	0.05	5
	surface12	25	0.05	1	10	0.05	5
	surface13	25	0.01	1	10	0.05	5
BULGE	surface14	25	2.5	3	10	0.05	5
	surface15	25	2.5	2.5	10	0.05	5
	surface16	25	2.5	2	10	0.05	5
	surface17	25	2.5	1.5	10	0.05	5
	surface18	25	2.5	1	10	0.05	5
	surface19	25	2.5	0.5	10	0.05	5
	surface20	25	2.5	0.25	10	0.05	5
	surface21	25	2.5	0.1	10	0.05	5
STDDEV	surface22	25	2.5	1.5	10	0.05	5
	surface23	25	2.5	1.5	6	0.05	5
	surface24	25	2.5	1.5	3	0.05	5
	surface25	25	2.5	1.5	1	0.05	5
	surface26	25	2.5	1.5	0.5	0.05	5
	surface27	25	2.5	1.5	0.2	0.05	5
	surface28	25	2.5	1.5	no_stddev	0.05	5
OFFSET	surface29	25	2.5	1.5	10	0.01	5
	surface30	25	2.5	1.5	10	0.02	5
	surface31	25	2.5	1.5	10	0.05	5
	surface32	25	2.5	1.5	10	0.1	5
	surface33	25	2.5	1.5	10	0.2	5
	surface34	25	2.5	1.5	10	0.5	5
	surface35	25	2.5	1.5	10	1	5
SUB	surface36	25	2.5	1.5	10	0.1	3
	surface37	25	2.5	1.5	10	0.1	4
	surface38	25	2.5	1.5	10	0.1	5
	surface39	25	2.5	1.5	10	0.1	6
	surface40	25	2.5	1.5	10	0.1	7
	surface41	25	2.5	1.5	10	0.1	8

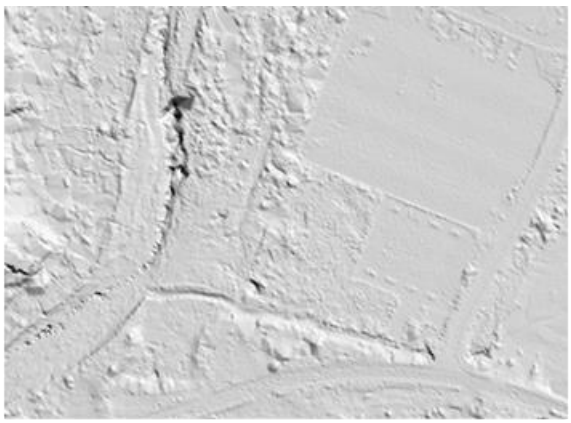

Bulge 2.5

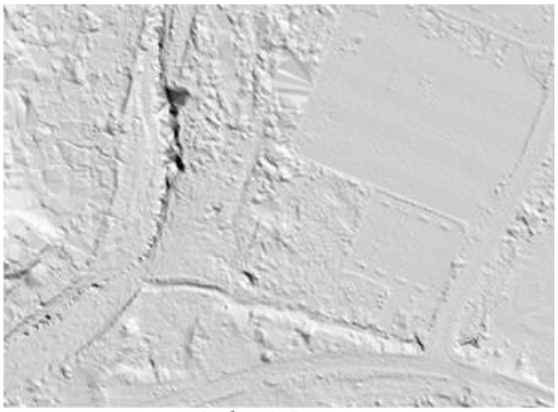

Bulge1.5

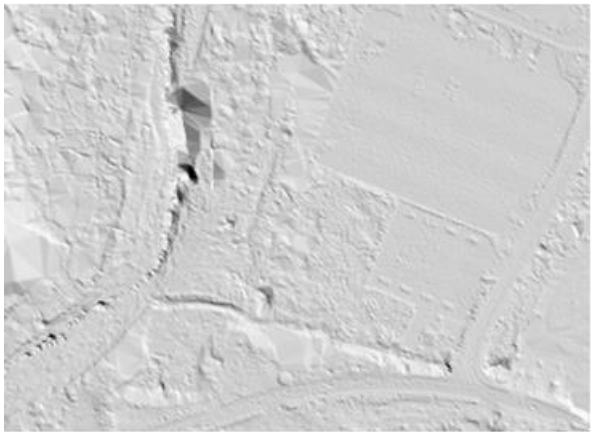

Bulge0.5

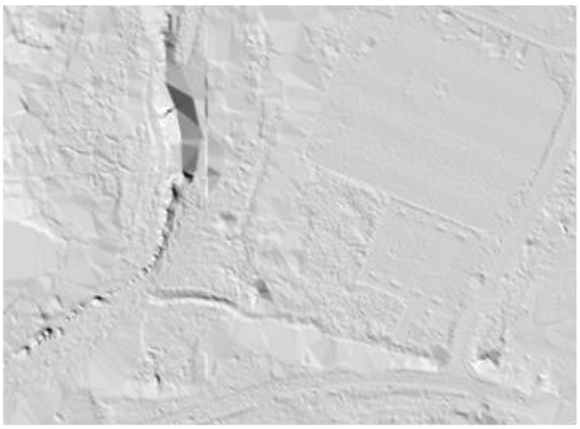

Bulge0.25

Figure 24: DIM bulge parameter optimization

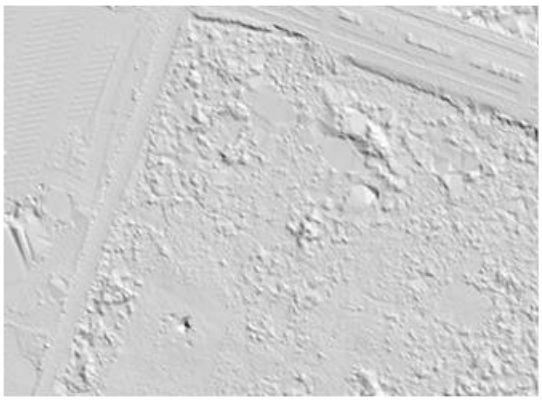

Stddev10

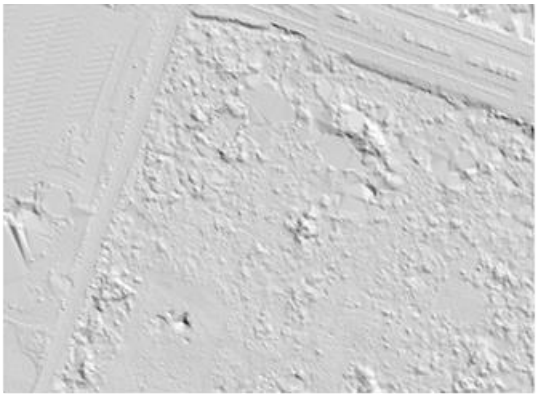

Stddev6

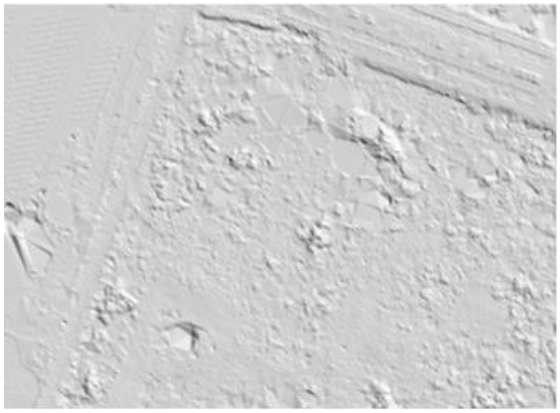

Stddev1

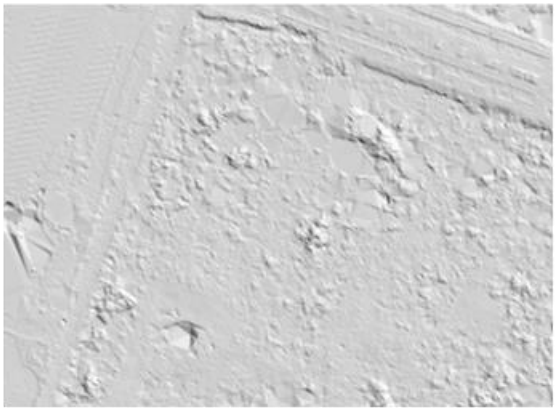

no stddev

Figure 25:DIM standard deviation parameter optimization

4.2.2. Filtering Quality check

To check the quality of the filtering, four (4) areas were identified, namely built-up, forest, pavement, and high vegetation. Two of the areas are where the researcher thinks the filtering worked well, and the other two are where it is suspected that the filtering did not work well. Only ground points were considered for this analysis. Figure 26 shows the selected areas for quality checking of the filtering.

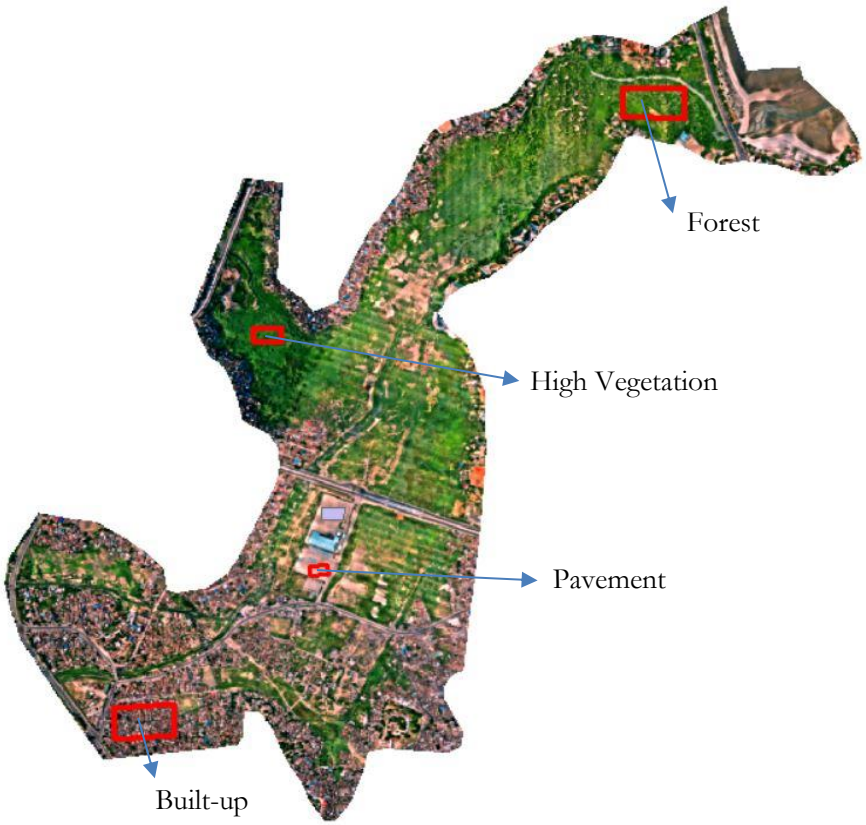

Figure 26: Areas for checking quality of filtering

CloudCompare, together with the lasview tool, was used to inspect the filtered point cloud in these four regions visually. The LiDAR point cloud, according to the analysis, showed the filtering worked well. However, the DIM point cloud though most of the buildings were removed, showed some misclassification as some roofs were classified as part of the ground. Overall, the filtering in this region is satisfactory, and the datasets performed as expected, this can be seen in figure 27(a). The forest area is where the filtering did not work well as there are a lot of huge mismatches between the LiDAR ground and the DIM ground. The LiDAR could not capture a lot of ground points in this region because the tree canopy was too dense for it also. The DIM for lack of penetration through the tree canopy was only able to capture the top of the trees. Interpolating in these areas to create a DTM creates a lot of spikes. This complicated landscape comprising a hill and some thick forest was too complicated for the algorithm when dealing with DIM data. This is seen in figure 27(b).

The concrete pavement was one area where it was expected that the filtering would work well, and figure 27(c) shows that the LiDAR and DIM data were filtered well. This was expected as this concrete surface is relatively flat and free from obstructions. Finally, the high vegetation cover area brings out a fascinating scenario as the pattern of the DIM ground points was a bit uneven, showing that there might be some

vegetation cover in the area. This might have caused the filtering of DIM data not to work well. This is seen in figure 27(d).

(a) Built-up: blue LiDAR ground points ,RGB DIM point

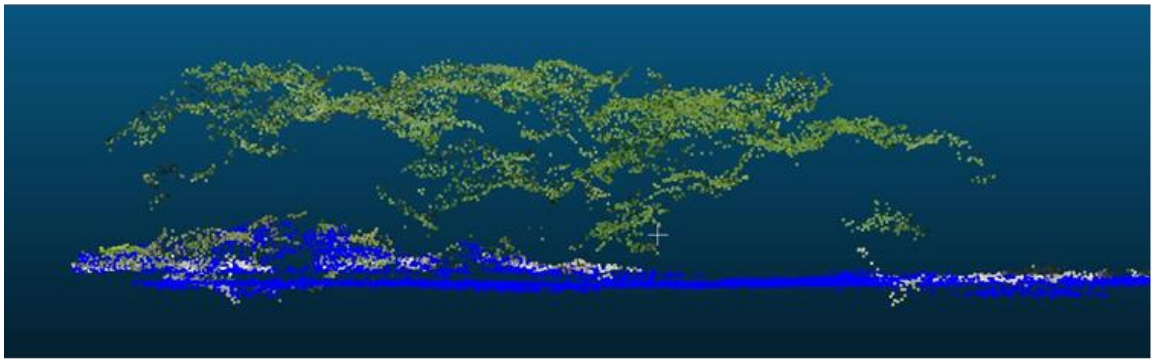

(b) Forest: blue LiDAR ground points ,RGB DIM ground points

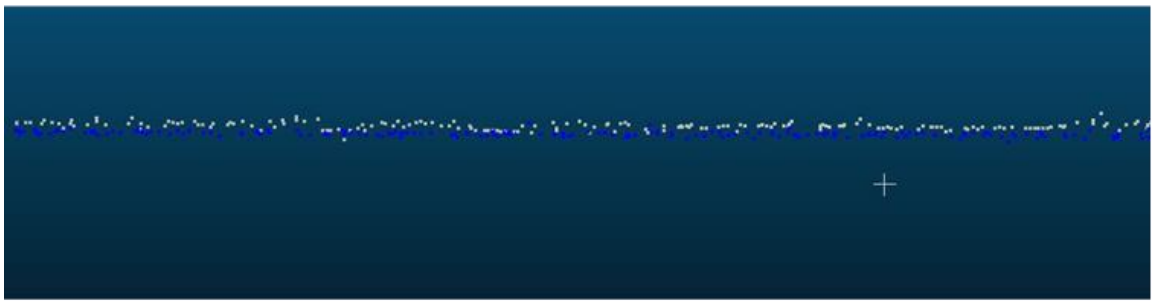

(c) concrete pavement: blue LiDAR ground points ,RGB DIM ground points

(d) high vegetation cover: blue LiDAR ground points ,RGB DIM

Figure 27: Profile sections of check areas for filtering quality check

4.3. Point cloud and DTM accuracy assessment

4.3.1. LiDAR Noise analysis in CloudCompare

This section reports on the noise analysis of 10 surfaces,5 LiDAR and 5 DIM, as derived from tuning the offset parameter in Tables 6 and 7. For these surfaces, all other parameters were kept constant except for the offset. The Root Mean Square (RMS) values obtained in this analysis are shown in Table 8, which shows how the parameter optimization affects the internal accuracy of the point cloud.

Table 8: RMS for offset parameter of LiDAR and DIM surfaces

DTM surface	LiDAR RMS (m)	DIM RMS (m)
surface29	0.086	0.093
surface30	0.086	0.093
surface31	0.090	0.093
surface32	0.097	0.093
surface33	0.103	0.093

From the analysis, it can be deduced that LiDAR surface29 and surface30 gave a small value,0.086m for the RMS, this according to the CloudCompare is the quadratic mean between the plane and point cloud. This error could also include noise in the point cloud. The values for the LiDAR increased as the value of the offset was being increased. For the DIM, it showed a minor change of an increase between the first and second surfaces, and then it was constant for the last three surfaces, but these were only observable to the 5th decimal place. At mm accuracy (3 decimals), this minor change is not noticeable. The reason for the LiDAR behaving like that might be that as the value of the offset increases, points with height variations and noise get added to the ground points, and eventually, the RMS tends to increase also.

The results from CloudCompare for surface29 for LiDAR and DIM are shown in figure 28.

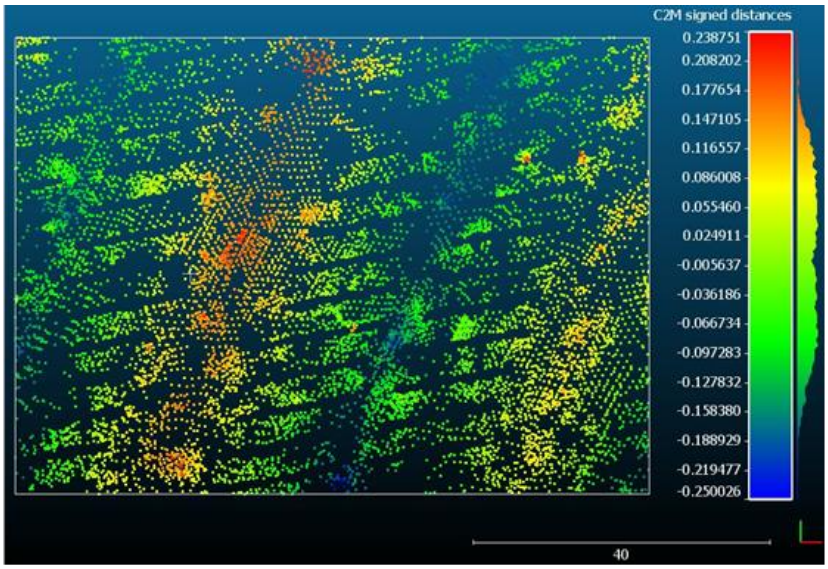

LiDAR surface

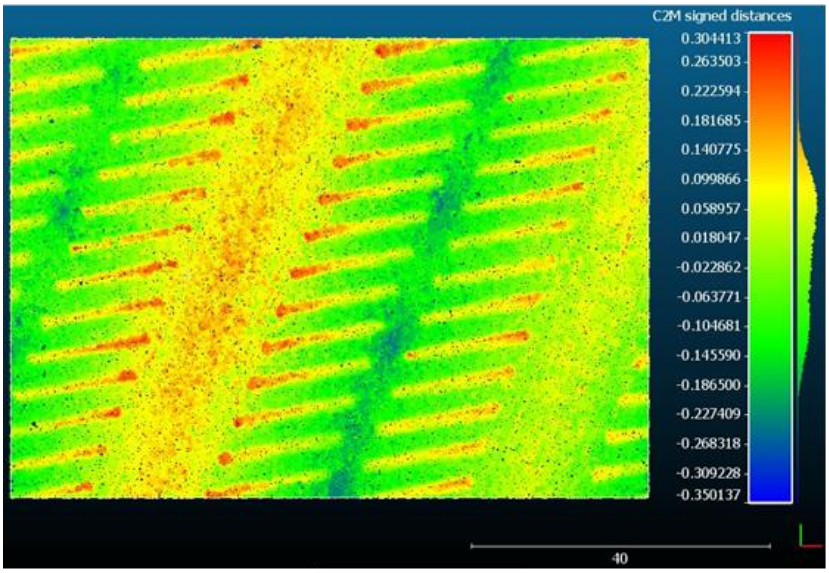

Figure 28: CloudCompare internal assessment of surfaces

4.3.2. Cloud to Mesh accuracy assessment

Figure 29 shows the test sites, namely test area 1 and test area 2, which are vegetated and built-up, respectively. The LiDAR point cloud was taken as the reference, so a mesh was created on the point clouds and then compared to the DIM to investigate the distances. The results from this analysis show that most of the differences between UAV LiDAR and DIM point clouds are found where there is some considerable vegetation. Generally, the performance of the two data sets in relatively flat terrain is almost the same, the green colour depicts this, the blue is for the DIM, and the red represents the high values of the LiDAR, this is seen in figure 30.

Table 9 shows the behavior as the bulge parameter is being tuned in the test sites. The mean distances for the two sites was different as it showed that in test site 1 it reduces by values 0.058m and 0.044m before increasing by 0.009m at bulge parameter 0.25m. The behavior in test site 2 shows that the pattern is different as it showed an increase of 0.009m, then reductions of 0.037m and 0.036m. Overall the behavior

of the mean values and standard deviation is such that they are lower in the built-up area than the vegetated one because of the differences caused by the filtering.

Figure 29:Orthophoto of subset

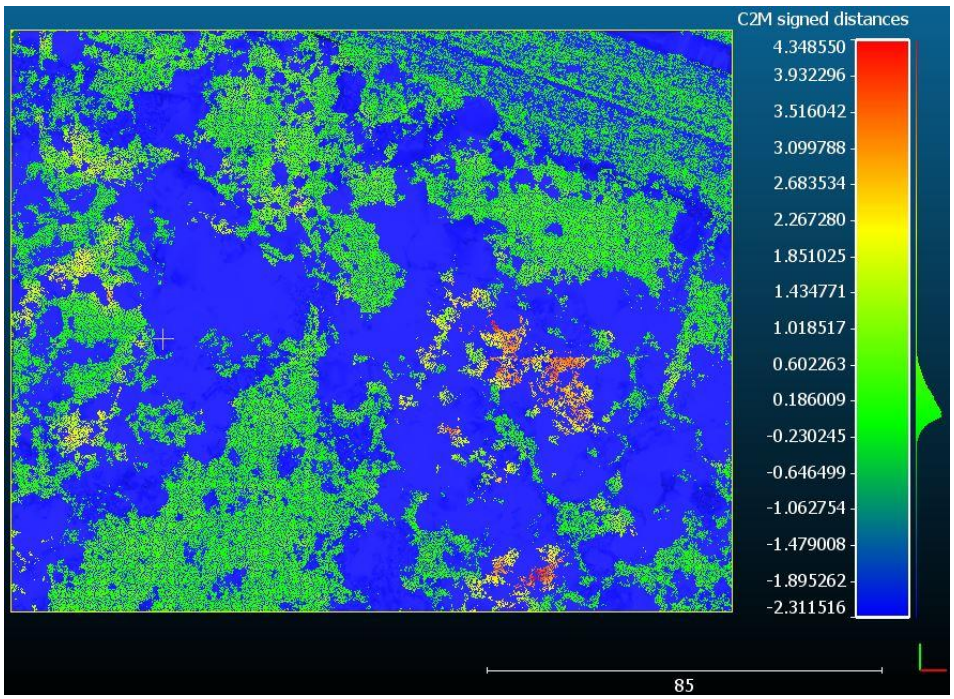

Figure 30: cloud to Mesh distance

Table 9: Mean distance and standard deviation for bulge parameter C2M analysis

Parameter	Section	Mean Distance (m)	Standard deviation (m)
Bulge	Test Area 1 surface15	0.253	0.453
	Test area 1 surface18	0.195	0.333
	Test Area 1 surface19	0.151	0.221
	Test Area 1 surface21	0.160	0.193
Bulge	Test area 2 surface15	0.142	0.404
	Test area 2 surface18	0.151	0.295
	Test area 2 surface19	0.114	0.161
	Test area 2 surface21	0.078	0.144

4.3.3. Cross-section accuracy assessment

This section analyses the nature of the terrain of LiDAR and DIM by looking at their cross sections in four landcover classes; built-up, vegetated, bare/open-grassland, and man-made/pavement. These cross-sections are shown in figures 31 to 34.

4.3.3.1. Built-up area

The built-up profile of the LiDAR and DIM has some similarities in their patterns. This shows that though they are obtained by different systems, the similarity of the pattern indicates that either of them can be used in this type of environment. However, this is dependent on how large the area is, the cost budget, and several other factors. Figure 31 shows the differences between the two DTMs.

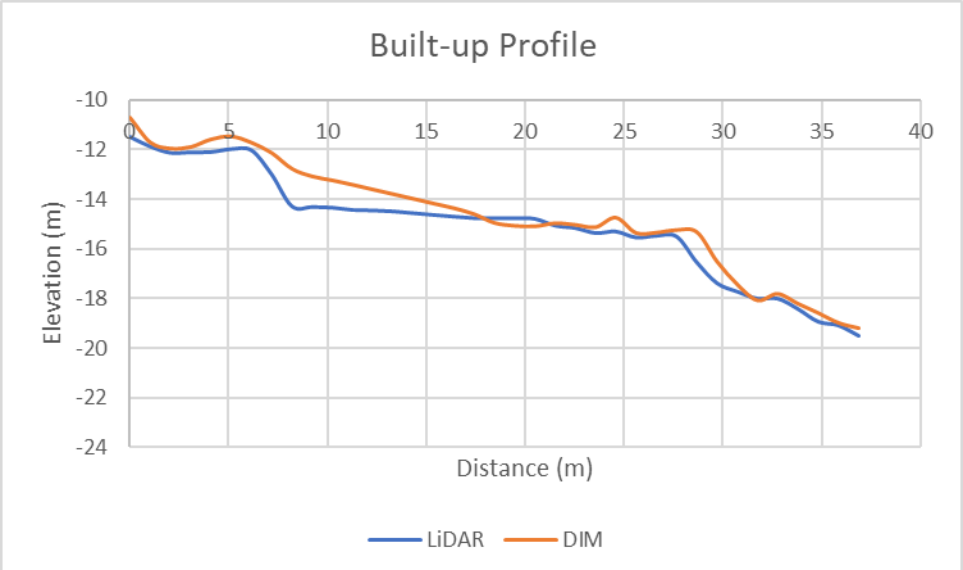

Figure 31: Built-up profile

4.3.3.2. Vegetated

The pattern in the vegetated area produced profiles that were very different from each other, as can be seen in figure 32. The DIM surface had a lot of points below or above the LiDAR. This is because DIM data performs poorly in areas of high vegetation hence the significant differences between the two DTMs. Also, the differences in profiles can be attributed to the dates of acquisition, and one was taken when the vegetation was less (September) and the other when the vegetation was grown (March).

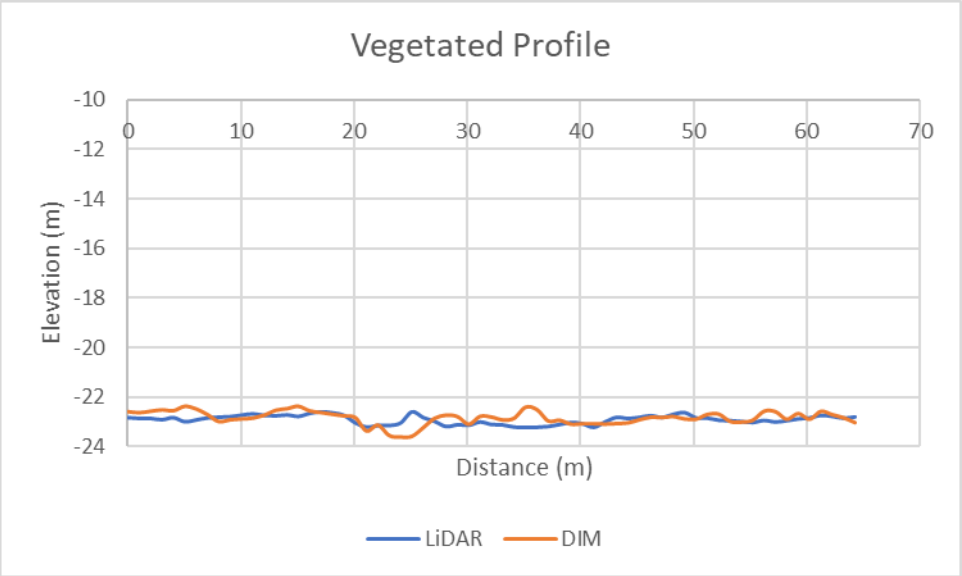

Figure 32: Vegetated profile

4.3.3.3. Bare/open grassland

This area, like the vegetated one, produced profile patterns that are very different from each other, see figure 33. This was unlike what was expected because, in such areas, the LiDAR and DIM data should produce similar patterns. This might have been due to some shrubs which formed some sort of closed-canopy, thereby preventing DIM ground capture.

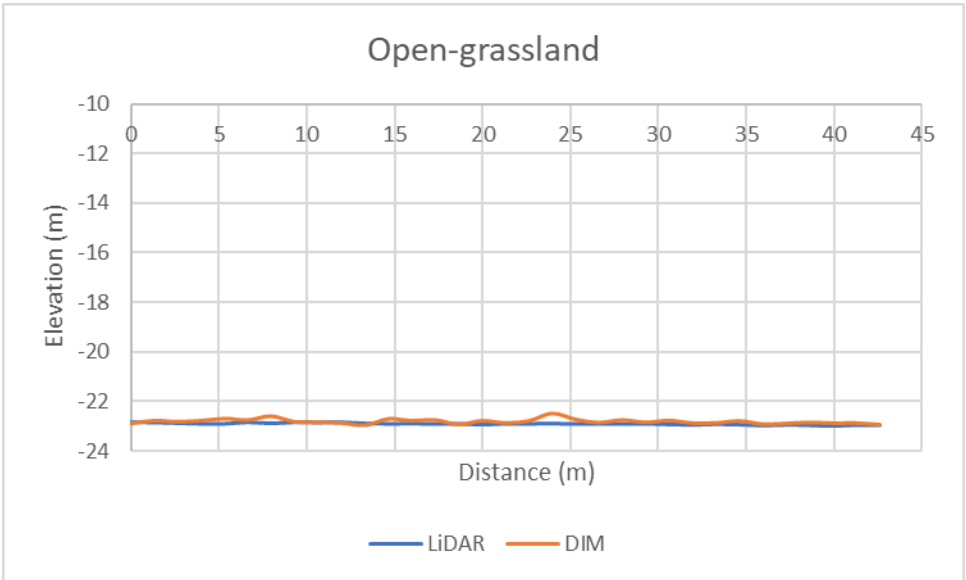

Figure 33: Bare/open grassland

4.3.3.4. Man-made concrete pavement

The surfaces obtained on the concrete pavement produced profile patterns that have similarities. This indicates that either LiDAR or DIM data can be used in regions with these same characteristics as this region. How the two surfaces compare to each other are shown in figure 34.

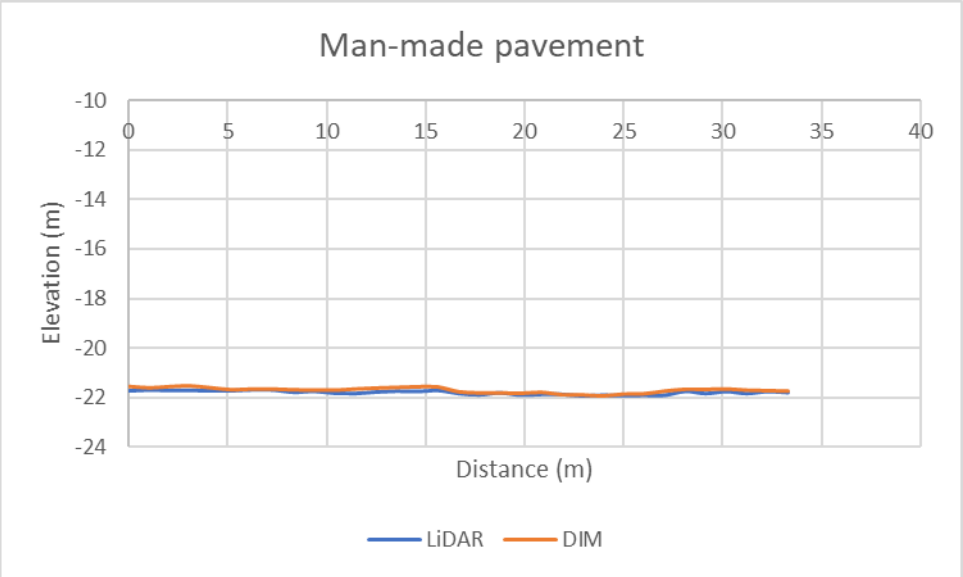

Figure 34:Man-made profile

4.3.4. DEM of difference

The LiDAR DTM was taken as the reference, so the Z value of the DIM DTM was subtracted from the LiDAR pixel by pixel. This yielded a surface that shows the differences between the two. This difference map displays the areas where the LiDAR and DIM data differ, and where there is little or no difference, as shown in figure 35. The areas where there is no difference indicate that either LiDAR or DIM data could be used in those areas. The areas where the significant differences suggest that only LiDAR can give the best results there because ground surface points are not easily captured by the Photogrammetric method. In this case, the areas with Red and green on the difference map are the ones where the LiDAR performs better than the DIM.

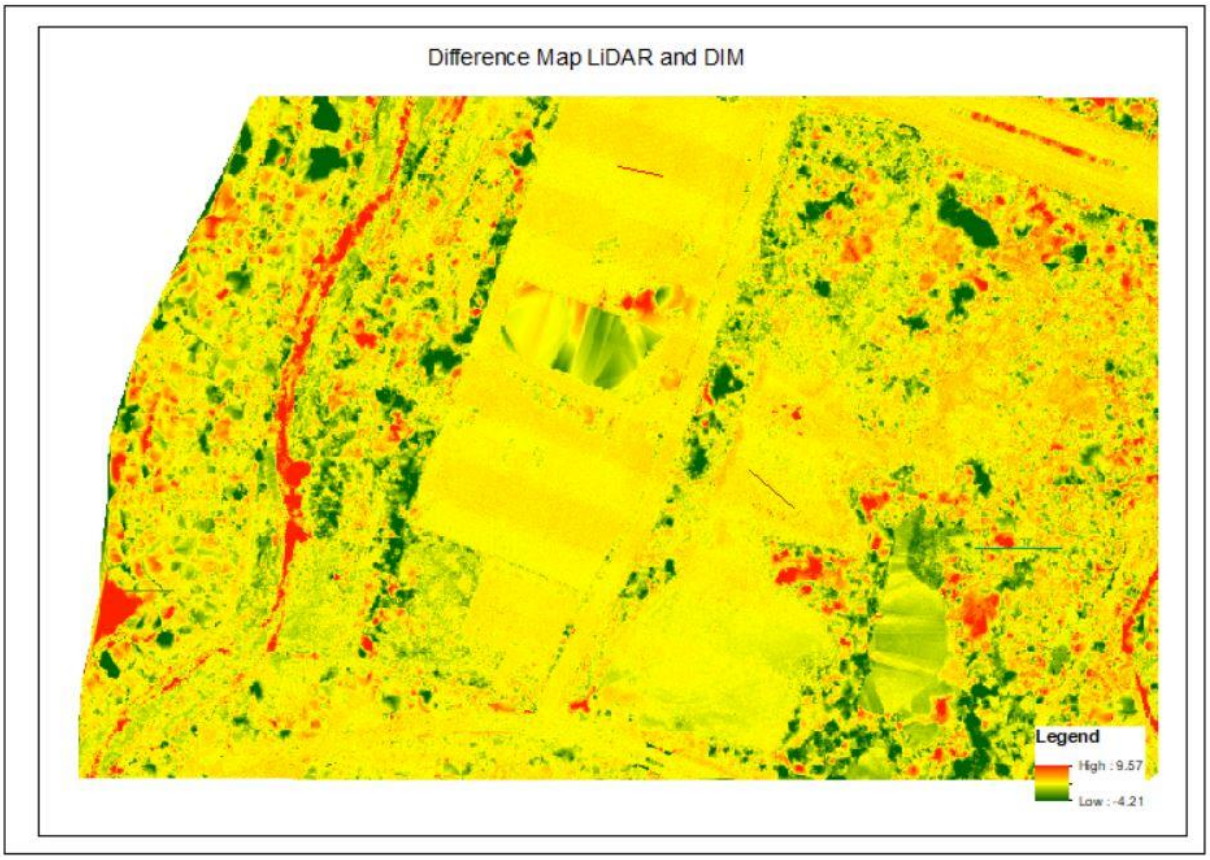

Figure 35:LiDAR and DIM DEM of Difference subset

4.3.5. DTM comparison using correlation coefficient

Correlation is a technique for investigating the linear relationship between two quantitative, continuous variables. Pearson's correlation(r) is a measure of the strength of the association between the two variables (Boslaugh, 2012). From Table 10, it can be seen that built-up and man-made areas gave quite high correlation coefficient values, which means that in these areas, both the performance of LiDAR and DIM are quite similar. Therefore, either of them can be used to conduct further analysis. The y-intercept in the linear regression denotes a level of bias; built-up has a value of -0.415m, which means that when the LiDAR data does not have a value in Z, the DIM will have a value of -0.415. The vegetated area gave a very high value; this means the bias is vast, in this area, the DIM performs very poorly.

The vegetated area gave the least value, which in this case makes sense because due to the vegetation cover in this area, LiDAR always outperforms DIM data because of its ability to penetrate through vegetation. The bare region was expected to yield a relatively high correlation, but the analysis yielded a lower one. This might be due to the presence of some low shrubs in the focus area. Gerard, Prospection, & Wiley (1999) used the correlation coefficient to compare how the heights in two DEMs compare to each other. Similarly, an evaluation of open-source DEM and LiDAR using the correlation coefficient was used by (Khalid et al., 2016). Therefore, the correlation coefficient is an excellent way to evaluate the differences between the two DTMs.

Table 10: LiDAR and DIM Correlation coefficient

	No. of sampled points	Correlation Coefficient (r)	Y-intercept
Bare	195	0.354	-10.054
Built-up	200	0.986	0.237
Man-made	200	0.764	-4.918
Vegetated	200	0.072	-17.799

4.4. DTM filtering Quality check through Flood simulation

4.4.1. Effect of optimized filtering parameters on flooding

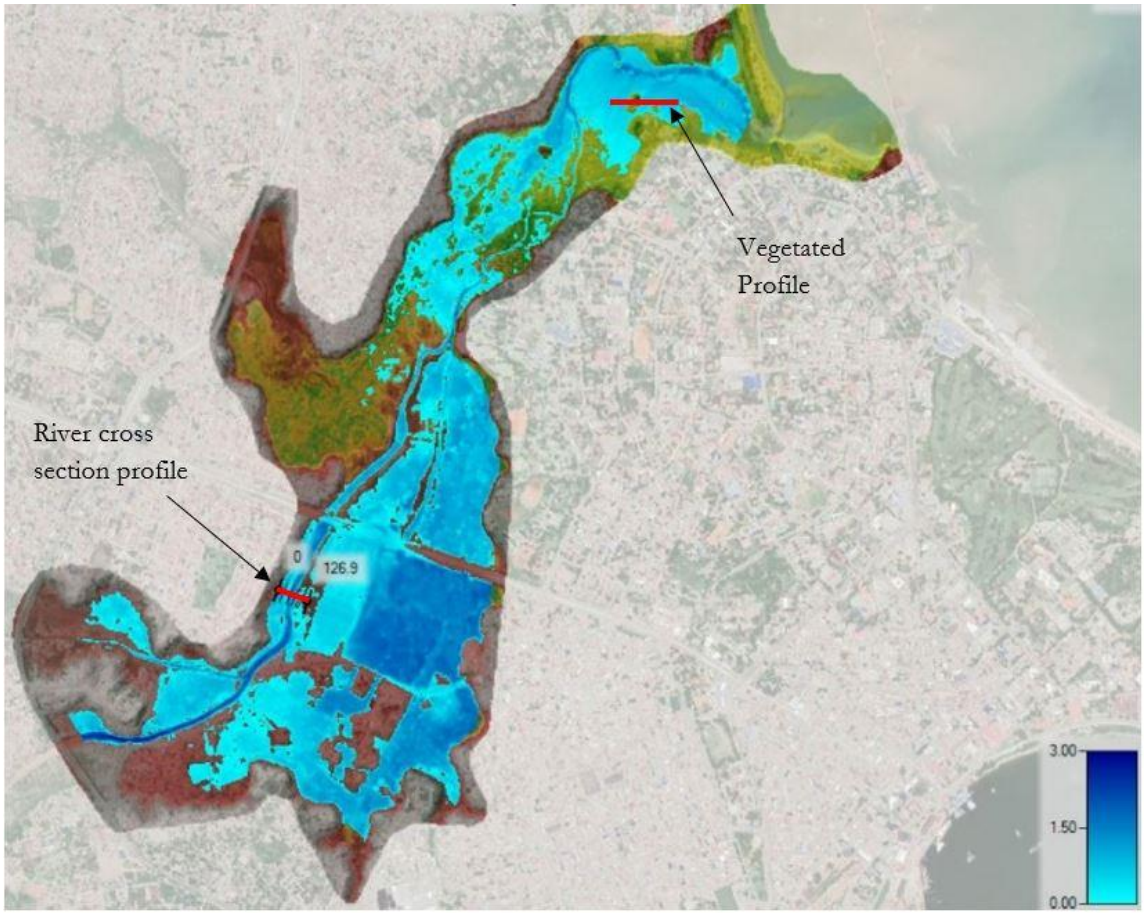

Figure 36: LiDAR flood extent with river and vegetated cross section

Figure 36 shows the flooding extents of the study area, using the optimized filtering parameters for LIDAR and DIM at DTM resolution of 1m. The flooding extent areas for the comparison shows that the LiDAR filtering parameters DTM shows more flooding than for the DIM DTM, as indicated in Table 11. In an area like the Msimbazi river basin characteristic of vegetation cover, which prevents photogrammetry from seeing some ground points, this is expected because, in this case, only the canopy cover is captured, not the ground. This inability of DIM data to contain ground points in these regions of high vegetation has a considerable impact on the DTM created. The produced DTM can have areas that

can block or divert flooding because the objects above the ground were not filtered well (Abdullah, 2012). These differences are further highlighted by the depth, velocity, and water surface elevation (WSE) in Table 11.

From Table 11, the maximum depth for the LiDAR is 1.977m, and that of DIM is 2.608m. These values were extracted from the river cross-section profile, which has a total length of 126.871m. This difference might be caused by the ground filtering around the region of the profile under investigation. The velocity along this profile line shows that the DIM surface has a higher one than the LiDAR; they have 0.186m/s, and 0.148m/s mean velocity, respectively. This might be caused by the DIM surface showing a lot of variation of slopes than the LiDAR. Figure 37 compares the WSE between the LiDAR and DIM profiles, which verifies that there is more flooding on the LiDAR surface than DIM because most of the terrain is inundated.

Table 11: Velocity, Depth, WSE and Inundation Area

		Velocity(m/s)	Depth(m)	WSE (m)	Inundated Area (Ha)
LiDAR	Max	0.000	0.000	-20.674	
	Min	0.261	1.977	-20.121	
	Mean	0.148	0.575	-20.491	162.423
DIM	Max	0.000	0.000	-20.477	
	Min	0.590	2.608	-19.243	
	Mean	0.186	0.562	-20.237	142.265

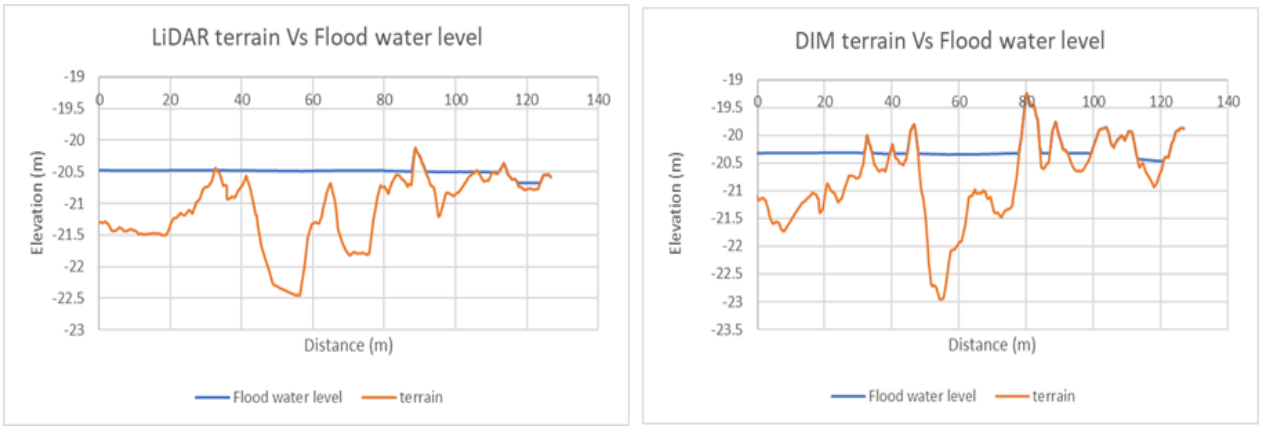

Figure 37: Flood water level of LiDAR and DIM surfaces on River cross section profile

4.4.2. Effects of different LiDAR and DIM DTMs resolutions on flooding

This section shows the effects of flooding caused by different resolutions of DTMs, 1m, 5m, 10m, and 20m. These DTMs were generated from the final optimized filtering parameters, for both LiDAR and DIM. The inundation area increases as the resolution of the DTM reduces from 1m to 10m, and then it decreases slightly at 20m resolution. As the resolution (cell size) of the DTM decreases, the generalization

of the surface occurs, which makes it deviate from the actual topography of the area under investigation. Hence, at the lower resolution, the flooding effects might be more exaggerated than at higher ones, because the estimated surface at higher resolution is closer to the actual terrain on the ground. Therefore, for flood modeling, it is observed that higher resolutions are the best. But for situations where it is not possible to obtain high-resolution data, then lower resolution DTMs can be used to have a rough estimate of the flooding effects. Figures 39 and 40 show how the generalization of the terrain occurs as the grid size increases in both the LiDAR and DIM DTM.

From Table 12, it can be observed that the lower the standard deviation for both LiDAR and DIM, the higher the inundation area. The DIM standard deviation is showing a trend where it is fluctuating, i.e., increase followed by a decrease, while the LiDAR standard deviation indicates a gradual decline, then increase. This might be because a higher standard deviation means there are some outliers, which means there are more significant deviations from the mean value, hence denoting surface roughness. However, regardless of the resolution, it can be observed that the inundation area for LiDAR was always higher than for DIM, as depicted in figure 38.

These observations on the effect of the resolution are similar to what Sithole & Vosselman (2004) stated that it is harder to separate ground and non-ground as the resolution of the data reduces. Further, Werner (2001) also showed that as the resolution becomes coarser, neighboring heights may be averaged. Hence, things such as embankments and riverbanks may be lost, thereby impacting on flood extent.

Table 12: WSE of 1m, 5m, 10m and 20m DTM at River cross-section profile

	WSE (m)	1m DTM	5m DTM	10m DTM	20m DTM
LiDAR	Max	-20.121	-20.393	-20.432	-20.075
	Min	-20.674	-20.642	-20.482	-20.559
	Mean	-20.491	-20.481	-20.452	-20.499
	stddev	0.066	0.052	0.012	0.110
DIM	Max	-19.243	-19.243	-19.562	-19.562
	Min	-20.477	-20.442	-20.383	-20.382
	Mean	-20.237	-20.239	-20.183	-20.159
	stddev	0.222	0.229	0.174	0.258

NB: WSE is the water surface elevation or flood water level

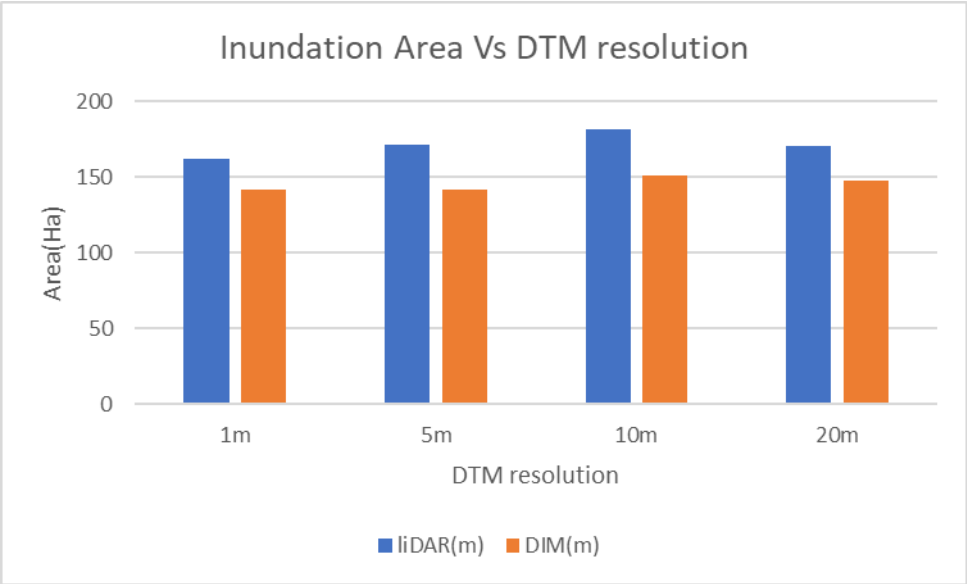

Figure 38: Inundation vs DTM resolution

Figures 39 and 40 show how the terrain and flood water level changes as the resolution of the DTM is reduced. The terrain tends to be generalized when the grid size increases or resolution is reduced.

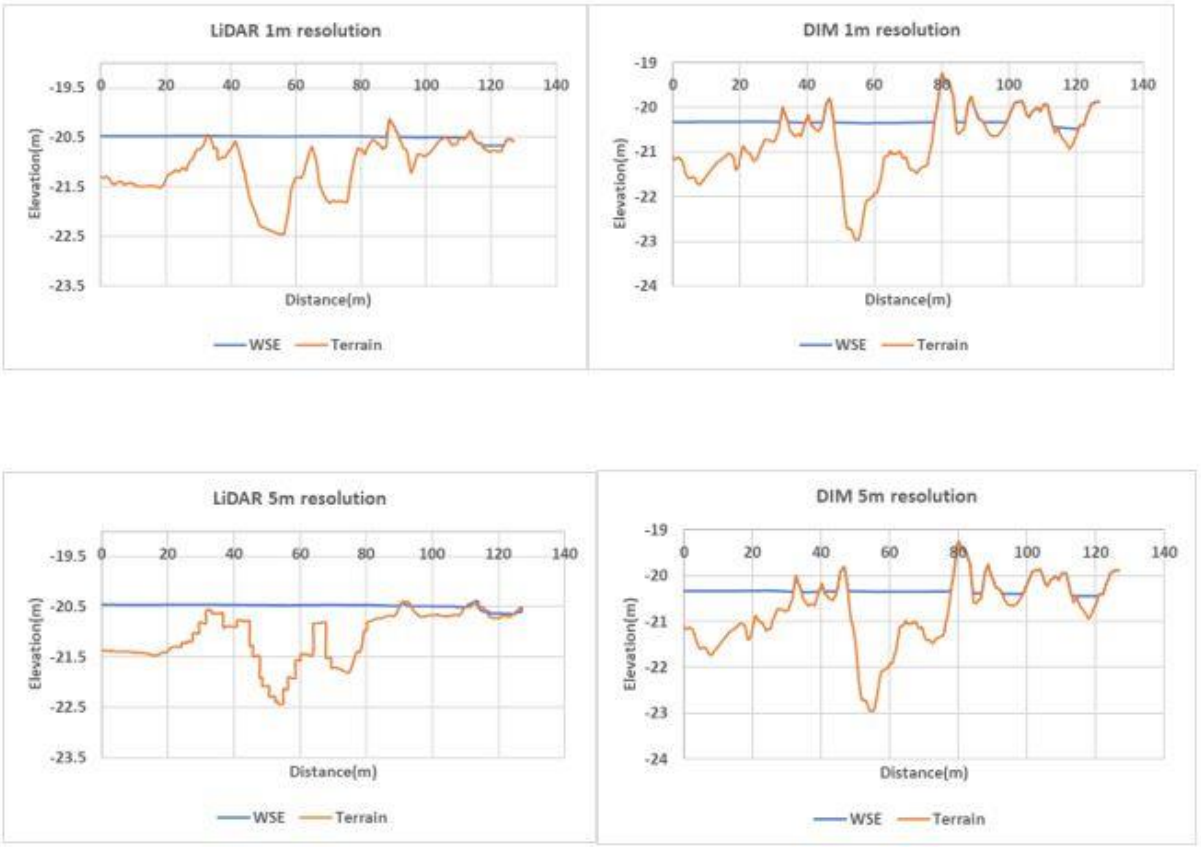

Figure 39: LiDAR and DIM 1m,5m resolution at River cross section profile

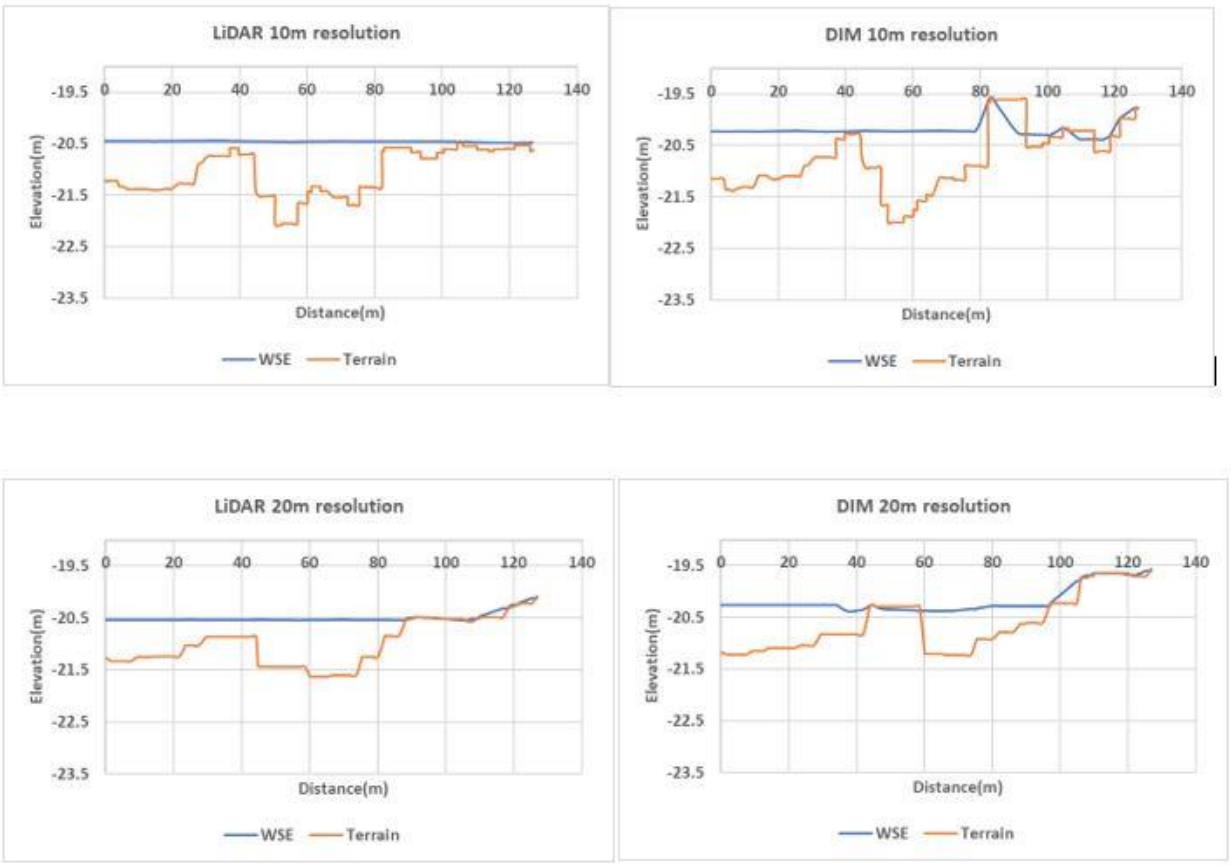

Figure 40: LiDAR and DIM 10m,20 resolution at river cross section profile

4.4.3. Effects of the optimized parameters on flooding

This section shows the differences between the optimized parameter DTMs from LiDAR and DIM. As the parameters are being optimized, this influences the inundation area, as shown in figure 41. As objects are being added or removed to the ground, this might affect flood depth, WSE, flood extent and velocity of the flood water by either increasing or decreasing them. This is so because objects being added or removed may make the surface smoother or coarser.

The central concept of the filtering is the inclusion or non-inclusion of points to either be part of the ground or not. In this vein, the more significant effect on the flooding in the LIDAR processing is on the standard deviation; this is because it changed from a value of 10cm to 1cm, which means that there was a reduction to the objects being included as part of the ground. This would eventually increase on the flooding extent, as can be seen in figure 42. This was an inundation area increase of 18.464 hectares.
For the DIM processing, the most significant change happened on the offset parameter. This is because this value changed from 0.05m to 0.1m, which means some objects which were not part of the ground get included as ground. This explains the reduction of flood extent because the flooding would encounter more resistance from the added objects which were not there before. The decrease in the inundation area is 21.638 hectares.

The choice of the profile, which is a river cross-section, was chosen to show that as the filtering is being done, the riverbank should be preserved as this is very vital when the resultant DTM is for flood modeling. Some of the filtering parameters end up flattening the riverbanks, curbs, etc. thereby increasing the flood extent, velocity, and adversely affecting the flood depth. The other parameter comparisons are shown in Appendix D.

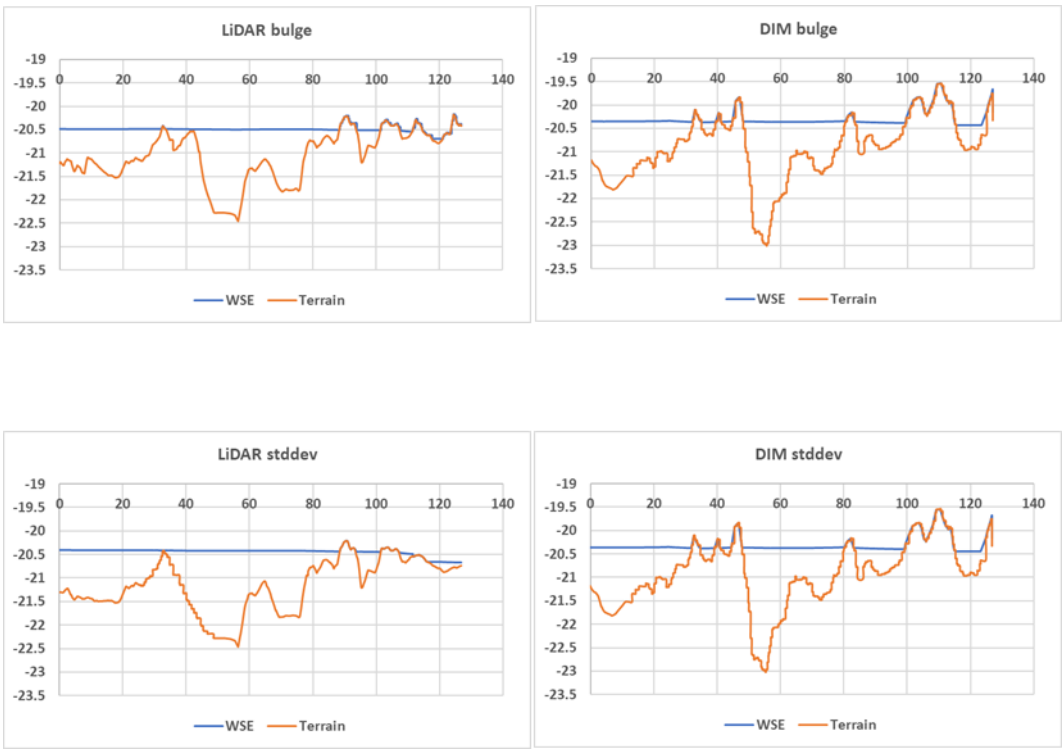

Figure 41:Comparison of bulge and stddev in LiDAR and DIM at river cross section profile

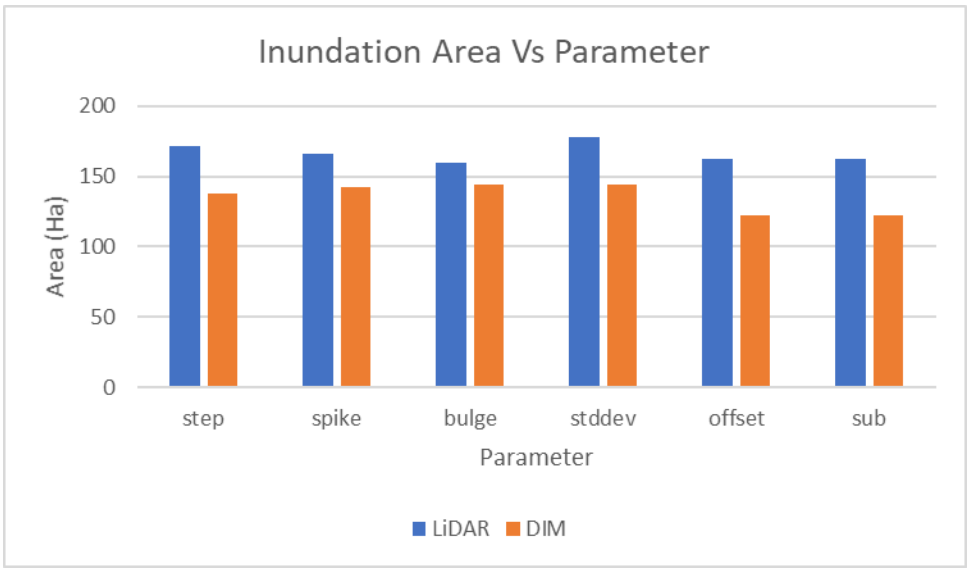

Figure 42:Inundation area vs optimised parameter

4.4.4. Effects of different parameters on flooding

In this section, the profile used is the vegetation profile. This profile was chosen to investigate the differences between LiDAR and DIM in terms of the effects of filtering on flooding in an area with a lot of tree cover. Silva et al. (2018) found that some ground filtering algorithms performed poorly in forest areas, as they tended to undervalue the DTM elevations, they further state that the most significant differences between the different algorithms also occurred in areas of steep slopes. This explains how the Lasground algorithm performed around this area with vegetation cover. Before any filtering is done in Lasground, the step size must be decided. The default for Lasground is 5m but various switches give defaults depending on the terrain characteristics of the study area.

Step parameter

The step parameter determines the size of non-ground objects that can be filtered. From figure 43, it can be observed that as the step size reduces, the filtering capability of the algorithm is affected because it is not able to filter out the bigger trees or buildings. This is very noticeable in the DIM DTM. The LiDAR parameter shows more flooding in the study area because ground points can easily be identified than in the DIM. As this parameter is being tuned LiDAR inundation area reduced by 3.197ha, 9.504ha and 1.439ha between step size 50m to 25m, 25m to 10m and 10m to 5m, respectively. The DIM also exhibits the same trend as it reduces by 14.662ha, 3.033ha and 3.986ha between step size 50m to 25m, 25m to 10m and 10m to 5m, respectively.

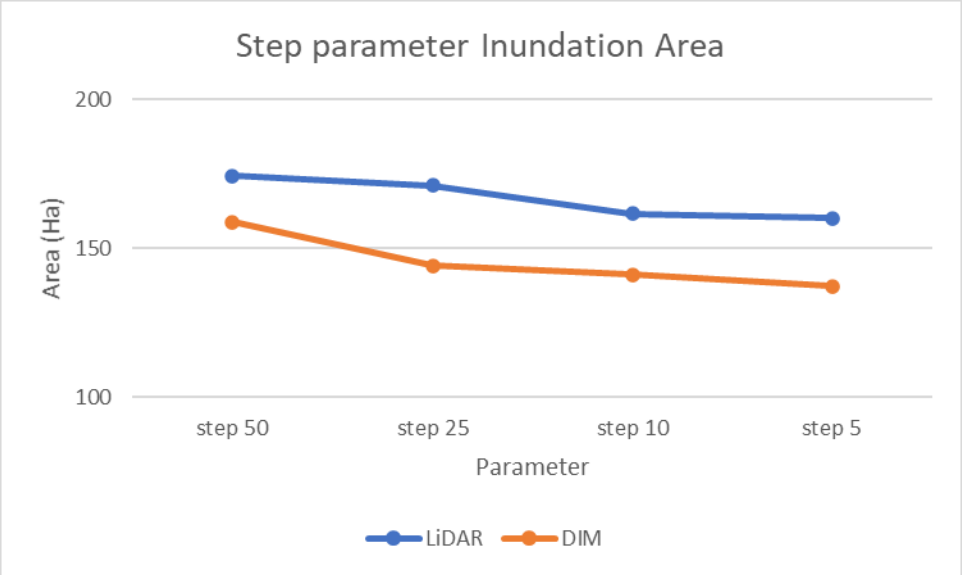

Figure 43:Step parameter inundation area

Spike parameter

The spike parameter determines at what height above and below spikes get removed, the below value is usually 10 times the above spike. The effect of the spike parameter is such that most of the terrain is inundated in the LiDAR scenario as opposed to the DIM, which again shows the advantage of LiDAR in such terrain. Figure 44 shows how the spike parameter affects the inundation areas. In the LiDAR, the area reduces by 0.606ha, increases by 0.552ha, and finally increases by 5.030ha. The DIM shows a similar trend of reduction, increment, and increment with values of 0.993ha,2.444ha, and 0.963ha, respectively.

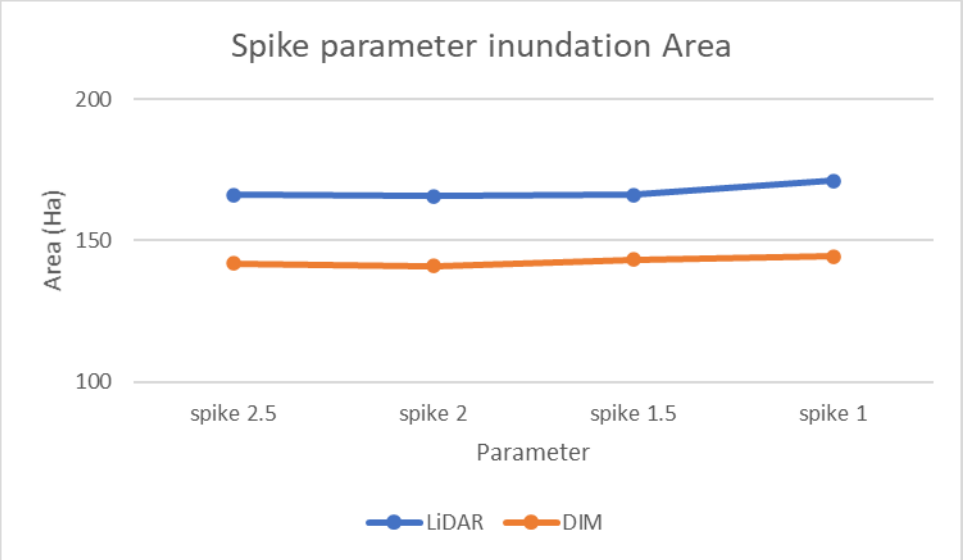

Figure 44:Spike parameter inundation area

Bulge parameter

The bulge parameter determines the acceptable bulge that the TIN surface can handle as points are being added to it during tuning. The default is one-tenth of the step when the step is 5m and one-fifth when the step size is less than 5m (Rapidlasso, n.d.-a). The bulge parameter in the LiDAR increases by 0.242ha, 6.045ha, and 18.731ha between bulge sizes 2.5m,1.5m,1m, and 0,25m. DIM increases by 2.167 between bulge 2.5m and 1.5m, then reduce between 1.5m and 1m by 2.265ha, then the inundation area increases by 10.727ha between 1.5m and 0.25m; this is highlighted in figure 45. This is because at lower values of the bulge, the algorithm only includes objects that fall within the small bulge threshold, and these would not impact so much on the flooding because they do not block the flow of the water.

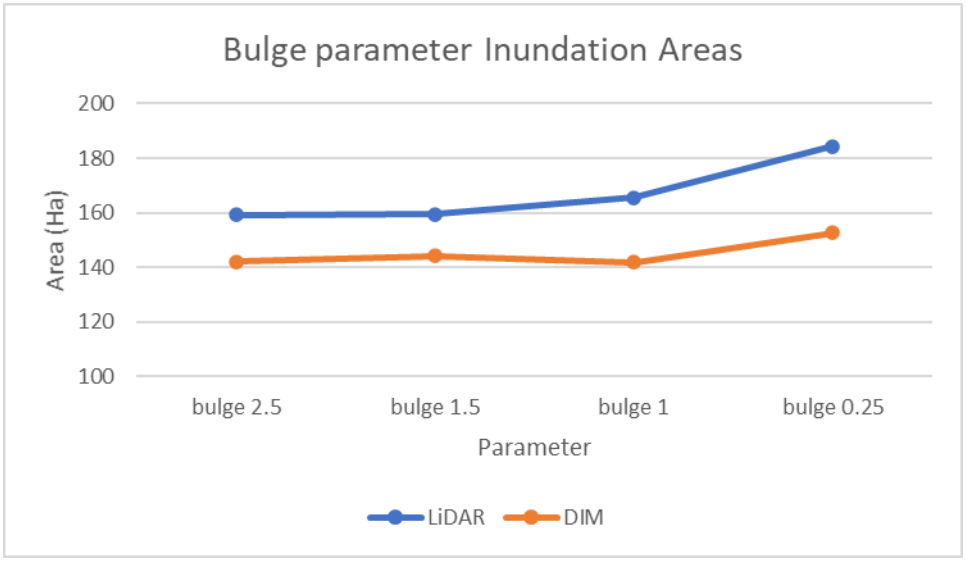

Figure 45:Bulge parameter inundation area

Standard Deviation parameter

The effect of the standard deviation on the inundation is such that for the LiDAR, it is constant between 10cm and 6cm. It increases by 3 hectares between 6cm and 1cm; after that, the area does not change between 1cm and no standard deviation. For the DIM, it reduces by 1 hectare both between 10cm to 6cm and 6cm to 1cm, after which it remains constant; this is depicted in figure 46.

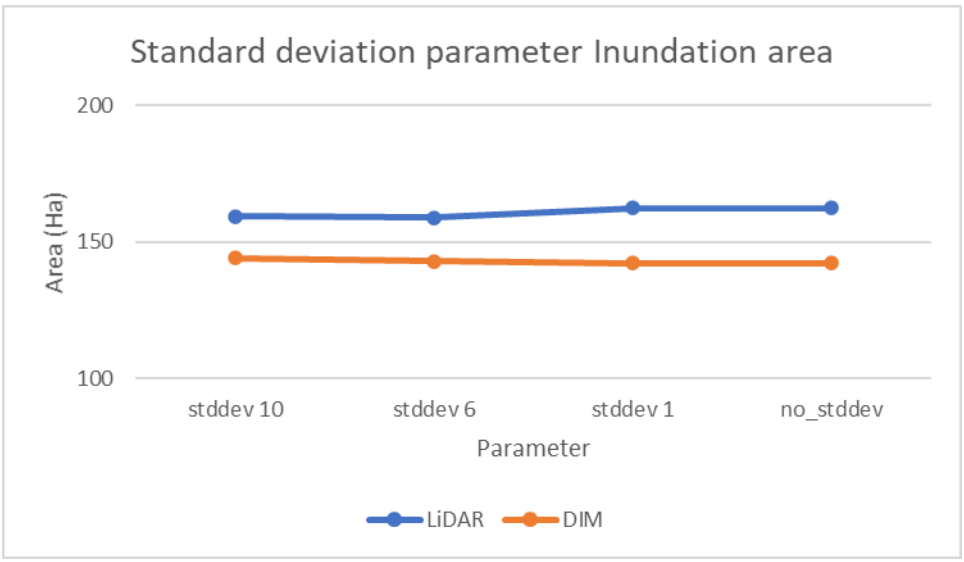

Figure 46: Standard deviation parameter inundation area

Offset parameter

The offset parameter is a threshold that determines the maximum height above the ground that points get included to the ground and has a default value of 0.05m. The effect of the offset parameter on the flooding seems to be more on the DIM than the LiDAR, though both show that there is a gradual decrease in inundation as the offset increases. This is shown in figure 47. In LiDAR there is a reduction of

0.868m,0.05m and 3.055m between offset 0.02m, 0.05m, 0.1m and 0.5m, respectively. The DIM data behaves differently as it reduces by 0.837ha,1.864ha,6.530ha between offset 0.02m,0.05m,0.1m, and 0.5m, respectively. The mean change in the inundation area for LiDAR and DIM is 1.324ha and 3.077ha, respectively. This is because a lot of objects are included as part of the ground as the offset value is increased, some of which might hinder the flow of water. An example of such a scenario is shown from the flooding extents of offset value 0.02 and 0.5 in figure 48, and the difference in flooding area is 3.972ha.

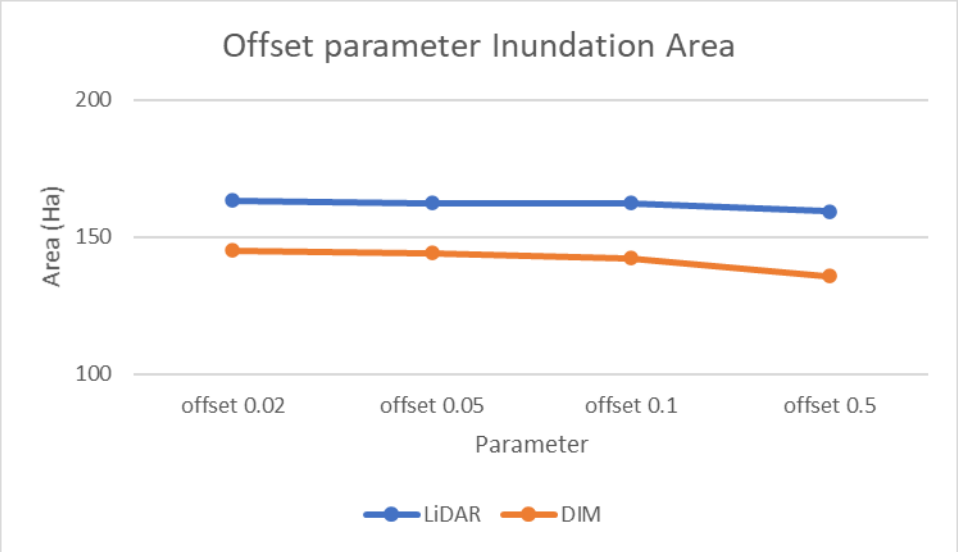

Figure 47:Offset parameter inundation area

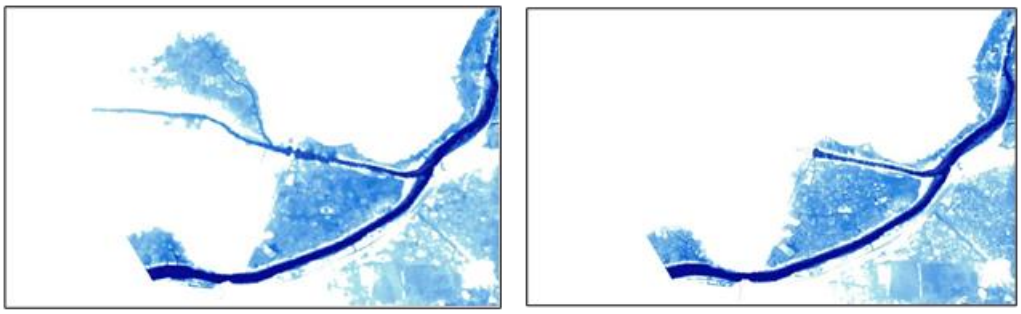

Figure 48:Flooding scenario at Lidar offset 0.02m and 0.5m

Sub parameter

The sub parameter denotes the initial search for the ground, and it ranges from coarse to extra fine corresponding to flat to very steep slopes. The effect of the sub parameter on the inundation is such that for the LiDAR, it increases by 0.448ha between sub3 and sub5, then reduces by 0.260ha between sub 5 and sub 6, then increases by 0.172ha between sub 6 and sub 8. The DIM reduces by 0.249ha between sub 3 and sub 5, then increases by 1.277ha between sub 5 and sub 6; finally, it decreases by 0.298ha between sub 6 and sub 8. This is seen in figure 49. The choice of which parameter to use is heavily dependent on the terrain in the study area(Silva et al., 2018).

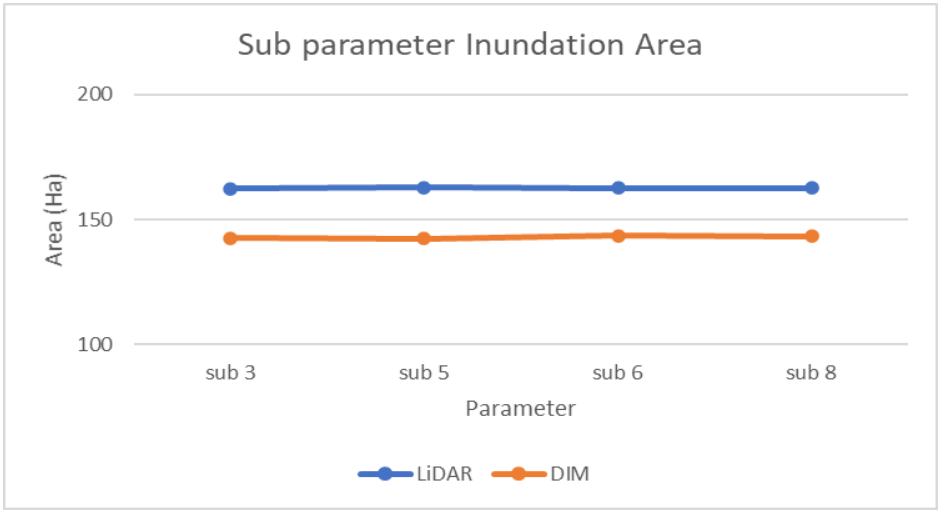

Figure 49: Sub parameter inundation area

Example showing the effect of spike parameter on flooding

Figures 50 and 51 show the effect of the spike parameter on flooding along the vegetation profile. It can be seen that a comparison of the LiDAR and DIM in this area shows that the ground points are not easily seen in the DIM data; hence there is little flooding along this profile compared to the LiDAR, which has considerable flooding as the parameters are being adjusted. A comparison of the other parameters is shown in appendix E.

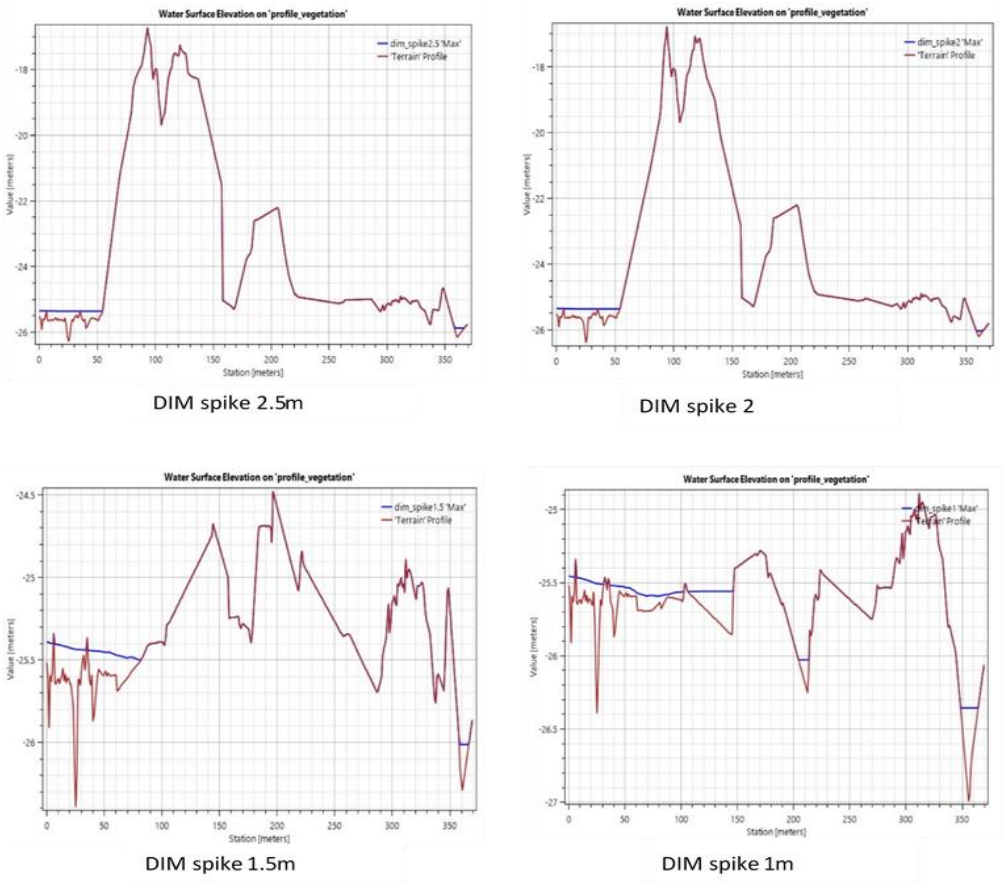

Figure 50: Effect of different DIM spike parameters on flooding

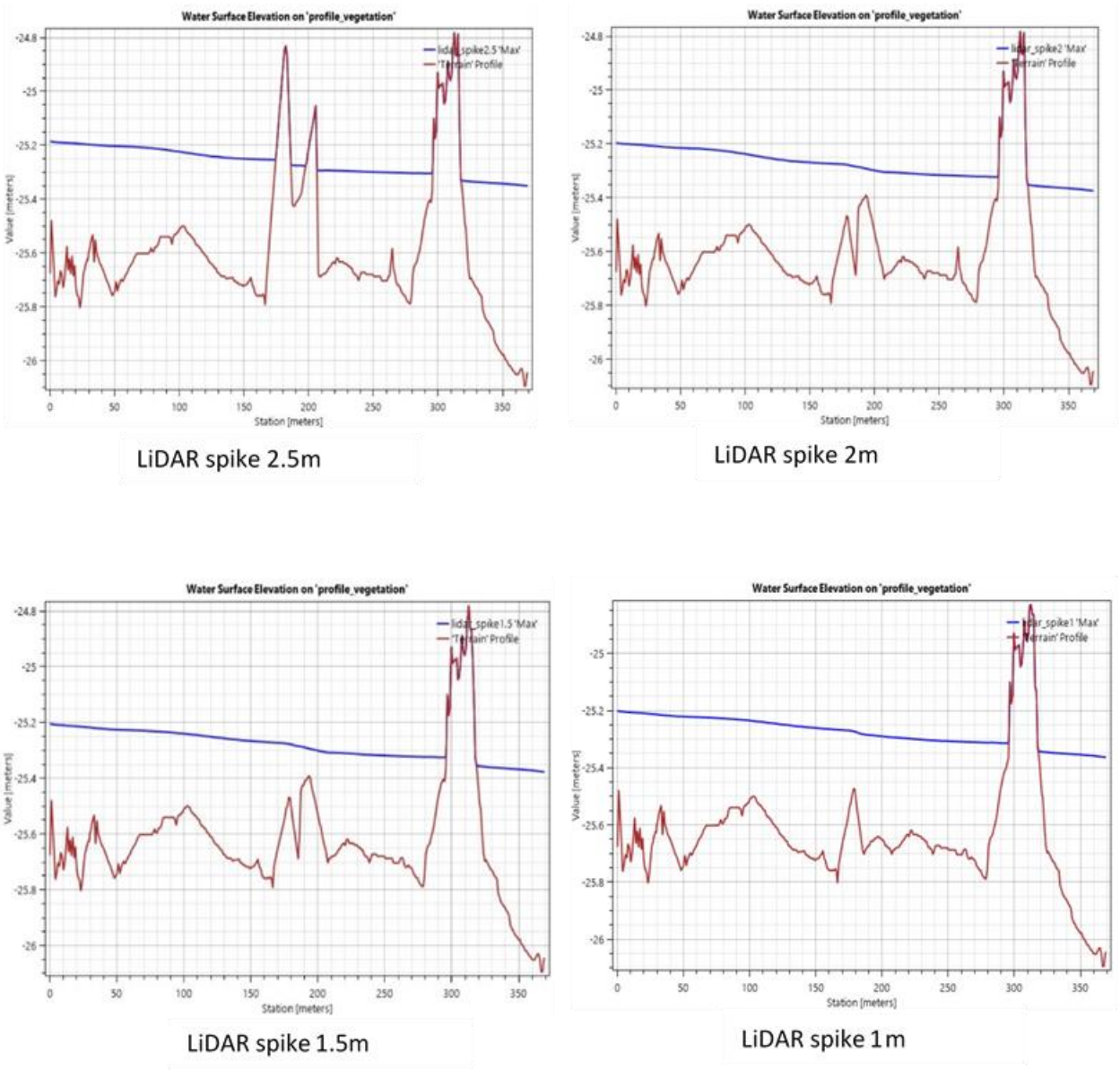

Figure 51: Effect of different LiDAR spike parameter on flooding

5. CONCLUSION AND RECOMMENDATIONS

5.1. Conclusion

In this study, an investigation was conducted to ascertain whether UAV LiDAR or UAV DIM data could be used for flood modeling. Lasground parameters of step, spike, bulge, standard deviation, offset, and sub were optimized to produce a DTM that meets the requirements of having ramps, curbs, dividers, and riverbanks preserved. At the same time, macro objects like buildings, vegetation, and bridges should be removed to have a bare earth DTM.

The findings from the comparison of the LiDAR and DIM DTMs and point clouds indicate that as the parameters are being tuned, this heavily influences what gets added to the produced surface. For example, when analyzing the LiDAR offset parameter, it showed that as the value of the offset increases, the RMS also increases. This means as more points are being added to the ground surface, the noise of the filtered surface and its distance also increases. Further, results from the cloud to cloud analysis on the bulge parameter showed that as the value of the parameter increases, so does the mean value and standard deviation. This gave mean distance and standard deviation values of 0.160m and 0.193m, and 0.078m and 0.144m for surface 21 in both test areas, respectively.

The analysis also showed that different landcover influence parameter settings. In vegetated areas, the difference between the LIDAR and DIM point clouds was higher than in the built-up. The relatively flat pavement showed no significant differences. Further, the high vegetation cover shows some significant differences also. This difference might be due to the season in which these data sets were captured; one was captured during the wet season (LiDAR) and the other during the dry season(DIM). This was likely to affect the vegetation cover and, consequently, on the filtering as well.

The analysis on grid size or resolution of the DTMs showed that as the resolution of the DTM is reduced, the flooding extent increased. That the flooding extent is significant is no sign that the model is good, it merely means that as the elevation in a coarser DTM is more generalized and hence the possibility of objects which either block or direct flow being removed are more in the coarser DTM. Thus this accounts for the more flooding in both LiDAR and DIM data. So, according to this analysis, the smaller resolutions can depict the flooding better because the produced DTMs are closer to the actual terrain characteristics. This means that to obtain a point density of at least 1.5 points/m2 using LiDAR, the UAV flights have to be flown at reduced heights to meet this requirement of producing a high-resolution DTM (Hsieh et al., 2016; Luo et al., 2016).

The flood simulation was able to show that different parameter settings either increase or decrease the flooding effects. From the analysis based on the mean flood extent areas for both LiDAR and DIM, six parameters were identified as those which influence flood modeling. These are bulge, step, spike, standard deviation, sub, and offset. It was observed that the effects of these parameters are different on the LiDAR and DIM data (Green, 2015). For the LiDAR data, the parameter with the most significant influence is the bulge with a mean flood area of 8,339 hectares.
In contrast, for DIM data, the one with the most significant influence is step with a mean area of 7.227 hectares. The bulge parameter, which is a measure of the acceptable bulge that the TIN surface can handle as points are being added. This parameter is much more flexible because of the curvature the TIN surface makes. Changing this value helps to improve ground classifying of particularly DIM data (Rapidlasso, n.d.-a). When tuning the DIM data, the parameters which seem to be very sensitive because of their high mean flood extent values are step, bulge, and offset. Hence, when processing the DIM data, the data processor should pay more attention to these, as a first guide. The LiDAR parameters most sensitive to the data are

bulge, step, and spike, so equally the processor when dealing with LiDAR data should pay more attention to these when tuning the filtering algorithm.

Therefore, apart from having different acquisition methods, LiDAR and DIM also have different ways in which the parameters affect the processing of the data. However, it should be noted that among all the parameters of the Lasground algorithm, the step parameter should be set before any other because this determines the size of non-ground objects to be filtered out (Green, 2015).

The results have shown that in open areas with low vegetation cover, the DIM data can be used for flood modeling. Also, the results have shown that parameter optimization of the ground filtering algorithm is essential as this adversely affects flooding depth, extent, and velocity. Further, the results have shown that parameter optimization is terrain dependent as the filtering has to suit the conditions of the local surface.

5.2. Recommendations

Data from gauging stations for checking the flood depth and for calibrating the model would be beneficial if this can be incorporated in future works. For a more realistic representation of the flood, and for obtaining a smoother DTM probably Lasground could be used in combination with another algorithm that can altogether remove bridges and low vegetation.

LIST OF REFERENCES

Abdullah, A. . (2012). *A methodology for processing raw lidar data to support urban flood modelling framework*.

Abdullah, A. ., Rahman, A. ., & Vojinovic, Z. (2009). LiDAR filtering algorithms for urban flood application: Review on current algorithms and filters test. *International Archives of Photogrammetry, Remote Sensing and Spatial Information Sciences*, *XXXVIII*(Part 3), 30–36.

Abdullah, A. ., Vojinovic, Z., Price, R. ., & Aziz, N. . . . . (2012). A methodology for processing raw LiDAR data to support urban fl ood modelling framework. *Journal of Hydroinformatics*, *14*(1), 75–92. https://doi.org/10.2166/hydro.2011.089

Alaghmand, S., Abdullah, R., & Abustan, I. (2014). *River Modelling for Flood Risk Map Prediction: A Case Study of Kayu Ara River Basin, Malaysia*. https://doi.org/10.15242/iae.iae1214510

Alho, P., Hyyppä, H., & Hyyppä, J. (2009). Consequence of DTM Precision for Flood Hazard Mapping : A Case Consequence of DTM Precision for Flood Hazard Mapping : A Case Study in SW Finland. *Nordic Journal of Surveying and Real Estate Research*, *6*(1), 21–39.

Alzahrani, A. S. (2017). *Application of Two-Dimensional Hydraulic Modeling in Riverine Systems Using Hec-Ras* (Issue March). https://etd.ohiolink.edu/!etd.send_file?accession=dayton1493135117254329&disposition=inline

Anders, N., Seijmonsbergen, A., Masselink, R., & Keesstra, S. (2016). Ground point filtering of UAV-based photogrammetric point clouds. *EGU General Assembly 2016, Held 17-22 April, 2016 in Vienna Austria, p.17966*, *18*, 17966. http://adsabs.harvard.edu/abs/2016EGUGA..1817966A

Anders, N., Valente, J., Masselink, R., & Keesstra, S. (2019). Comparing Filtering Techniques for Removing Vegetation from UAV-Based Photogrammetric Point Clouds. *Drones*, *3*(3), 61. https://doi.org/10.3390/drones3030061

Anuar bin Md, A. (2018). *Flood Inundation Modeling and Hazard Mapping under Uncertainty in the Sungai Johor Basin , Malaysia*.

Axelsson, P. (2000). DEM generation from laser scanner data using adaptive TIN models. *International Archives of Photogrammetry and Remote Sensing*, *33*(4), 110–117. https://www.isprs.org/proceedings/XXXIII/congress/part4/111_XXXIII-part4.pdf

Begashaw, S. (2018). *Accuracy of DTM derived from UAV imagery and its effect on canopy height model compared to airborne lidar in part of tropical rain forests of Berklah, Malaysia*. https://library.itc.utwente.nl/papers_2018/msc/nrm/berhanu.pdf

Ben Khalfallah, C., & Saidi, S. (2018). Spatiotemporal floodplain mapping and prediction using HEC-RAS - GIS tools: Case of the Mejerda river, Tunisia. *Journal of African Earth Sciences*, *142*, 44–51. https://doi.org/10.1016/j.jafrearsci.2018.03.004

Berteška, T., & Ruzgienė, B. (2013). Photogrammetric Mapping Based on Uav Imagery. *Geodesy and Cartography*, *39*(4), 158–163. https://doi.org/10.3846/20296991.2013.859781

Boslaugh, S. (2012). Pearson Correlation Coefficient. *Encyclopedia of Epidemiology*, *April 2014*. https://doi.org/10.4135/9781412953948.n342

Bout, B., & Jetten, V. G. (2018). The validity of flow approximations when simulating catchment-integrated flash floods. *Journal of Hydrology*, *556*, 674–688. https://doi.org/10.1016/j.jhydrol.2017.11.033

Briese, C. (2010). Extraction of Digital Terrain Models. In G. Vosselman, H-G Maas (Ed.), *Airborne and Terrestrial Laser Scanning* (pp. 135–167). Whittles Publishing.

Brunner, G. W. (2016). *HEC-RAS River Analysis System 2D Modeling User ' s Manual* (Issue February).

Cao, L., Liu, H., Fu, X., Zhang, Z., Shen, X., & Ruan, H. (2019). Comparison of UAV LiDAR and digital aerial photogrammetry point clouds for estimating forest structural attributes in subtropical planted forests. *Forests*, *10*(2), 1–26. https://doi.org/10.3390/f10020145

Căţeanu, M., & Arcadie, C. (2017). Als for terrain mapping in forest environments: An analysis of lidar filtering algorithms. *EARSeL EProceedings*, *16*(1), 9–20. https://doi.org/10.12760/01-2017-1-02

CDR international. (2019). *Bathymetric and UAV-LiDAR topographic survey of Msimbazi river area,Tanzania*.

Chow, V. T. (1959). *Open Channel Hydraulics*. McGraw Hill Inc.

Chu, H. J., Chen, R. A., Tseng, Y. H., & Wang, C. K. (2014). Identifying LiDAR sample uncertainty on terrain features from DEM simulation. *Geomorphology*, *204*, 325–333. https://doi.org/10.1016/j.geomorph.2013.08.016

Coveney, S., & Fotheringham, A. S. (2011). The impact of DEM data source on prediction of flooding and erosion risk due to sea-level rise. *International Journal of Geographical Information Science*, *25*(7), 1191–

1211. https://doi.org/10.1080/13658816.2010.545064
Coveney, S., & Roberts, K. (2017). Lightweight UAV digital elevation models and orthoimagery for environmental applications: data accuracy evaluation and potential for river flood risk modelling. *International Journal of Remote Sensing*, *38*(8–10), 3159–3180. https://doi.org/10.1080/01431161.2017.1292074
de Risi, R., Jalayer, F., de Paola, F., Iervolino, I., Giugni, M., Topa, M. E., Mbuya, E., Kyessi, A., Manfredi, G., & Gasparini, P. (2013). Flood risk assessment for informal settlements. *Natural Hazards*, *69*(1), 1003–1032. https://doi.org/10.1007/s11069-013-0749-0
Dorn, H., Vetter, M., & Höfle, B. (2014). GIS-based roughness derivation for flood simulations: A comparison of orthophotos, LiDAR and Crowdsourced Geodata. *Remote Sensing*, *6*(2), 1739–1759. https://doi.org/10.3390/rs6021739
Escobar Villanueva, J. ., Iglesias Martínez, L., & Pérez Montiel, J. I. (2019). DEM Generation from Fixed-Wing UAV Imaging and Flood Estimations. *Sensors*, *19*(14), 3205. https://doi.org/https://doi.org/10.3390/s19143205
Fintling, C. (2006). *Flood Risk Perception in Tanzania* [Stockholms University]. https://www.diva-portal.org/smash/get/diva2:189999/FULLTEXT01.pdf
Gerard, J., Prospection, A., & Wiley, J. (1999). *MODELLING OF INDIVIDUAL MONUMENTS FROM STEREO PAIRS OF*. *0763*(199912).
Green, V. (2015). *Towards Systematic Selection of Terrain- and Ground Cover-Specific LiDAR Filtering Parameters* [University of Arkansaa]. https://pdfs.semanticscholar.org/96c3/1d882f98752fc9f9a60ac9bfe30c8ba83c86.pdf
Guo, Q., Li, W., Yu, H., & Alvarez, O. (2010). Effects of Topographic Variability and Lidar Sampling Density on Several DEM Interpolation Methods. *American Society for Photogrammetry and Remote Sensing*, *6*(12), 701–712. https://doi.org/10.14358/PERS.76.6.701
Habonimana, H. V. (2016). *Integrated Flood Modeling in Lubigi Catchment Kampala INTEGRATED FLOOD MODELING KAMPALA*. *February 2014*. https://doi.org/10.13140/RG.2.1.3285.4645
Harwin, S., & Lucieer, A. (2012). Assessing the accuracy of georeferenced point clouds produced via multi-view stereopsis from Unmanned Aerial Vehicle (UAV) imagery. *Remote Sensing*, *4*(6), 1573–1599. https://doi.org/10.3390/rs4061573
Hashemi-Beni, L., Jones, J., Thompson, G., Johnson, C., & Gebrehiwot, A. (2018). Challenges and opportunities for UAV-based digital elevation model generation for flood-risk management: A case of princeville, north carolina. *Sensors (Switzerland)*, *18*(11), 3843. https://doi.org/10.3390/s18113843
Höhle, J., & Potuckova, M. (2011). Assessment of the quality of Digital Terrain Medels. *Official Publication - EuroSDR*, *60*.
Hsieh, Y., Chan, Y., & Hu, J. (2016). Digital Elevation Model Differencing and Error Estimation from Multiple Sources : A Case Study from the Meiyuan Shan Landslide in Taiwan. *Remote Sens*, *8*(3), 199. https://doi.org/10.3390/rs8030199
Hui, Z., Li, D., Jin, S., Ziggah, Y. Y., Wang, L., & Hu, Y. (2019). Automatic DTM extraction from airborne LiDAR based on expectation-maximization. *Optics and Laser Technology*, *112*, 43–55. https://doi.org/10.1016/j.optlastec.2018.10.051
Ismail, Z., Zulkarnain, M., Rahman, A., Radhie, M., Salleh, M., Razak, A., & Yusof, M. (2015). Accuracy Assessment of LIDAR-Derived Elevation Value Over Vegetated Terrain in Tropical Region. *Jurnal Teknologi*, *73*(5), 171–177. https://doi.org/https://jurnalteknologi.utm.my/index.php/jurnalteknologi/article/view/4335
Izumida, A., Uchiyama, S., & Sugai, T. (2017). Application of UAV-SfM photogrammetry and aerial lidar to a disastrous flood: Repeated topographic measurement of a newly formed crevasse splay of the Kinu River, central Japan. *Natural Hazards and Earth System Sciences*, *17*(9), 1505–1519. https://doi.org/10.5194/nhess-17-1505-2017
Jakovljevic, G., Govedarica, M., Alvarez-Taboada, F., & Pajic, V. (2019). Accuracy assessment of deep learning based classification of LiDAR and UAV points clouds for DTM creation and flood risk mapping. *Geosciences (Switzerland)*, *9*(7), 323. https://doi.org/10.3390/geosciences9070323
Javernick, L., Brasington, J., & Caruso, B. (2014). Modeling the topography of shallow braided rivers using Structure-from-Motion photogrammetry. *Geomorphology*, *213*, 166–182. https://doi.org/10.1016/j.geomorph.2014.01.006
Kalyanapu, A. J., Burian, S. J., & McPherson, T. N. (2009). Effect of land use-based surface roughness on hydrologic model output. *Journal of Spatial Hydrology*, *9*(2), 51–71.
Khalid, N. F., Din, A. H. M., Omar, K. M., Khanan, M. F. A., Omar, A. H., Hamid, A. I. A., & Pa'Suya,

M. F. (2016). Open-source digital elevation model (DEMs) evaluation with gps and lidar data. *International Archives of the Photogrammetry, Remote Sensing and Spatial Information Sciences - ISPRS Archives*, *42*(4W1), 299–306. https://doi.org/10.5194/isprs-archives-XLII-4-W1-299-2016

Langhammer, J., Janský, B., Kocum, J., & Mina, R. (2018). 3-D reconstruction of an abandoned montane reservoir using UAV photogrammetry , aerial LiDAR and fi eld survey. *Applied Geography*, *98*(February), 9–21. https://doi.org/10.1016/j.apgeog.2018.07.001

Leitão, J. . P., & Sousa, L. M. (2018). Towards the optimal fusion of high-resolution Digital Elevation Models for detailed urban fl ood assessment. *Journal of Hydrology*, *561*(December 2017), 651–661. https://doi.org/10.1016/j.jhydrol.2018.04.043

Leitão, J. ., Vitry, M. M. De, Scheidegger, A., & Rieckermann, J. (2016). Assessing the quality of digital elevation models obtained from mini unmanned aerial vehicles for overland flow modelling in urban areas. *Hydrology and Earth System Sciences*, *20*(4), 1637–1653. https://doi.org/10.5194/hess-20-1637-2016

Liu, X. (2008). Airborne LiDAR for DEM generation: Some critical issues. *Progress in Physical Geography*, *32*(1), 31–49. https://doi.org/10.1177/0309133308089496

Luo, S., Chen, J. M., Wang, C., Xi, X., Zeng, H., Peng, D., & Li, D. (2016). Effects of LiDAR point density , sampling size and height threshold on estimation accuracy of crop biophysical parameters. *Opt. Express*, *24*(11), 11578–11593. https://doi.org/10.1364/OE.24.011578

Mantong, H. I. (2018). *Retrieval of a High Resolution DEM from UAV Photogrammetry for defining the Flood water level extents detected with SAR images*. https://library.itc.utwente.nl/login/2018/msc/wrem/mantong.pdf

Mark, O., Weesakul, S., Apirumanekul, C., Aroonnet, S. B., & Djordjevic, S. (2004). Potential and limitations of 1D modelling of urban flooding. *Journal of Hydrology*, *299*(3–4), 284–299. https://doi.org/10.1016/j.jhydrol.2004.08.014

Martínez-Carricondo, P., Agüera-Vega, F., Carvajal-Ramírez, F., Mesas-Carrascosa, F. J., García-Ferrer, A., & Pérez-Porras, F. J. (2018). Assessment of UAV-photogrammetric mapping accuracy based on variation of ground control points. *International Journal of Applied Earth Observation and Geoinformation*, *72*(May), 1–10. https://doi.org/10.1016/j.jag.2018.05.015

Meesuk, V. (2017). *Point Cloud Data Fusion for Enhancing 2D Urban Flood Modelling*.

Meesuk, V., Vojinovic, Z., Mynett, A. E., & Abdullah, A. F. (2015). Advances in Water Resources Urban flood modelling combining top-view LiDAR data with ground-view SfM observations. *ADVANCES IN WATER RESOURCES*, *75*, 105–117. https://doi.org/10.1016/j.advwatres.2014.11.008

Micheletti, N., Chandler, J. . ., & Lane, S. . . (2015). Structure-from-motion photogrammetry. In *British Society for Geomorphology* (p. Chap.2,sec.2.2).

Moudrý, V., Klápště, P., Fogl, M., Gdulová, K., Barták, V., & Urban, R. (2020). Assessment of LiDAR ground filtering algorithms for determining ground surface of non-natural terrain overgrown with forest and steppe vegetation. *Measurement: Journal of the International Measurement Confederation*, *150*. https://doi.org/10.1016/j.measurement.2019.107047

Muller, J. (2015). *Comparing high quality digital elevation models to estimate ponding in urban systems*.

Nandurkar, R., More, R., & Deshpandhe, S. (2017). Urban Flash Flood Modelling Using Remotely Sensed Data And Hec-RAS : Pune Case Study. *Conference Paper*, *November*.

Nex, F., & Remondino, F. (2014). UAV for 3D mapping applications: A review. *Applied Geomatics*, *6*(1), 1–15. https://doi.org/10.1007/s12518-013-0120-x

Nie, S., Wang, C., Dong, P., Xi, X., Luo, S., & Qin, H. (2017). A revised progressive TIN densification for filtering airborne LiDAR data. *Measurement: Journal of the International Measurement Confederation*, *104*, 70–77. https://doi.org/10.1016/j.measurement.2017.03.007

Obeng-manu, C. (2019). *Assessing the accuracy of UAV-DTM generated under different forest canopy density and its effect on estimation of aboveground carbon in Asubima forest, Ghana*. https://library.itc.utwente.nl/papers_2019/msc/nrm/obeng-manu.pdf

Pa'suya, M. F., Md Din, A. H., Mat Amin, Z., & Omar, K. M. (2019). Evaluation of Global Digital Elevation Model for Flood Risk Management in Perlis. *Lecture Notes in Civil Engineering*, 1007–1017. https://doi.org/10.1007/978-981-10-8016-6

Peterson, S., Lopez, J., & Munjy, R. (2019). COMPARISON of UAV IMAGERY-DERIVED POINT CLOUD to TERRESTRIAL LASER SCANNER POINT CLOUD. *ISPRS Annals of the Photogrammetry, Remote Sensing and Spatial Information Sciences*, *4*(2/W5), 149–155. https://doi.org/10.5194/isprs-annals-IV-2-W5-149-2019

Podobnikar, T. (2009). Methods for visual quality assessment of a digital terrain model. *Sapiens*, *2*(2).
Podobnikar, T., & Vrečko, A. (2012). Digital Elevation Model from the Best Results of Different Filtering of a LiDAR Point Cloud. *Transactions in GIS*, *16*(5), 603–617. https://doi.org/10.1111/j.1467-9671.2012.01335.x
Polat, N., & Uysal, M. (2015). Investigating performance of Airborne LiDAR data filtering algorithms for DTM generation. *Measurement: Journal of the International Measurement Confederation*, *63*, 61–68. https://doi.org/10.1016/j.measurement.2014.12.017
Polat, N., & Uysal, M. (2017). DTM generation with UAV based photogrammetric point cloud. *International Archives of the Photogrammetry, Remote Sensing and Spatial Information Sciences - ISPRS Archives*, *42*(4W6), 77–79. https://doi.org/10.5194/isprs-archives-XLII-4-W6-77-2017
Polat, N., & Uysal, M. (2018). An Experimental Analysis of Digital Elevation Models Generated with Lidar Data and UAV Photogrammetry. *Journal of the Indian Society of Remote Sensing*, *46*(7), 1135–1142. https://doi.org/10.1007/s12524-018-0760-8
Pratomo, R. A. (2015). *Flash flood behaviour on a small Caribbean island : a comparison of two watersheds in Grenada* [University of Twente]. https://ezproxy2.utwente.nl/login?url=https://library.itc.utwente.nl/login/2015/msc/aes/pratomo.pdf
Ramirez, J. R. (2006). A new approach to relief representation. *Surveying and Land Information Science*, *66*(1), 19–25.
Rapidlasso. (n.d.-a). *Lasground read me file*. Retrieved June 22, 2020, from http://lastools.org/download/lasground_README.txt
Rapidlasso. (n.d.-b). *LAStools*. Retrieved June 22, 2020, from https://rapidlasso.com/lastools/
Rapidlasso. (2019). *Category Archives: photogrammetry*. https://rapidlasso.com/category/photogrammetry/
Remondino, F., Barazzetti, L., Nex, F., Scaioni, M., & Sarazzi, D. (2012). Uav Photogrammetry for Mapping and 3D Modeling – Current Status and Future Perspectives. *ISPRS - International Archives of the Photogrammetry, Remote Sensing and Spatial Information Sciences*, *XXXVIII-1/*(September), 25–31. https://doi.org/10.5194/isprsarchives-xxxviii-1-c22-25-2011
Rizaldy, A. (2018). *Deep Learning-Based Dtm Extraction From Lidar Point Cloud.* https://library.itc.utwente.nl/papers_2018/msc/gfm/rizaldy.pdf
Salach, A., & Bakuła, K. (2018). Accuracy Assessment of Point Clouds from LiDAR and Dense Image Matching Acquired Using the UAV Platform for DTM Creation. *International Journal of Geographical Information*, *7*(9), 342. https://doi.org/10.3390/ijgi7090342
Shahbazi, M., Sohn, G., Théau, J., & Menard, P. (2015). Development and evaluation of a UAV-photogrammetry system for precise 3D environmental modeling. *Sensors (Switzerland)*, *15*(11), 27493–27524. https://doi.org/10.3390/s151127493
Silva, C. A., Klauberg, C., Hentz, Â. M. K., Corte, A. P. D., Ribeiro, U., & Liesenberg, V. (2018). Comparing the performance of ground filtering algorithms for terrain modeling in a forest environment using airborne LiDAR data. *Floresta e Ambiente*, *25*(2). https://doi.org/10.1590/2179-8087.015016
Sithole, G., & Vosselman, G. (2004). Experimental comparison of filter algorithms for bare-Earth extraction from airborne laser scanning point clouds. *ISPRS Journal of Photogrammetry and Remote Sensing*, *59*(1–2), 85–101. https://doi.org/10.1016/j.isprsjprs.2004.05.004
Siwiec, J. (2019). Comparison of Airborne Laser Scanning of Low and High Above Ground Level for Selected Infrastructure Objects. *Journal of Applied Engineering Sciences*, *8*(2), 89–96. https://doi.org/10.2478/jaes-2018-0023
Syme, W. J. (2008). Flooding in Urban Areas-2D Modelling Approaches for Buildings and Fences. *9th National Conference on Hydraulics in Water Engineering*, *September*, 23–26.
Tamiru, A., & Rientjes, T. H. M. (2001). *Effects of LiDAR DEM resolution in flood modelling: a model sensitivity study for the city of Tegucigalpa, Honduras*. https://webapps.itc.utwente.nl/librarywww/papers_2005/conf/rientjes_eff.pdf
Uysal, M., Toprak, A. S., & Polat, N. (2015). DEM generation with UAV Photogrammetry and accuracy analysis in Sahitler hill. *Measurement: Journal of the International Measurement Confederation*, *73*, 539–543. https://doi.org/10.1016/j.measurement.2015.06.010
Wallace, L., Lucieer, A., Malenovskỳ, Z., Turner, D., & Vopěnka, P. (2016). Assessment of forest structure using two UAV techniques: A comparison of airborne laser scanning and structure from motion (SfM) point clouds. *Forests*, *7*(3), 1–16. https://doi.org/10.3390/f7030062
Werner, M. G. F. (2001). Impact of grid size in GIS based flood extent mapping using a 1D flow model.

Physics and Chemistry of the Earth, Part B: Hydrology, Oceans and Atmosphere, *26*(7–8), 517–522. https://doi.org/10.1016/S1464-1909(01)00043-0

Wilson, J. ., & Gallant, J. . (2000). *Terrain Analysis: Principles and Applications*. JOHN WILEY & SONS,INC.

WorldBank. (2019). *Wading Out the Storm – Flood Risk and Poverty in Dar es Salaam*. https://www.worldbank.org/en/news/feature/2019/10/01/wading-out-the-storm---flood-risk-and-poverty-in-dar-es-salaam#:~:text=In May 2019%2C uninterrupted rainfall,was not a one-off.

Yang, B., & Chen, C. (2015). Automatic registration of UAV-borne sequent images and LiDAR data. *ISPRS Journal of Photogrammetry and Remote Sensing*, *101*, 262–274. https://doi.org/10.1016/j.isprsjprs.2014.12.025

Yilmaz, C., & Gungor, O. (2018). Comparison of the performances of ground filtering algorithms and DTM generation from a UAV-based point cloud. *Geocarto International*, *33*(5), 522–537. https://doi.org/10.1080/10106049.2016.1265599

Zeybek, M., & Şanlıoğlu, İ. (2019). Point cloud filtering on UAV based point cloud. *Measurement: Journal of the International Measurement Confederation*, *133*, 99–111. https://doi.org/10.1016/j.measurement.2018.10.013

Zhang, Z., Gerke, M., Vosselman, G., & Yang, M. Y. (2018). Filtering photogrammetric point clouds using standard lidar filters towards DTM generation. *ISPRS Journal of Photogrammetry and Remote Sensing*, *IV*, 4–7.

APPENDICES

Appendix A : Rainfall Data extraction script in R

```
library(raster)
library(rgdal)
library(spatial)
install.packages("")
getwd()
dir()
setwd("G:\\Msc_Thesis\\openLISEM\\rainfall4_may2019_N\\output_new1")
Rain_data <- list.files(path = ".", pattern = "tif$", full.names = FALSE)
Rain_Stack <- stack(Rain_data)
rainfall <- c(1, Rain_data)
# Checking the data source / information
Rain_Stack[[1]]

# Plot data for individual raster

plot(Rain_Stack[[1]])
plot(Rain_Stack[[2]])

# Getting the cell
colFromX(Rain_Stack, 39.2)
rowFromY(Rain_Stack, -6.8)
cellFromRowCol(Rain_Stack, 1, 2)

# Getting cell data
Rain_Stack[2]
View(Rain_Stack[285])

#putting the cell data in a vector
x <- c(Rain_Stack[2])

#plot the vector
plot(x,xlab="Time step (min)", ylab="Rainfall (mm)", main="May 2019 rainfall")
lines(x, lty=1)
```

Appendix B
Appendix B-1 : Modified Batch Processing script for DIM data

```
:: a batch script for converting a photogrammetry points into a
:: number of products with a tile-based multi-core batch pipeline
:: add LAStools\bin directory to PATH to run script from anywhere

set PATH=%PATH%;C:\software\LAStools\bin

:: specify the number of cores to use

set NUM_CORES=4

:: create a lasinfo report and a 0.5 m RGB raster for input LAZ file

rmdir .\1_quality /s /q
mkdir .\1_quality

lasinfo -i 0_photogrammetry\*.laz ^
        -cd ^
        -o 1_quality\Dar_UAV.txt

lasgrid -i 0_photogrammetry\*.laz ^
        -step 0.5 ^
        -rgb ^
        -fill 1 ^
        -o 1_quality\Dar_UAV.png

:: use lastile to create a buffered tiling from the original
:: photogrammetry points of Msimbazi river basin. we use '-tile_size 200'
:: to specify the tile size and request a buffer of 30 meters
:: around every tile with '-buffer 30' and '-flag_as_withheld'
:: all the buffer points so they can easily be dropped later.
:: the '-olaz' flag requests LASzip compressed output tiles to
:: lower the I/O bottleneck.

rmdir .\2_tiles_raw /s /q
mkdir .\2_tiles_raw

lastile -i 0_photogrammetry\*.laz ^
        -tile_size 200 -buffer 30 -flag_as_withheld ^
        -o 2_tiles_raw\Dar_UAV.laz -olaz

rmdir .\3_tiles_temp1 /s /q
mkdir .\3_tiles_temp1

:: give the point closest to the 20th elevation percentile per
:: 90 cm by 90 cm cell the classification code 8 (but only do
```

```
:: this for cells containing 20 or more points) using lasthin
lasthin -i 2_tiles_raw\*.laz ^
       -step 0.9 ^
       -percentile 20 20 ^
       -classify_as 8 ^
       -odir 3_tiles_temp1 -olaz ^
       -cores %NUM_CORES%
:: considering only points with classification code 8 (ignoring
:: those with classification code 0) change to code from 8 to 12
:: for all "overly isolated" points using lasnoise. the check
:: for isolation uses cells of size 200 cm by 200 cm by 50 cm
:: and marks points in cells whose neighbourhood of 27 cells has
:: only 3 or fewer points in total (see lasnoise_README.txt)

rmdir .\3_tiles_temp2 /s /q
mkdir .\3_tiles_temp2

lasnoise -i 3_tiles_temp1\*.laz ^
        -ignore_class 0 ^
        -step_xy 2 -step_z 0.5 -isolated 3 ^
        -classify_as 12 ^
        -odir 3_tiles_temp2 -olaz ^
        -cores %NUM_CORES%
:: considering only the surviving points with classification
:: code 8 (ignoring those with classification code 0 or 12)
:: change their classification code from 8 either to ground (2)
:: or to non-ground (1) using lasground. the temporary ground
:: surface defined by the resulting ground points will be used
:: to classify points below it as noise in the next step.

rmdir .\3_tiles_temp3 /s /q
mkdir .\3_tiles_temp3

lasground -i 3_tiles_temp2\*.laz ^
         -ignore_class 0 12 ^
         -step 25 -spike 2.5 -bulge 1.5 -stddev 10 -offset 0.1 -sub 5 ^
         -odir 3_tiles_temp3 -olaz ^
         -cores %NUM_CORES%
:: classify all points that are 20 cm or more below the surface
:: that results from Delaunay triangulating the temporary ground
:: points as noise (7) and all others as unclassified (1)

rmdir .\4_tiles_denoised /s /q
mkdir .\4_tiles_denoised

lasheight -i 3_tiles_temp3\*.laz ^
         -classify_below -0.2 7 ^
         -classify_above -0.2 1 ^
```

```
        -odir 4_tiles_denoised -olaz ^
        -cores %NUM_CORES%

:: classify the lowest points per 25 cm by 25 cm cell that is *not*
:: noise (i.e. classification other than 7) as 8 using lasthin

rmdir .\5_tiles_thinned_lowest /s /q
mkdir .\5_tiles_thinned_lowest

lasthin -i 4_tiles_denoised\*.laz ^
      -ignore_class 7 ^
      -step 0.25 ^
      -lowest ^
      -classify_as 8 ^
      -odir 5_tiles_thinned_lowest -olaz ^
      -cores %NUM_CORES%

:: classify points considering only the points with classification code 8
:: (i.e. ignore classification 1 and 7) into ground (2) and non-ground (1)
:: points using lasground with options '-town -extra_fine -bulge 0.1'

rmdir .\6_tiles_ground /s /q
mkdir .\6_tiles_ground

lasground -i 5_tiles_thinned_lowest\*.laz ^
        -ignore_class 1 7 ^
        -step 25 -spike 2.5 -bulge 1.5 -stddev 10 -offset 0.1 -sub 5 ^
        -odir 6_tiles_ground -olaz ^
        -cores %NUM_CORES%

:: interpolate points classified as 2 into a TIN and raster a 1m DTM
:: but cutting out only the center 200 meter by 200 meter tile but not
:: rasterizing the buffers. the DTM raster is stored as gridded LAZ for
:: maximal compression

rmdir .\7_tiles_dtm /s /q
mkdir .\7_tiles_dtm

las2dem -i 6_tiles_ground\*.laz ^
      -keep_class 2 ^
      -step 1 ^
      -use_tile_bb ^
      -odir 7_tiles_dtm -olaz ^
      -cores %NUM_CORES%

:: we merge the gridded LAZ files for the DTM into one input and create
:: a 1m hillshaded DTM raster in PNG format
```

```
blast2dem -i 7_tiles_dtm\*.laz -merged ^
        -hillshade ^
        -step 1 ^
        -odir 7_tiles_dtm -o dtm_hillshaded.png

:: create clean folder for the final DTM raster

rmdir .\8_tiles_dtm_final /s /q
mkdir .\8_tiles_dtm_final

blast2dem -i 7_tiles_dtm\*.laz -merged ^
          -elevation ^
          -step 1 ^
         -odir 8_tiles_dtm_final -o final_dtm_UAV.tif
```

Appendix B-2 : Modified Batch Processing script for LiDAR DIM data

```
:: a batch script for processing LiDAR data into
:: a number of products with a tile-based multi-core batch pipeline
:: include LAStools in PATH to allow running script from anywhere

set PATH=%PATH%;..;

:: specify the number of cores to use

set NUM_CORES=4

:: create clean folder for the raw tiles with buffer

rmdir .\1_tiles_raw /s /q
mkdir .\1_tiles_raw

:: use lastile to create a buffered tiling from the original
:: flight strips. the flag '-files_are_flightlines' assures
:: that points from different flight lines will get a unique
:: flight lines ID stored in the 'point source ID' attribute
:: that makes it possible to later identify from which points
:: belong to the same flight strip. we use '-tile_size 200'
:: to specify the tile size and request a buffer of 30 meters
:: around every tile with '-buffer 30'. this buffer helps to
:: reduce edge artifacts at tile boundaries in a tile-based
:: processing pipeline.

lastile -i 0_strips_raw\*.laz -files_are_flightlines ^
        -tile_size 200 -buffer 30 ^
            -utm 37south -vertical_wgs84 ^
        -o 1_tiles_raw\dar.laz -olaz

:: create clean folder for the ground-classified tiles

rmdir .\2_tiles_ground /s /q
mkdir .\2_tiles_ground

:: use lasground to find the bare-earth points in all tiles
:: with the optimisation parameter values for step, spike, bulge,stddev,offset and sub
:: (initial ground estimate)
:: (see: lasground_README.txt).

lasground -i 1_tiles_raw\*.laz ^
          -step 25 -spike 2 -bulge 1.5 -stddev 1 -offset 0.1 -sub 5 ^
              -compute_height ^
          -odir 2_tiles_ground -olaz ^
```

```
        -cores %NUM_CORES%
:: create clean folder for the denoised tiles

rmdir .\3_tiles_denoised /s /q
mkdir .\3_tiles_denoised

:: use lasheight to remove low and high outliers that are often
:: just noise (e.g. clouds or birds). by default lasheight uses
:: the points classified as ground to construct a TIN and then
:: calculates the height of all other points in respect to this
:: ground surface TIN. with '-drop_above 40 -drop_below -3' all
:: points that are 40 meters above the ground or 3 meters below
:: the ground are removed from the output LAZ tiles that are to
:: be stored in the '3_tiles_denoised' folder. if we have multiple
:: input files this process runs on %NUM_CORES% many cores.

lasheight -i 2_tiles_ground\*.laz ^
        -drop_above 40 -drop_below -3 ^
        -odir 3_tiles_denoised -olaz ^
        -cores %NUM_CORES%

:: create clean folder for the classified tiles

rmdir .\4_tiles_classified /s /q
mkdir .\4_tiles_classified

:: use lasclassify to identify buildings and trees in all denoised
:: tiles.

lasclassify -i 3_tiles_denoised\*.laz ^
            -ignore_class 7 ^
          -odir 4_tiles_classified -olaz ^
          -cores %NUM_CORES%

:: create clean folder for the final tiles (stripped of the buffer)

rmdir .\5_tiles_final /s /q
mkdir .\5_tiles_final

:: use lastile to remove the buffer from the classified tiles which
:: is requested with the option '-remove_buffer'.

lastile -i 4_tiles_classified\*.laz ^
       -remove_buffer ^
       -odir 5_tiles_final -olaz

:: create clean folder for the raster DTMs in ESRI ASCII format
```

```
rmdir .\6_tiles_dtms /s /q
mkdir .\6_tiles_dtms

:: run las2dem on the ground-classified tiles to create raster DTMs
:: in bil format for each individual tile. important
:: is the '-keep_class 2' flag that activates a filter letting only
:: the points classified as 'ground' through. in addition we use the
:: '-thin_with_grid 0.5' filter to have only one ground point per
:: 0.5m by 0.5m area. this assures that we construct and sample a
:: TIN appropriate for the output resolution of 1.0m by 1.0m that is
:: set by '-step 1.0'. very important is the '-use_tile_bb' parameter
:: that limits rasterizating the TIN to the tile area *without* the
:: buffer added by lastile in the 'tile_based_lidar_preparation.bat'
:: batch script thereby avoiding any potential edge artifacts along
:: the tile boundaries.

las2dem -i 2_tiles_ground\*.laz ^
      -keep_class 2 -thin_with_grid 0.5 -step 1.0 -use_tile_bb ^
      -odir 6_tiles_dtms -obil ^
      -cores %NUM_CORES%

:: create clean folder for the hillshaded DTM rasters

rmdir .\7_tiles_hillshaded_dtms /s /q
mkdir .\7_tiles_hillshaded_dtms

:: use blast2dem to create individual 1m hillshaded DTM rasters from the
:: LiDAR points that were classified as ground in each tile. .

blast2dem -i 6_tiles_dtms\*.bil -merged ^
      -step 1.0 -hillshade -utm 37south -vertical_wgs84 ^
      -odir 7_tiles_hillshaded_dtms -opng ^
      -cores %NUM_CORES%

:: create clean folder for the final DTM raster

rmdir .\8_tiles_dtm_final /s /q
mkdir .\8_tiles_dtm_final

:: use blast2dem to create a single tif TM raster from on-the
:: fly merged bil rasters.


blast2dem -i 6_tiles_dtms\*.bil -merged ^
      -step 1.0 -elevation -utm 37south -vertical_wgs84 ^
      -odir 8_tiles_dtm_final -o dtm_liDAR.tif
```

Appendix C : R script for calculating correlation coefficient and Y-intercept

```
# correlation coefficient for Vegetated area

vegetated <- read.csv('vegetated_corr.csv')
head(vegetated)
cor.test(vegetated$lidar,vegetated$dim)
mymodel <- lm(vegetated$dim ~ vegetated$lidar)
summary(mymodel)

# correlation coefficient for built-up area

builtup <- read.csv('builtup_corr.csv')
head(builtup)
cor.test(builtup$lidar,builtup$dim)
mymodel1 <- lm(builtup$dim~builtup$lidar)
summary(mymodel1)

# correlation coefficient for bare area

bare <- read.csv('bare_corr.csv')
head(bare)
cor.test(bare$lidar,bare$dim)
mymodel2 <- lm(bare$dim~bare$lidar)
summary(mymodel2)

# correlation coefficient for man-made area

man_made <- read.csv('man_made_corr.csv')
head(man_made)
cor.test(man_made$lidar,man_made$dim)
mymodel3 <- lm(man_made$dim~man_made$lidar)
summary(mymodel3)
```

Appendix D: Effects of optimised parameters on flooding

Appendix D-1 : WSE from Optimised parameters DTMs :left LiDAR Step & spike and right DIM step & spike (River cross-section profile)

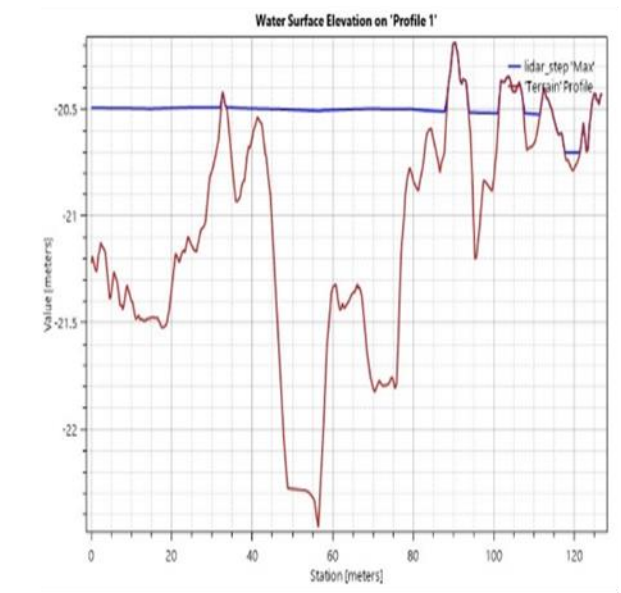

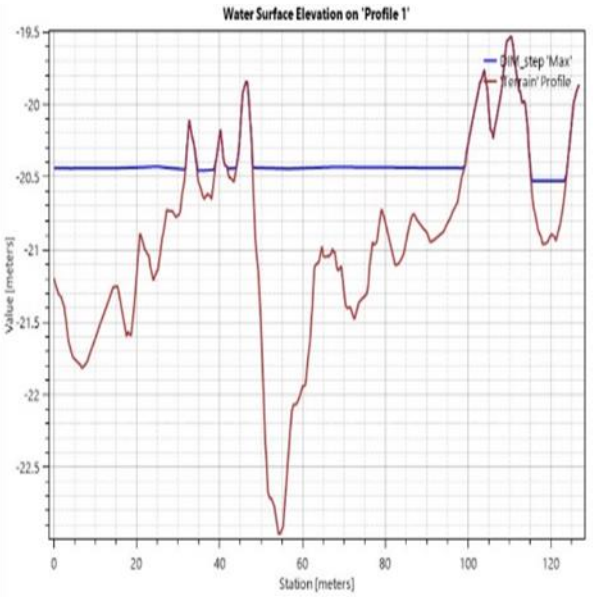

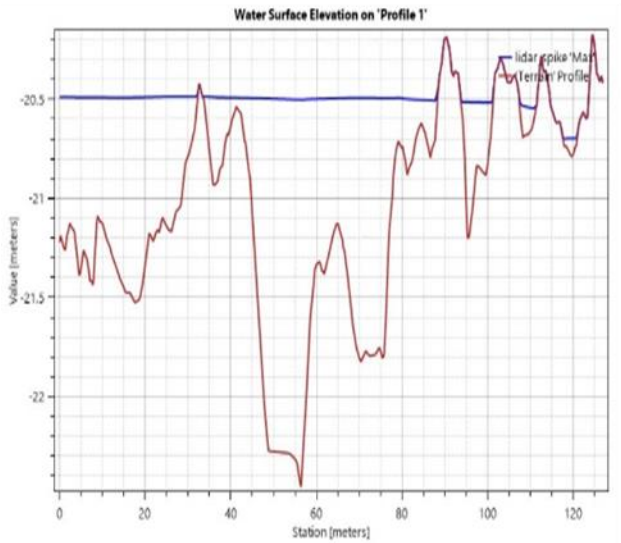

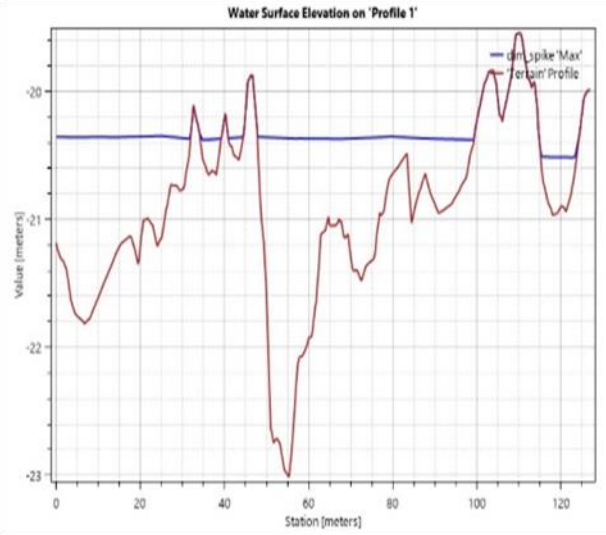

Appendix D-2 : WSE from Optimised parameters DTMs :left LiDAR bulge & stddev and right DIM bulge & stddev (River cross-section profile)

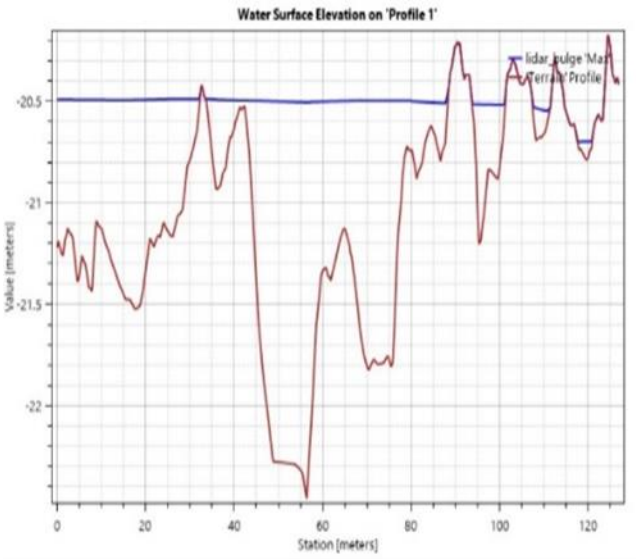

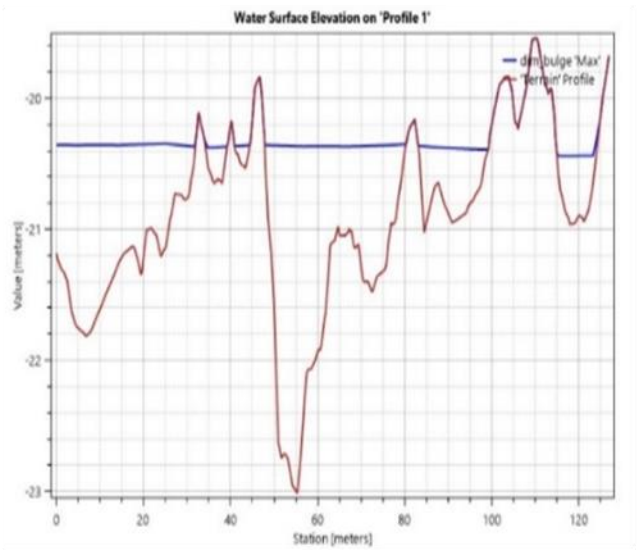

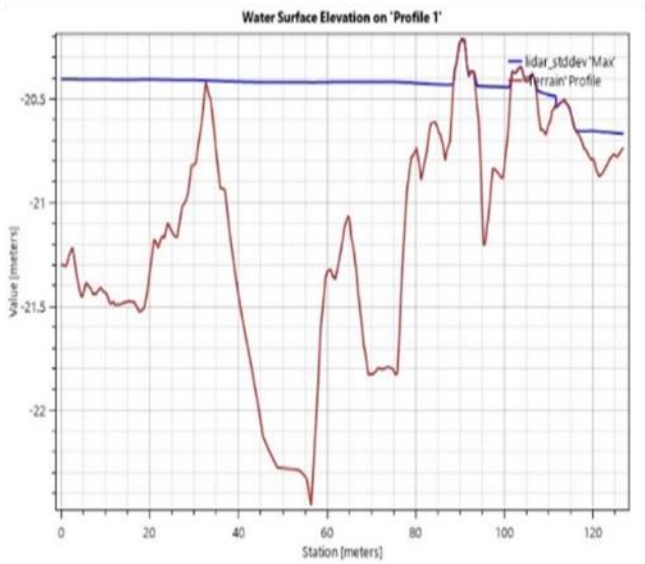

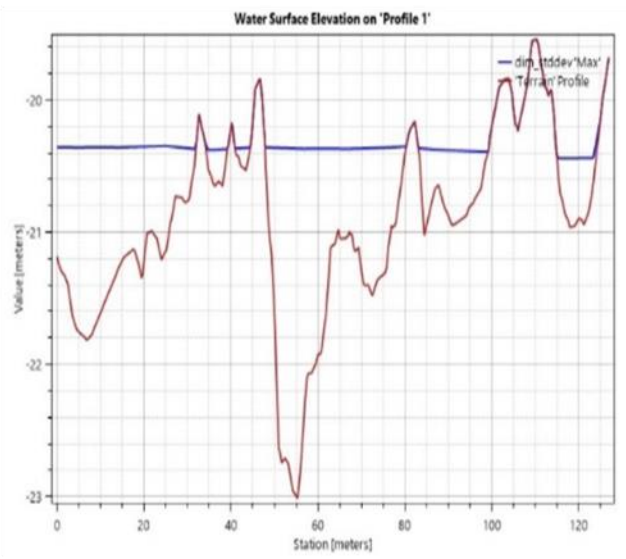

Appendix D-3 : WSE from Optimised parameters DTMs :left LiDAR offset & sub and right DIM offset & sub (River cross-section profile)

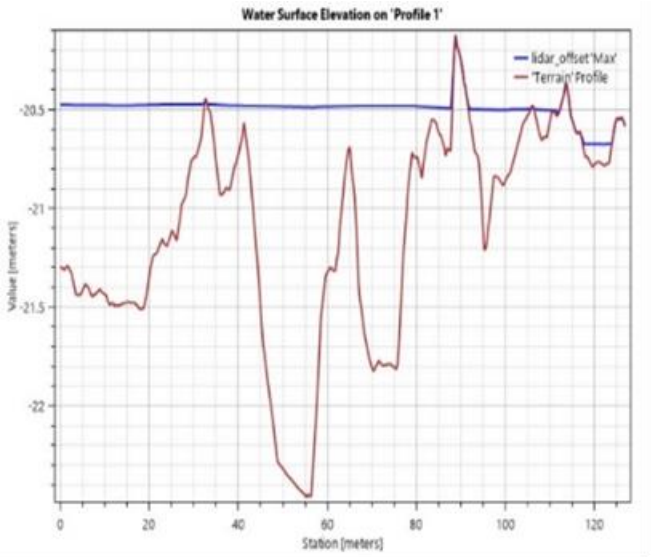

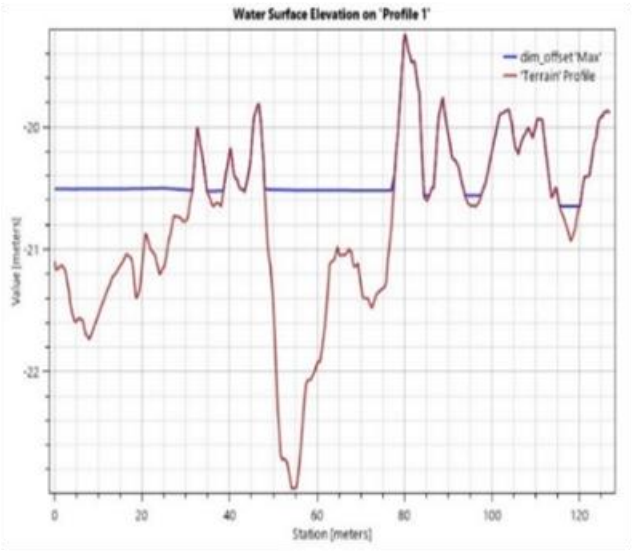

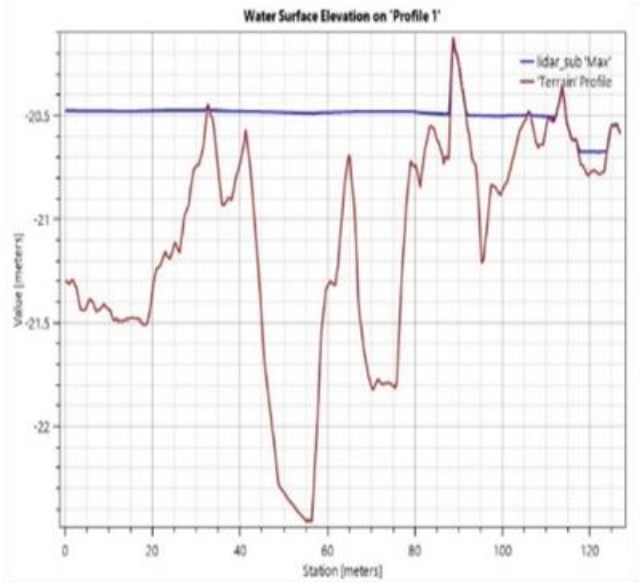

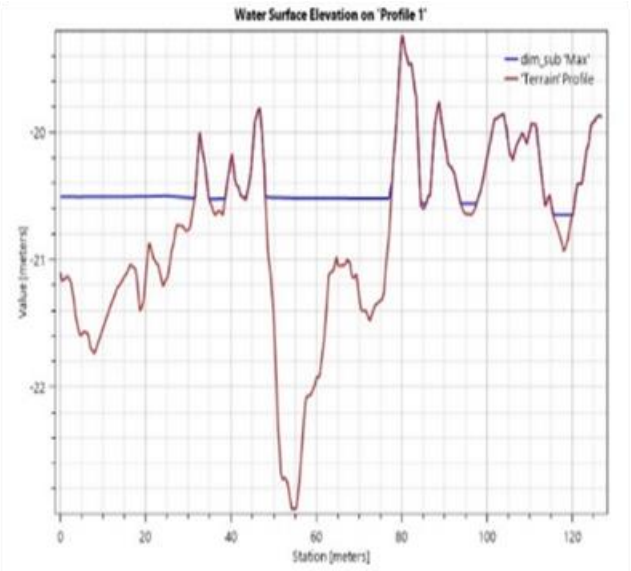

Appendix E: Effects of different parameters on flooding

Appendix E-1: LiDAR Step parameter effect on inundation (Vegetation profile)

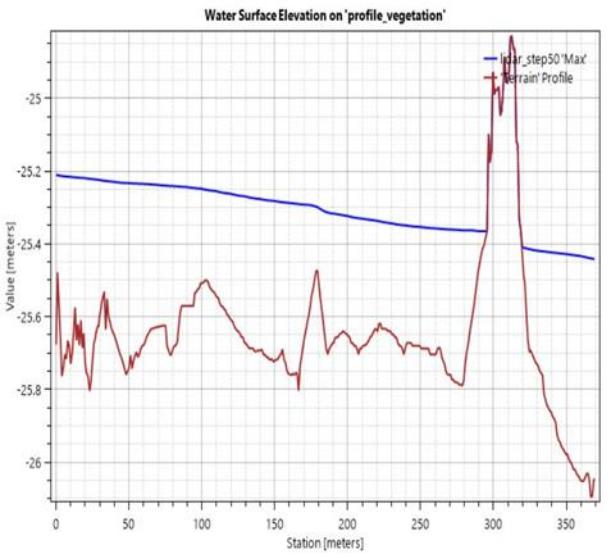

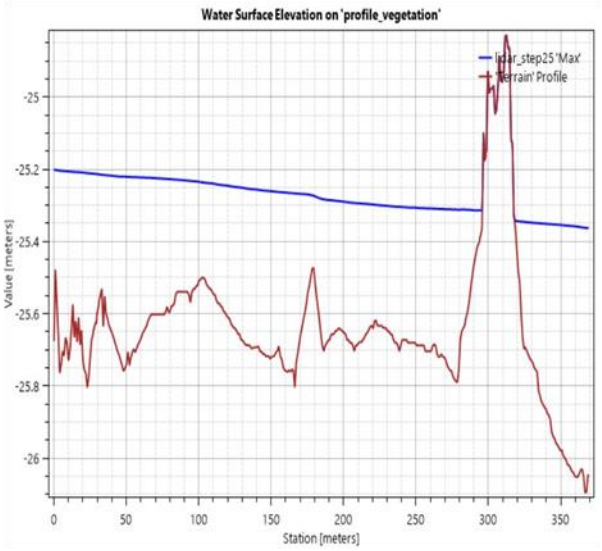

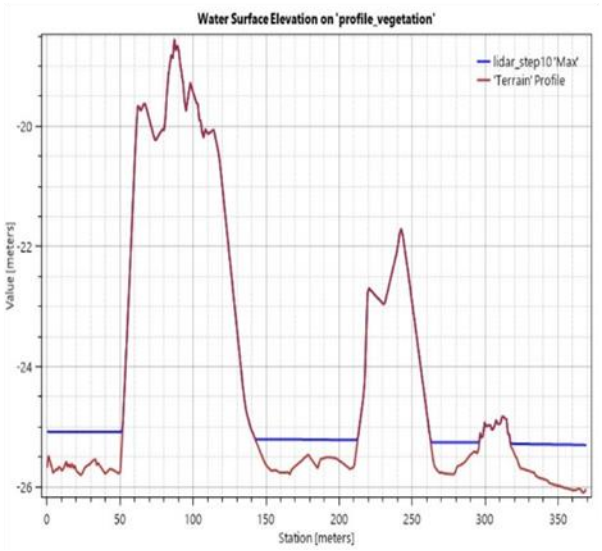

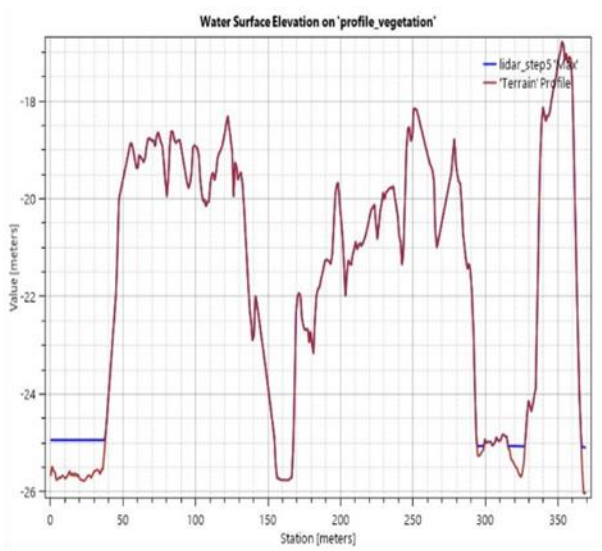

Appendix E-2: DIM Step parameter effect on inundation (Vegetation profile)

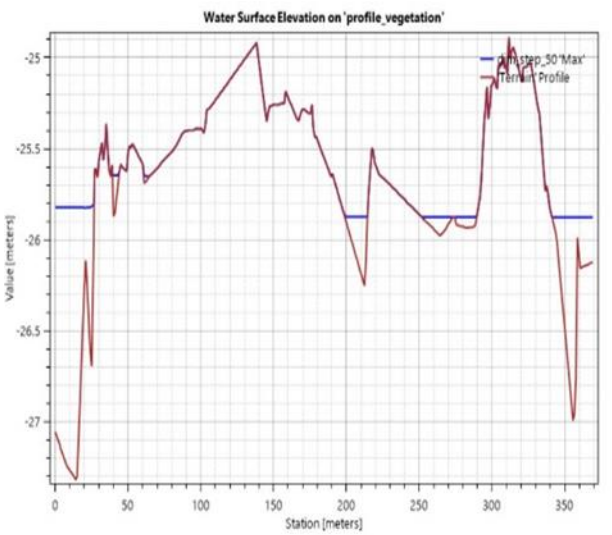

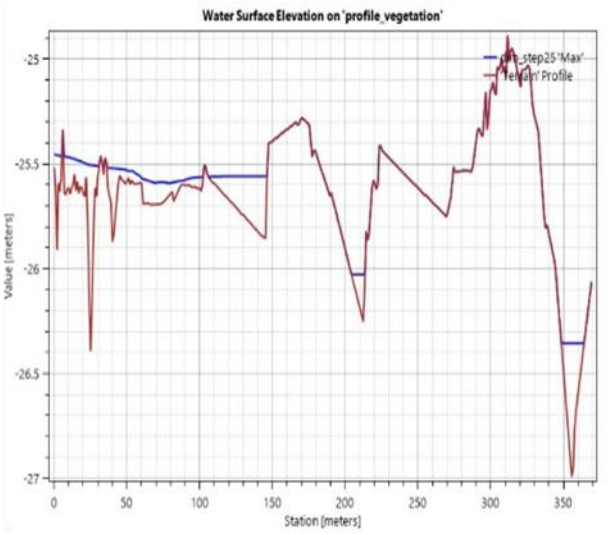

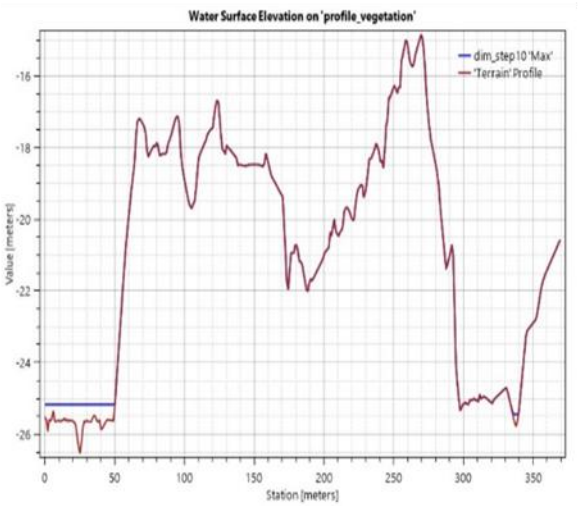

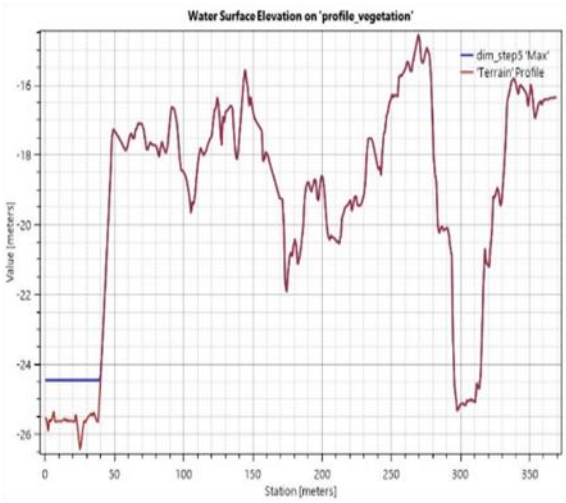

Appendix E-3 : LiDAR Spike parameter effect on inundation (Vegetation profile)

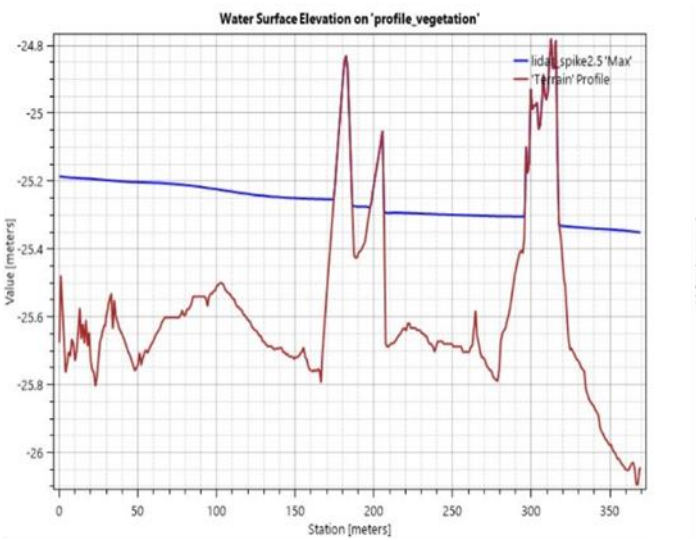

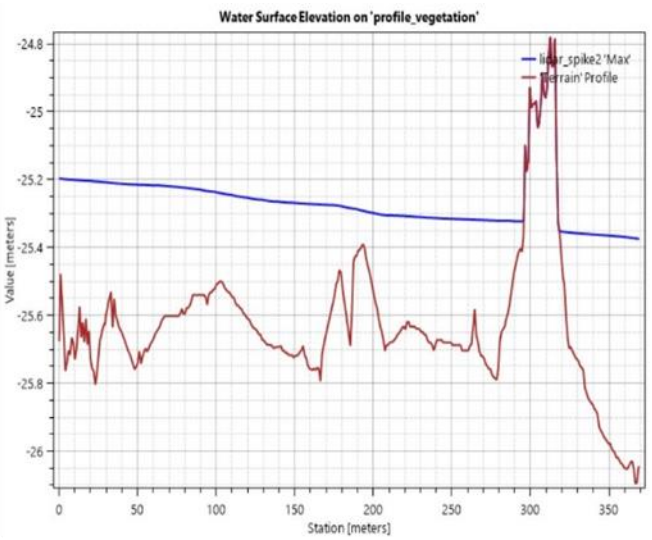

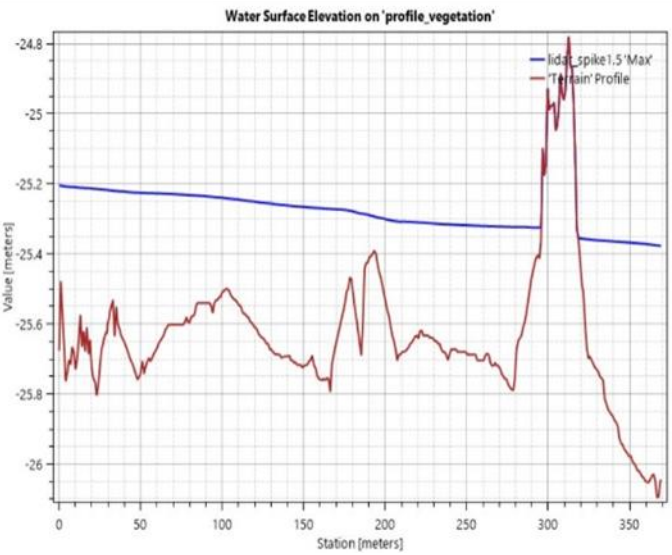

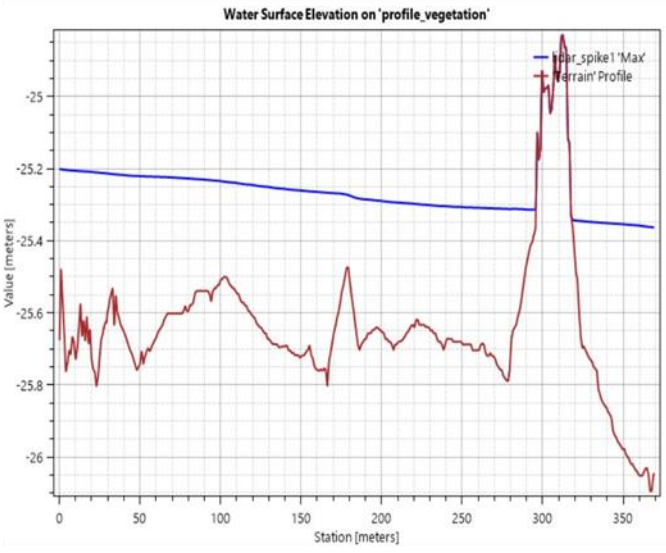

Appendix E-4 : DIM Spike parameter effect on inundation (Vegetation profile)

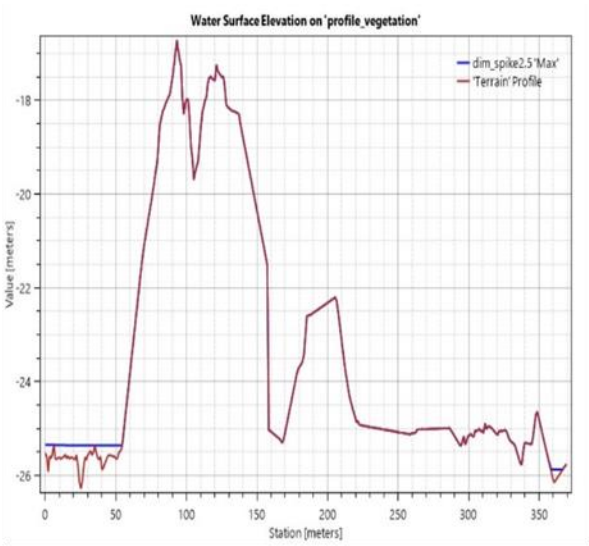

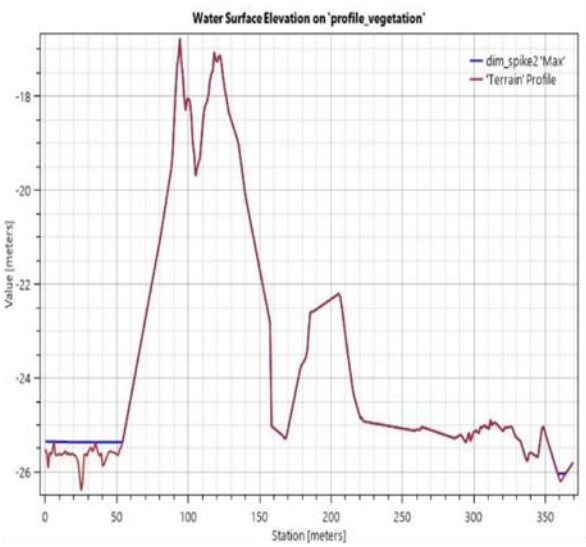

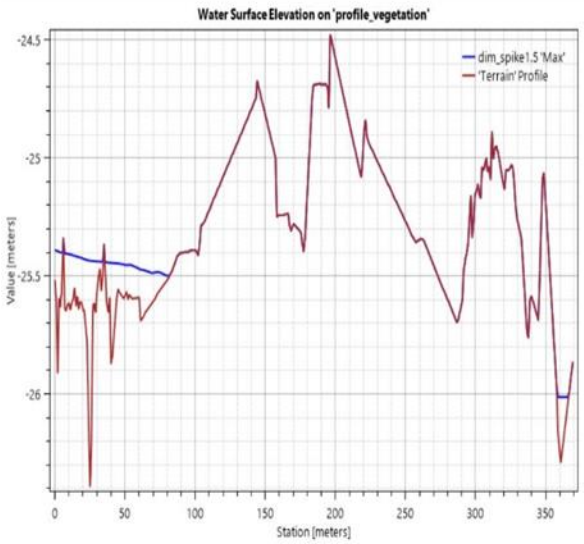

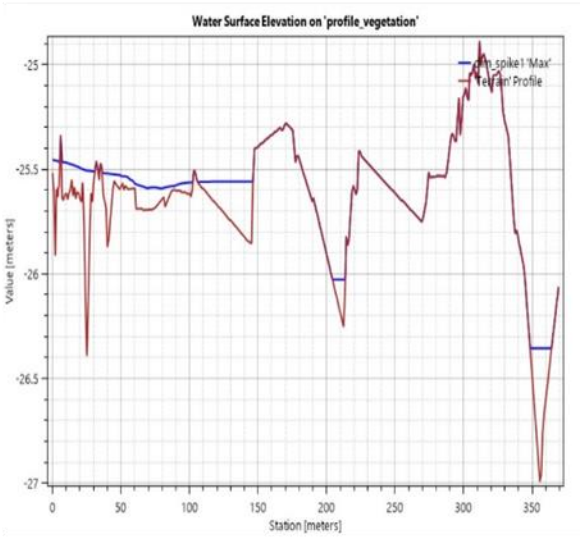

Appendix E-5: LiDAR offset parameter effect on inundation (Vegetation profile)

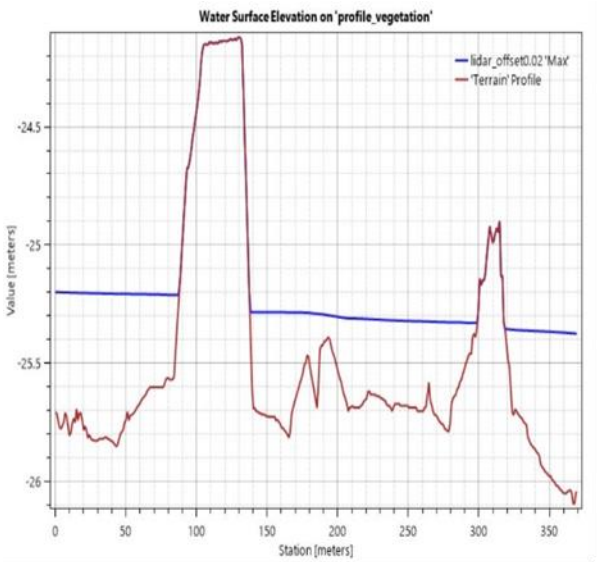

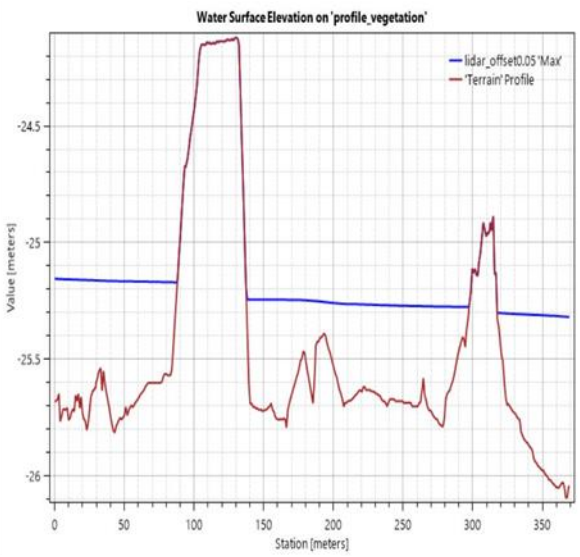

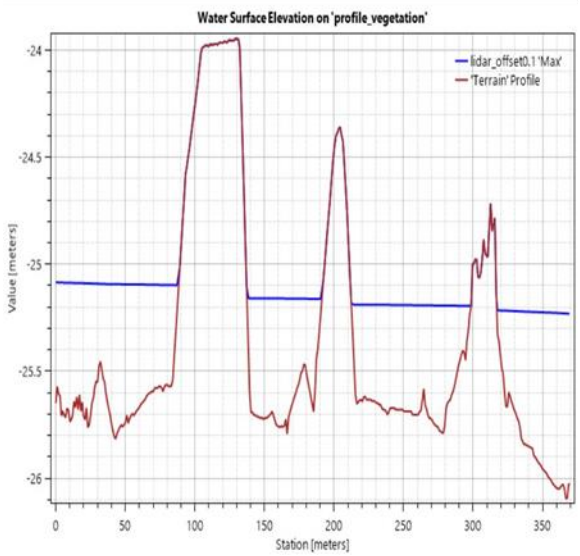

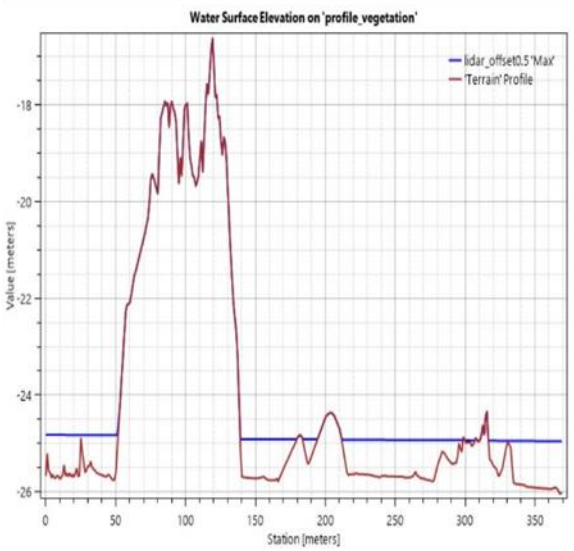

Appendix E-6: LiDAR Step parameter effect on inundation (Vegetation profile)